Investigation of the effects of hydrogen peroxide in combination with ionising radiation in cancer

Samantha Nimalasena

Thesis submitted to the University of London in accordance with the requirements for the degree of Doctor of Medicine MD (Res)

2022
Institute of Cancer Research

Declaration

I declare that this thesis has been composed solely by myself and that it has not been submitted, in whole or in part, in any previous application for a degree. Except where it states otherwise by reference or acknowledgment, the work presented is entirely my own.

Abstract

Introduction

In the early 2000s, Japanese colleagues reported sensitisation of normal and tumour cell lines to cytotoxic doses of ionising radiation (IR) by low concentrations of hydrogen peroxide (H_2O_2), research that prompted clinical studies testing intratumoural (IT) injections of 0.5% H_2O_2 in 1% sodium hyaluronate gel during radiotherapy in patients with inoperable breast cancer. Five-year local control rates were substantially higher than expected from the radiotherapy dose intensities used, with no additional late adverse effects.

Methods

Using the radioresistant cell lines HCT116 and HN5, the effect of H_2O_2 + IR was investigated in 2D clonogenic survival and 3D spheroid growth assays. A dual hypoxia marker technique was used to capture the effect of IT H_2O_2 in murine xenografts. In parallel, a Phase I clinical trial of IT H_2O_2 + radiotherapy was conducted in 12 patients with breast cancer to evaluate safety and acute toxicity.

Results

2D clonogenic assays did not confirm sensitisation of HCT116 or HN5 under normoxic conditions. Growth inhibition was demonstrated in HCT116 spheroids treated with H_2O_2 + IR, compared with H_2O_2/IR alone. Xenograft tumours injected with H_2O_2 + sodium hyaluronate exhibited a reduction in hypoxia staining compared to baseline. A significant difference in pimonidazole versus CCI-103F staining was demonstrated in H_2O_2-injected tumours ($p=0.02$), with no significant difference in the control groups. The Phase I clinical trial confirmed safety with no additional toxicity compared to RT alone.

Conclusion

3D spheroid results are in keeping with clinical reports of enhancement of radiation effect by H_2O_2. Reoxygenation by IT H_2O_2 may be an important mechanism by which tumour response is enhanced for therapeutic gain, and which has implications for scheduling of H_2O_2 relative to radiotherapy in the clinical setting. If this method of increasing oxygen delivery to tumours is confirmed to be successful, it has potential to be utilised in several other tumour types.

Acknowledgements

Foremost, I owe a sincere debt of gratitude to my supervisors: Dr Navita Somaiah, Dr Carol Box, Dr Simon Robinson and Professor John Yarnold for the unwavering support, scholarly advice, knowledge, and wisdom they provided whilst I undertook this research. Their constant dedication, keen interest, and meticulous approach have been a source of inspiration to me. It is an understatement to say that all their guidance (and limitless patience) was invaluable through all the stages of the writing process. Each of my supervisors gave generously of their time, always readily available to keep me motivated and to read multiple thesis drafts. I would also like to acknowledge Professor Alan Melcher, for agreeing to be my back-up supervisor.

When I started out in the laboratory with no prior experience and not even able to use a pipette, Dr Carol Box patiently and painstakingly taught me the laboratory skills I required to proceed with my experiments. I extend particular thanks to her, as without this supervision, it would not have been possible. Similarly, to Dr Simon Robinson for his invaluable advice on the practicalities and design of the *in vivo* experiments. I would also like to offer special thanks to Dr Selva Anbalagan, for giving so generously of his time and wealth of experience, continuous IT expertise, and keeping me fed and watered during long days in the lab!

I give my heartfelt thanks for the assistance of numerous colleagues (too many to mention), without whom I would not have been able to conduct this work. Firstly, to Dr Jessica Boult and Nigel Bush for helping me and giving me the confidence to carry out the *in vivo* experiments. To Nigel Bush for expertly setting up and operating the ultrasound during intratumoural injection of xenograft tumours. I am grateful to Dr Ruth Riisnaes for her assistance in sectioning of cryopreserved xenograft tumours prior to staining. Furthermore, to Dr Sheng Yu for performing the computational analysis of plasma biomarker results obtained in the Phase I clinical study. I would also like to acknowledge Professors Peter Wardman and Peter O'Neill for their guidance and readiness to impart their expert knowledge on ROS biology.

I would like to thank the other students and staff at the CCI and BSU for their good humour and always being approachable. I am also extremely grateful to Lone Gothard and Dr Harriet Steel for their time and diligence in providing IT support during the writing of this thesis.

I extend my gratitude to Professor Yasuhiro Ogawa and colleagues in Japan for performing the preliminary work on H_2O_2 and irradiation, which provided the basis for this research project. I am grateful for the expert training provided by Professor Ogawa and colleagues, which enabled the UK Phase I clinical trial to proceed. A special mention is given to the patients who participated in the Phase I clinical trial, who gave freely of their time and for their motivation to advance research in this area. I would also like to acknowledge the generous funding bodies that enabled me to undertake this work; KORTUC Inc. and the National Institute for Health and Care Research (NIHR).

Finally, I wish to say thank you to my family without whom I would not have been able to complete this work. To my parents, for their consistent support and encouragement, readiness to help with childcare and making delicious meals to keep me going. To my husband Jonathan, and children Amelie, Toby, and Henry for allowing me the time and space to work, and never complaining.

Table of Contents

List of Abbreviations

BSA	Bovine Serum Albumin
CO_2	Carbon Dioxide
CR	Complete Response
CTCAE	Common Toxicity Criteria for Adverse Events
CTG	CellTiter-Glo®
CTV	Clinical Target Volume
DAMPs	Damage Associated Molecular Patterns
DMEM	Dulbecco's Modified Eagle Medium
DMSO	Dimethyl Sulfoxide
DNA	Deoxyribonucleic acid
EDTA	Ethylenediamine tetra-acetic acid
EGF	Epidermal Growth Factor
EGFR	Epidermal Growth Factor Receptor
ELISA	Enzyme-linked Immunoassay
EPO	Erythropoietin
EQD_2	Equivalent Dose in 2Gy Fractions
ER	Oestrogen Receptor
ERK	Extracellular signal-regulated kinase
FITC	Fluorescein Isothiocyanate
FSD	Focus to Skin Distance
H_2DCFA	2,7-Dichlorodihydrofluorescein
H_2O_2	Hydrogen Peroxide
HBSS	Hank's Balanced Salt Solution
HER2	Human Epidermal Growth Factor-2
HIF-1	Hypoxia Inducible Factor-1
IDMC	Independent Data Monitoring Committee
IL-1β	Interleukin-1β
IL-4	Interleukin-4
IP	Intraperitoneal
IR	Ionising Radiation
IS-MRI	Intrinsic Susceptibility Magnetic Resonance Imaging
IT	Intratumoural
JNK	Jun N-terminal kinase
KORTUC	Kochi-Oxydol-Radiation Therapy for Unresectable Carcinomas
LET	Linear Energy Transfer
MAPK	Mitogen-activated Protein Kinase
MFH	Malignant Fibrous Histiocytoma
MHRA	Medicines Healthcare products Regulatory Agency
MIP-1α	Macrophage inflammatory protein-1α
mM	Millimolar
MRI	Magnetic Resonance Imaging
MSOT	Multispectral Opto-acoustic Tomography
MTOR	Mammalian Target of Rapamycin
MV	Megavoltage
NF-κB	Nuclear factor kappa B
NO	Nitric Oxide
OCR	Oxygen Consumption Rate
OCT	Optimum Cutting Temperature
OE-MRI	Oxygen Enhanced Magnetic Resonance Imaging

OER	Oxygen Enhancement Ratio
OVA	Ovalbumin
PBS	Phosphate-buffered saline
PCR	Polymerase Chain Reaction
PDGF	Platelet Derived Growth Factor
PE	Plating Efficiency
PET	Positron Emission Tomography
ATM	Ataxia Telangiectasia Mutated
PI	Propidium Iodide
PR	Progesterone Receptor
REC	Research Ethics Committee
RIPK-3	Receptor Interacting Protein Kinase-3
RNS	Reactive Nitrogen Species
ROS	Reactive Oxygen Species
RPMI	Roswell Park Memorial Institute
RT	Radiotherapy
SF	Surviving Fraction
SOD	Superoxide Dismutase
SRB	Sulforhodamine B
SRUS	Super Resolution Ultrasound
STAT-6	Signal Transducer and Activator of Transcription 6
STR	Short Tandem Repeat
TCA	Trichloroacetic acid
TGFβ	Transforming Growth Factor
TH2	T Helper 2
TNFα	Tumour Necrosis Factor α
TRAIL	TNF-related apoptosis-inducing ligand
UPR	Unfolded Protein Response
US	Ultrasound
VAM	Vascular Architecture Mapping
VEGF	Vascular Endothelial Growth Factor

List of Figures

List of Tables

Chapter 1

Introduction

1.1 Radiotherapy

1.1.1 Radiotherapy in clinical practice

The discovery of X-rays in 1895 by Wilhelm Röntgen paved the way for the therapeutic use of radiation in the management of malignant disease. Radiotherapy remains one of the cornerstones in the management of many cancers, and modern techniques used in combination with chemotherapy and surgery have significantly improved outcomes for patients (Hope-Stone, 1986). On average 50% of cancer patients receive radiotherapy alone or in combination with chemotherapy and/or surgery during their treatment. It is estimated that radiotherapy accounts for approximately 40% of curative treatments (Baskar, Lee, Yeo, & Yeoh, 2012). It is also an effective modality for palliation and symptom control in patients with advanced or recurrent malignancy (Lutz, Jones, & Chow, 2014).

A unique feature of radiotherapy is that the dose delivered to the tumour is relatively uniform, usually within a few percentage points of the prescription dose. This is in contrast to systemic chemotherapy, where the delivered dose is heterogeneous and dependent on factors such as tumour physiology, vasculature, target expression and properties of the drug (Citrin & Mitchell, 2014). The aim of radiotherapy is to deliver as much dose to the tumour as possible whilst sparing normal tissues in and around the target volume (known as the therapeutic index). Technological advances such as image-guided, intensity-modulated, and stereotactic radiotherapy have enabled dose escalation and/or reduction in toxicity when compared to conventional techniques (Busk, Horsman, Overgaard, & Jakobsen, 2020).

Ionising radiation causes potentially lethal DNA damage, and the tumour cell's ability to repair this determines its radiosensitivity. Cancer cells that sustain irreparable DNA damage stop replicating and die. Cell death can occur via several processes: apoptosis, mitotic catastrophe, necrosis, senescence and autophagy (Baskar et al., 2012).

Ionising radiation can cause cell damage via “direct” or “indirect” means as illustrated in Figure 1.1. The former (the dominant process) refers to the effects of x-rays on biomolecules such as DNA, protein, and lipids. Radiation effects on DNA occur via damage to base pairs, single- and double-strand breaks, the latter being the most lethal (Wang, Mu, He, & Zhang, 2018). Indirect damage is caused by x-rays interacting with molecules within the target, resulting in primary or secondary ionisation. The resulting free electrons can exert damage to biomolecules other than DNA, or interact with water, forming hydroxyl radicals and other reactive oxygen species (Sharma et al., 2016). Direct and indirect effects are illustrated in Figure 1.1.

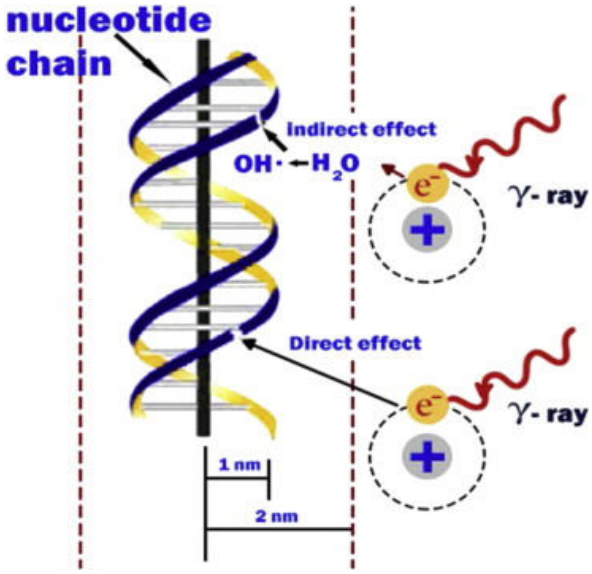

Figure 1.1 Direct and Indirect effects of radiation. Direct action involves absorption of an x-ray photon resulting in secondary electrons interacting with DNA. In indirect action, the secondary electron interacts with another biomolecule (e.g., H_2O with production of hydroxyl radicals (OH·) which damage DNA (image reproduced from E. J. Hall & Giaccia, 2006)

However, tumour radioresistance remains a significant clinical problem. Factors including tumour size, hypoxia, high antioxidant levels, genetic instability and deregulated growth mechanisms contribute to radioresistance (Morgan & Lawrence, 2015). In addition to the DNA damage response, the tumour microenvironment, immune system, and cell-cell signalling (the bystander effect) can also affect response to radiotherapy (Busk et al., 2020; Prise & O'Sullivan, 2009).

1.1.2 The five Rs of radiotherapy

A set of classic factors, the “five Rs of radiotherapy” have been identified which regulate the cellular/tissue response to radiation. These are Repair, Redistribution, Repopulation and Reoxygenation, and intrinsic Radiosensitivity. They can guide radiobiological research into treatment strategies that may modulate radiation response (Hall, 1978; Steel, 1989). In simple terms, Repair and Repopulation lead to radioresistance, and Reoxygenation and Redistribution render the tumour more radiosensitive.

“Repair” relates to the restoration of damage to macromolecules following ionising radiation. Reactive oxygen species (ROS) generated by ionising radiation primarily affect DNA, leading to loss of clonogenic potential. Characterisation of DNA repair mechanisms have uncovered targets which can modulate DNA-repair capacity, thereby potentially sensitising cells to IR. ‘Repopulation” occurs when surviving cells proliferate to replace those that have been eliminated by a dose of radiation, and this remains an important obstacle in treatment success.

“Redistribution” describes that the cellular response to irradiation varies as the cell progresses through the cell cycle. “Reoxygenation” describes a process whereby hypoxic regions within the tumour become more oxygenated following a dose of radiation. This is relevant as tumour oxygen concentration dramatically affects tumour radiosensitivity (by a factor of 2.5-3), and this is discussed in detail in Chapter 4. In addition, the phenomenon of reoxygenation illustrates that oxygenation within a tumour is not static. “Intrinsic radiosensitivity” refers to the variation in radiosensitivity between cell types, which can be expressed as SF2, the fraction of cells surviving following a single 2 Gy dose of radiation. The mechanisms underlying this variation in radiosensitivity are likely to be multifactorial (Steel, 1989). Anticancer treatments which target the processes related to these R’s of radiotherapy are possible modulators of radiosensitivity (Oehler et al., 2007).

1.1.3 Modifying radiation response

The rationale for combining radiotherapy and drug treatment is to optimise therapeutic outcome. As described by Steel et al, combining radiotherapy and chemotherapy or other systemic agents can achieve an improved outcome by spatial (anatomical) co-operation, exploitation of independent toxicities, selective protection of normal tissues, or selective enhancement of tumour response (Steel, Hill, & Peckham, 1978).

Although the primary endpoint in many trials of drug-radiotherapy combinations is overall survival, locoregional control of disease is also paramount. Control of local and regional disease can have a positive impact on cancer survival. This is explained by the concept that uncontrolled local disease can act as a reservoir for metastatic spread. Furthermore, uncontrolled local disease can result in significant morbidity and impact negatively on quality of life. This is especially relevant in patients where distant disease is controlled by systemic therapy, and the prognosis of the patient may extend to years (Citrin & Mitchell, 2014).

1.1.4 Sensitisation

Many agents tested in the laboratory and used in a clinical setting have cytotoxic or cytostatic effects that can be exploited to enhance the effectiveness of radiation in the ways described above.

Sensitisation is a special case, referring to the effects of agents causing no clinical, tissue or cellular toxicity when used alone, but which enhance the cytotoxic effects of radiation. There are few examples of true sensitisers, as the majority used in the clinical context demonstrate a degree of cytotoxicity when used alone (Citrin & Mitchell, 2014).

1.1.5 Radiosensitisers in clinical practice

There are many obstacles which make it difficult to achieve cure with radiotherapy alone. These include the number and radiosensitivity of cancer stem cells, tumour hypoxia and repopulation, and other environmental influences such as angiogenesis and tumour metabolism. Radiosensitisers aim to improve the

efficacy of radiotherapy by modifying specific causes of clinical resistance (Wang et al., 2018).

Initial studies in the 1970s involved giving sequential or concurrent chemotherapy with radiation, hypothesising that a synergistic effect could be achieved by chemotherapy-mediated disruption of DNA repair mechanisms. Radiosensitisation has been demonstrated using sub-cytotoxic doses of platinum drugs, 5-fluorouracil, and mitomycin C, and temozolomide, which work by reducing the intrinsic radioresistance of tumour cells (Higgins, O'Cathail, Muschel, & McKenna, 2015). These drugs are effective as they add to the DNA damage induced by radiotherapy, thereby increasing cell death.

The drawback from this strategy is that there is no specificity for tumour cells and normal tissue toxicity is also increased (Moding, Kastan, & Kirsch, 2013). Aside from the combination of cytotoxic chemotherapy with radiotherapy, there has been limited progress in bringing targeted therapy and radiotherapy combinations into clinical practice, and there have been more failures than successes (Sharma et al., 2016). The reasons why these treatments have not lived up to expectations include the paucity of validated biomarkers, and the unacceptable side-effect profiles of the drugs used. Despite this, there remains cause for optimism.

1.1.6 Cancer biology and radiation response

Radiobiology research has benefited from improvements in our understanding of signal transduction pathways, genetic/epigenetic alterations, and differences in DNA damage response between tumour and normal tissue. These developments have identified molecular pathways that can be pharmacologically exploited in combination with radiotherapy. Such radiation-drug combination strategies may include the use of: DNA damage response inhibitors, inhibitors of pro-survival signalling pathways, hypoxic cell sensitizers, metabolic inhibitors, immune modulators, growth factor inhibitors, anti-invasive drugs, and anti-angiogenic agents (Falls et al., 2018; Oehler et al., 2007).

1.1.7 Modulation of oxidative stress as a treatment strategy

ROS play a crucial role in regulating cell proliferation, apoptosis, DNA repair, stemness, metabolic reprogramming, and the tumour microenvironment. All have been implicated in resistance to radiotherapy.

During radiotherapy, ROS, including the superoxide anion (O_2^-), hydroxyl radicals (OH^-) and hydrogen peroxide (H_2O_2), are formed by the radiolysis of water, and these highly reactive molecules are toxic to both tumour cells and normal tissues (O'Neill & Wardman, 2009). Approximately two-thirds of the low-LET DNA damage induced by radiation in mammalian cells occurs due to the hydroxyl radical (Lv et al., 2014). In addition, radiation can induce endogenous ROS generation in mitochondria and influence mitochondrial membrane permeability, which then further stimulates ROS production. Excessive levels of ROS can also cause oxidative stress by reacting with biological molecules such as lipids, proteins, and DNA. To counteract this, endogenous antioxidant systems protect against radiation-induced oxidative stress by scavenging free radicals. For example, O_2^- can be converted to H_2O_2 by superoxide dismutases (SODs), and catalase and peroxidases can convert H_2O_2 to water and O_2. In this context, increased ROS production and inhibition of the antioxidant system represent credible targets to enhance tumour radiosensitivity (Kim et al., 2019).

1.2 Hydrogen Peroxide

It is well recognised that oxidative stress is a cause of cell damage and associated with the development and progression of many conditions, such as neurodegenerative diseases, diabetes and cancer (Veal, Day, & Morgan, 2007). Hydrogen Peroxide (H_2O_2) is a ubiquitous member of the ROS family, along with the hydroxyl radical OH• and the superoxide ion ($O2^{\bullet-}$). They are distinct from the reactive nitrogen species (RNS) family, which include compounds such as nitric oxide (NO) (Di Meo, Reed, Venditti, & Victor, 2016). H_2O_2 is generated in response to numerous stimuli, including cytokines and growth factors. It is formed *in vivo* by dismutation of superoxide and plays a pivotal role in redox signalling and homeostasis at physiological concentrations (1-10 nM) (Halliwell, Clement,

& Long, 2000; Sies, 2017). Downstream signalling events that are influenced by H_2O_2 include calcium mobilisation, protein phosphorylation and gene expression. In its role as a messenger molecule, it readily diffuses through cells and tissues to stimulate such effects as alterations in cell shape, cell proliferation, and immune cell recruitment (Sies, 2017).

1.2.1 History

H_2O_2 was first synthesised in 1818 by the French chemist Louis-Jacques Thenard, who termed it “oxygenated water”, and realised that it caused painful blotches when applied to the skin. Subsequent detection of H_2O_2 production by pneumococcus and aspergillus focused on cell-killing properties, but it wasn’t until 1970 that the role of H_2O_2 in normal physiology and metabolism in mammals was recognised (Sies, 2017).

1.2.2 Everyday uses

Nowadays, there are many commercial and cosmetic household applications utilising the oxidant properties of H_2O_2, examples which include bleaching agents and hair dyes. H_2O_2 in vaporised form can also be used in sterilisation processes, for materials that are unable to tolerate high temperatures and humidity. In more concentrated forms, it is a component of fuel additive for rockets and planes, and in the medical field H_2O_2 has long been used as an antiseptic in mouthwashes and wound cleansers.

1.2.3 Molecular and cellular effects

H_2O_2 is produced by certain cell types (e.g., phagocytes), in response to growth and injury, mediated by epidermal growth factor (EGF), VEGF and platelet-derived growth factor (PDGF) (Y. Fang et al., 2013; Wang et al., 2018). In comparison to other ROS, H_2O_2 is nonpolar and can traverse cell membranes easily, and exhibits a low bioactivity. In many cancer cells, upregulated H_2O_2-dependent signalling pathways contribute toward cell differentiation, growth, and survival, whilst higher concentrations of H_2O_2 may promote cell cycle arrest or apoptosis (Lennicke, Rahn, Lichtenfels, Wessjohann, & Seliger, 2015).

In view of the fact that a cytotoxic chemical such as H_2O_2 also functions as a signalling molecule, it is unsurprising that a carefully balanced system of

antioxidant enzymes is required to maintain redox homeostasis within the cell. These enzymes are often upregulated in tumour cells to protect themselves against cell damage induced by ROS (Lennicke et al., 2015). A characteristic feature of tumour cells is enhanced metabolic activity and high levels of ROS. The main antioxidant enzymes which eliminate H_2O_2 are catalase, glutathione peroxidase, and the peroxiredoxins (Doskey et al., 2016; Giandomenico, Cerniglia, Biaglow, Stevens, & Koch, 1997).

An important question is how the biological response to H_2O_2 in any given cell is determined. At supraphysiological concentrations (>100 nM), H_2O_2 causes nuclear single and double strand DNA breaks, although the former predominates and are rapidly repaired (Prise, Davies, & Michael, 1989). Depending on the dose, H_2O_2 can trigger DNA damage response (DDR) pathways that may promote DNA repair, cell-cycle arrest, or apoptosis (Vilema-Enriquez, Arroyo, Grijalva, Amador-Zafra, & Camacho, 2016).

Detrimental effects of H_2O_2 also arise by interaction with transition metal ions (e.g. Fe^{2+}) in the Fenton reaction (Prise et al., 1989). This results in cytosolic conversion of H_2O_2 to the highly reactive hydroxyl radical ($^{\bullet}OH$), and the production of labile Fe^{3+} ions which permeabilise and depolarise the mitochondrial membrane causing apoptosis (Halliwell, 2000; Wardman & Candeias, 1996). Figure 1.2 illustrates the differential effects of H_2O_2 within the cell, which are concentration dependent.

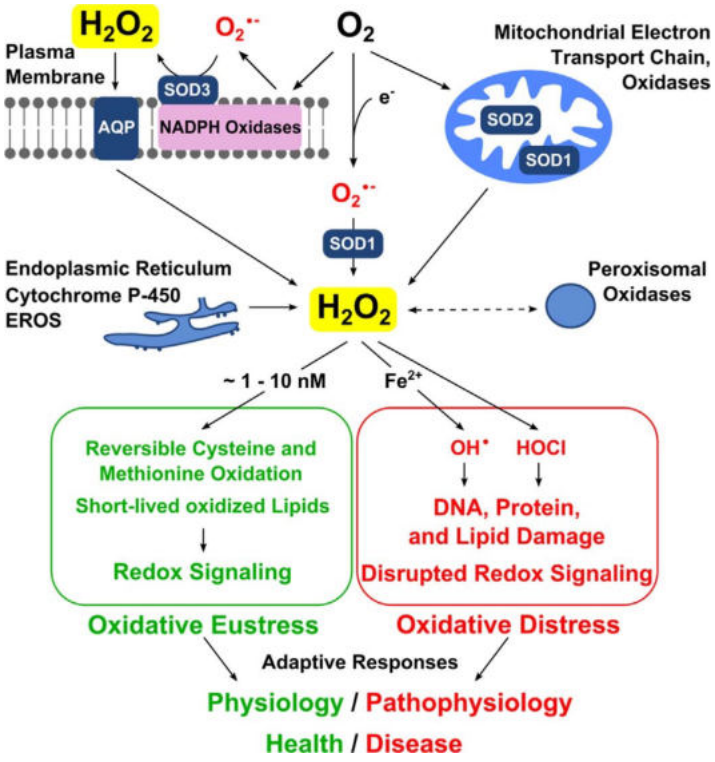

Figure 1.2. Hydrogen peroxide in oxidative stress. Bottom left (green) shows physiological redox signalling (oxidative eustress), in contrast to deranged signalling and oxidative stress (red) characterised by damage to biomolecules. (Image reproduced from H. Sies, 2017)

In a study on fibroblasts and the CAL-27 cell line, 3 different patterns of cell death were observed following exposure to H_2O_2. Concentrations up to 10 mM caused rapid cell death (60-90 minutes) without detectable evidence of apoptosis, moderate concentrations (1-10 mM) led to DNA cleavage and morphological features of apoptosis, and the lowest concentrations (0.1 mM-0.5 mM) resulted in delayed cytotoxicity at 24-28 hours, but without measurable evidence of apoptosis (Gardner et al., 1997). Prise et al demonstrated significant levels of DNA double strand breaks with induced cell death, when Chinese hamster V79 cells were exposed to H_2O_2 concentrations greater than 0.001 mM (Prise et al., 1989).

Figure 1.3 below illustrates the diversity of cellular outcomes with variation in H_2O_2 concentration below 1 mM concentration.

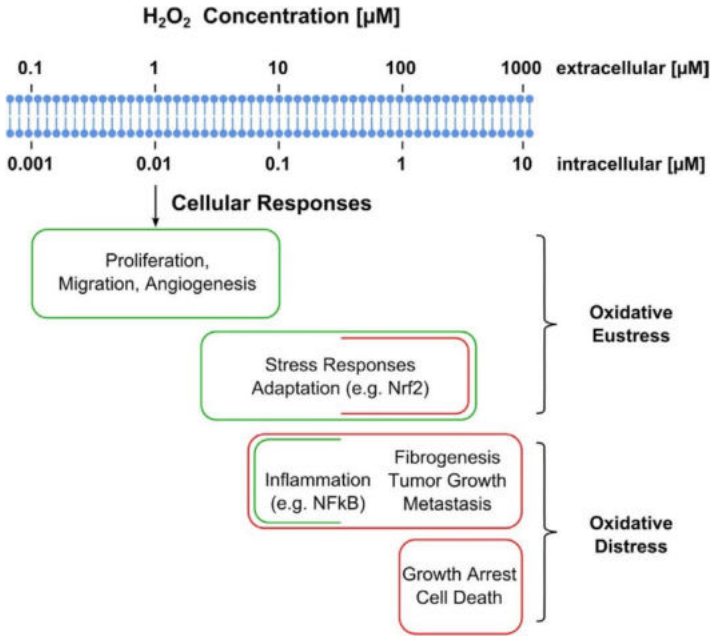

Figure 1.3 Variation in cellular responses according to extracellular vs. intracellular H_2O_2 concentrations, with the physiological effects (green) occurring up to 100 nM with deleterious outcomes (red) at higher concentrations. (Image reproduced from H.Sies, 2017)

At high H_2O_2 concentrations (5-10 mM) cell necrosis occurs, while lower concentrations (<1 mM) induce apoptosis. This suggests that the extent of oxidative insult influences which pathway is operative (Gardner et al., 1997). It is well-recognised that high (>50 µM) concentrations have a cytotoxic effect in a range of cells in culture, although the duration and mode of cell death varies by cell type, H_2O_2 concentration, and length of exposure (Halliwell, 2000). The concentration of H_2O_2 required to cause apoptosis of mammalian cells can vary by up to 20-fold (Veal et al., 2007).

1.2.4 Hydrogen Peroxide in combination with radiation (preclinical studies)

An application of H_2O_2 to radiosensitisation identified by Ogawa et al (Kochi University, Japan) arose from studying a highly radioresistant human osteosarcoma cell line (Hs-Os-1). Following a single 30 Gy IR dose, only minimal oxidative DNA damage (8-OxoG) or cell killing was detectable (by fluorescence of ROS-sensitive dichlorodihydrofluorescein diacetate (H_2DCFA) (Ogawa, Takahashi, Kobayashi et al., 2003). It was postulated that high levels of

intracellular antioxidants were responsible for this radioresistant phenotype, also seen in human chondrocytes (Ogawa, Takahashi, Kobayashi, et al., 2003).

It was discovered that the radioresistance of Hs-Os-1 cells and of normal chondrocytes was overcome by adding 0.1 mM H_2O_2 to the culture medium 4 hours before IR (Ogawa, Takahashi, Kobayashi, et al., 2003). This finding was reproduced in the prostate cancer cell line, PC-3, where apoptosis was observed in 4.9% cells 48 hours after 10 Gy alone, 1.9% after 0.1 mM H_2O_2 alone and 28.4% cells after exposure to both agents (Kariya et al., 2009). Interestingly, the high sensitivity of PC-3 cells and of normal chondrocytes to IR + H_2O_2 was completely abrogated by ammonium chloride (NH_4Cl) in the culture medium, a compound known to increase lysosomal pH and to inactivate lysosomal hydrolases (Kariya et al., 2009).

H_2O_2 + IR also demonstrated enhanced cytotoxicity (by lysosomal apoptosis) in the melanoma cell line MeWo (HTB-65). The effect of 0.05 mM H_2O_2 administered 24 hours prior to IR was investigated in a clonogenic assay. In comparison to the control group, there was decreased colony formation in MeWo cells treated with H_2O_2 alone, and further inhibition of colony growth following H_2O_2 + IR in combination (Y. J. Fang et al., 2013).

Two *in vivo* studies have demonstrated superior tumour growth inhibition (including near complete responses) in murine tumours treated with an intratumoural gel mixture comprising H_2O_2 and sodium hyaluronate, and single dose IR (Akima et al., 2016a, 2016b; Takaoka et al., 2017). This is further discussed in Chapter 4.

1.2.5 Clinical experience: H_2O_2 and radiotherapy

Ogawa et al developed a treatment using H_2O_2 (Oxydol)- soaked gauze applied to superficial tumours in patients with melanoma, malignant fibrous histiocytoma (MFH) and breast cancer, during a course of radiotherapy. This was referred to as Kochi Oxydol-Radiation Therapy for Unresectable Carcinomas (KORTUC I). 2/5 patients in this cohort exhibited a clinical complete response at 3 months post-treatment, and 3/5 achieved a partial response of greater than 50% reduction in

tumour volume compared to baseline. Treatment was well tolerated with the main toxicity being Grade 1 radiation induced dermatitis (Ogawa et al., 2008).

It was hypothesised that when tumours are irradiated in presence of H_2O_2, there is inactivation of peroxidase and catalase, and the oxygen molecules produced as a product of H_2O_2 breakdown facilitate oxidative damage and increased radiosensitivity (Ogawa et al., 2008). A slow-release formulation comprising 0.5% H_2O_2 in 1% sodium hyaluronate gel (KORTUC II), was developed for clinical use in Japan. Sodium hyaluronate was incorporated to increase viscosity and slow the degradation of H_2O_2. It also served to improve tolerability, as H_2O_2 can be irritant upon injection (Ogawa et al., 2009). Intratumoural injection of 2.5-5.0 ml of KORTUC under ultrasound (US) guidance can be completed in minutes, and is guided by the immediate release of oxygen microbubbles lasting for up to 48 hours (Tokuhiro et al., 2010).

Ogawa initially reported on 17 patients with locally advanced breast cancer (stage IIIB-IVA) given KORTUC injections twice-weekly during weeks 2-4 of radiotherapy (RT) (49.5 Gy/18#). Treatment was well tolerated, and imaging (US and contrast enhanced MRI) confirmed complete response (CR) in all primary breast tumours (17/17) at a median follow up period of 13 months (Miyatake et al., 2010). A subsequent non-randomised cohort study in 72 patients with breast cancer reported 68/70 (97%) alive with no evidence of local disease at 51 months mean follow up (Ogawa et al., 2015). A contemporary cohort study of 108 Japanese patients with earlier stage (I-IIIA) breast cancer reported that comparable systemic therapies plus RT alone achieved a 36% (39/108) CR rate (Mukai et al., 2013). KORTUC has since been used to treat small numbers of patients with other tumour types, including melanoma, squamous cell skin cancer, and sarcoma, with high response rates (Ogawa et al., 2011). More recent developments include a slower-release formulation of KORTUC requiring once-weekly administration (Morita-Tokuhiro et al., 2016).

1.2.6 UK KORTUC Phase 1 trial

In January 2017, a Phase 1 trial was initiated (at the Royal Marsden Hospital), testing intratumoural KORTUC with breast radiotherapy (RT) in patients with locally advanced/metastatic breast cancer who required RT for local disease control. Recruitment of 12 patients was completed in June 2018, with the demonstration that treatment is safe and well tolerated. Follow-up data show that 11/12 patients had a maintained partial or complete response at a median follow up of 12 months (Nimalasena et al., 2020). A multi-centre Phase II study testing the efficacy of KORTUC+RT vs. RT alone commenced in 2020 and is currently recruiting patients.

1.3 Aims and Hypotheses of laboratory research

The rationale for laboratory research related to the KORTUC trial, was to gain insight into mechanisms of therapeutic relevance. The 3 main hypotheses were:

1. *Under normoxic conditions, nanomolar-millimolar concentrations of H_2O_2 sensitise cells to the cytotoxic effects of IR.*

2. *Under radiobiological hypoxia, H_2O_2 leads to tumour reoxygenation, which contributes to enhanced cell killing by IR.*

3. *Intratumoural H_2O_2 in combination with radiotherapy is a safe and tolerable treatment in patients with locally advanced/recurrent breast cancer.*

It was important to understand the effects of H_2O_2 in isolation prior to investigating the effects of the combination with IR. If the *in vitro* evidence pertaining to the effects of H_2O_2 and IR were suggestive of an additive effect of the two agents, the order in which the treatments are delivered may not be crucial. However, if a true synergistic, or greater-than-additive process were demonstrated, this would indicate that the presence of intratumoural H_2O_2 at the time of IR is imperative. Understanding the interaction between H_2O_2 and IR, both at the “cellular” and “tissue” levels, would allow identification of factors relevant to treatment scheduling (i.e., timing of H_2O_2 injections relative to RT), dosing and normal tissue

toxicity. Also relevant is the potential application of KORTUC-based treatment to tumour histologies other than breast cancer. This has been explored by colleagues in Japan with promising results to date; hence this treatment may have wider reaching applications if efficacy is demonstrated in the ongoing Phase II trial.

References

Akima, R., Ogawa, Y., Morita-Tokuhiro, S., Tsuzuki, A., Yaogawa, S., Kariya, S., Hamada, N., Nishioka, A., Masunaga, S., & Ono, K. (2016a). Experimental Study of a New Enzyme-Targeting Radiosensitizer (KORTUC) Containing Hydrogen Peroxide & Sodium Hyaluronate for Intra-Tumoral Injection Using Mice Transplatned with SCCVII Tumor. *Cancers (MDPI), 8*. doi:10.3390/

Akima, R., Ogawa, Y., Morita-Tokuhiro, S., Tsuzuki, A., Yaogawa, S., Kariya, S., Hamada, N., Nishioka, A., Masunaga, S., & Ono, K. (2016b). New enzyme-targeting radiosensitizer (KORTUC) containing hydrogen peroxide & sodium hyaluronate for intra-tumoral injection using mice transplanted with SCCVII tumor. *Int J Cancer Clin Res, 3*(2), 1-6.

Baskar, R., Lee, K. A., Yeo, R., & Yeoh, K. W. (2012). Cancer and radiation therapy: current advances and future directions. *Int J Med Sci, 9*(3), 193-199. doi:10.7150/ijms.3635

Busk, M., Horsman, M. R., Overgaard, J., & Jakobsen, S. (2020). In vitro hypoxia responsiveness of [(18)F] FDG and [(18)F] FAZA retention: influence of shaking versus stagnant conditions, glass versus polystyrene substrata and cell number down-scaling. *EJNMMI Radiopharm Chem, 5*(1), 14. doi:10.1186/s41181-020-00099-5

Citrin, D. E., & Mitchell, J. B. (2014). Altering the response to radiation: sensitizers and protectors. *Semin Oncol, 41*(6), 848-859. doi:10.1053/j.seminoncol.2014.09.013

Di Meo, S., Reed, T. T., Venditti, P., & Victor, V. M. (2016). Role of ROS and RNS Sources in Physiological and Pathological Conditions. *Oxid Med Cell Longev, 2016*, 1245049. doi:10.1155/2016/1245049

Falls, K. C., Sharma, R. A., Lawrence, Y. R., Amos, R. A., Advani, S. J., Ahmed, M. M., Vikram, B., Coleman, C. N., & Prasanna, P. G. (2018). Radiation-Drug Combinations to Improve Clinical Outcomes and Reduce Normal Tissue Toxicities: Current Challenges and New Approaches: Report of the Symposium Held at the 63rd Annual Meeting of the Radiation Research Society, 15-18 October 2017; Cancun, Mexico. *Radiat Res, 190*(4), 350-360. doi:10.1667/RR15121.1

Fang, Y., Moore, B. J., Bai, Q., Cook, K. M., Herrick, E. J., & Nicholl, M. B. (2013). Hydrogen peroxide enhances radiation-induced apoptosis and inhibition of melanoma cell proliferation. *Anticancer Res, 33*(5), 1799-1807.

Gardner, A. M., Xu, F. H., Fady, C., Jacoby, F. J., Duffey, D. C., Tu, Y. P., & Lichtenstein, A. (1997). Apoptotic vs nonapoptotic cytotoxicity induced by hydrogen peroxide. *Free Radical Biology and Medicine, 22*(1-2), 73-83. doi:Doi 10.1016/S0891-5849(96)00235-3

Giandomenico, A. R., Cerniglia, G. E., Biaglow, J. E., Stevens, C. W., & Koch, C. J. (1997). The importance of sodium pyruvate in assessing damage produced by hydrogen peroxide. *Free Radical Biology and Medicine, 23*(3), 426-434. doi:Doi 10.1016/S0891-5849(97)00113-5

Hall, E. J. (1978). Radiobiology for the radiologist. 2nd Edition. Publisher: Medical Department, Harper & Row. ISBN: 0061410748, 9780061410741.

Hall, E. J., & Giaccia, A. J. (2006). *Radiobiology for the radiologist* (6th ed.). Philadelphia: Lippincott Williams & Wilkins.

Halliwell, B., Clement, M. V., & Long, L. H. (2000). Hydrogen peroxide in the human body. *FEBS Lett, 486*(1), 10-13. doi:Doi 10.1016/S0014-5793(00)02197-9

Higgins, G. S., O'Cathail, S. M., Muschel, R. J., & McKenna, W. G. (2015). Drug radiotherapy combinations: Review of previous failures and reasons for future optimism. *Cancer Treatment Reviews, 41*(2), 105-113. doi:10.1016/j.ctrv.2014.12.012

Hope-Stone, H. F. (1986). Radiotherapy in clinical practice. Publisher: Butterworth-Heinemann Ltd (January 1, 1986). ISBN-10: 0407003207. ISBN-13: 978-0407003200.

Kariya, S., Sawada, K., Kobayashi, T., Karashima, T., Shuin, T., Nishioka, A., & Ogawa, Y. (2009). Combination treatment of hydrogen peroxide and X-rays induces apoptosis in human prostate cancer PC-3 cells. *Int J Radiat Oncol Biol Phys, 75*(2), 449-454. doi:10.1016/j.ijrobp.2009.04.092

Kim, W., Lee, S., Seo, D., Kim, D., Kim, K., Kim, E., Kang, J., Seong, K. M., Youn, H., & Youn, B. (2019). Cellular Stress Responses in Radiotherapy. *Cells, 8*(9). doi:10.3390/cells8091105

Lennicke, C., Rahn, J., Lichtenfels, R., Wessjohann, L. A., & Seliger, B. (2015). Hydrogen peroxide - production, fate and role in redox signaling of tumor cells. *Cell Commun Signal, 13*, 39. doi:10.1186/s12964-015-0118-6

Lutz, S. T., Jones, J., & Chow, E. (2014). Role of radiation therapy in palliative care of the patient with cancer. *J Clin Oncol, 32*(26), 2913-2919. doi:10.1200/JCO.2014.55.1143

Lv, H., Yan, M., Zhang, M., Niu, L., Zeng, H., & Cui, S. (2014). Efficacy of capecitabine-based combination therapy and single-agent capecitabine maintenance therapy in patients with metastatic breast cancer. *Chin J Cancer Res, 26*(6), 692-697. doi:10.3978/j.issn.1000-9604.2014.12.13

Miyatake, K., Kubota, K., Ogawa, Y., Hamada, N., Murata, Y., & Nishioka, A. (2010). Non-surgical care for locally advanced breast cancer: radiologically assessed therapeutic outcome of a new enzyme-targeting radiosensitization treatment, Kochi Oxydol-Radiation Therapy for Unresectable Carcinomas, Type II (KORTUC II) with systemic chemotherapy. *Oncol Rep, 24*(5), 1161-1168.

Moding, E. J., Kastan, M. B., & Kirsch, D. G. (2013). Strategies for optimizing the response of cancer and normal tissues to radiation. *Nature Reviews Drug Discovery, 12*(7), 526-542. doi:10.1038/nrd4003

Morgan, M. A., & Lawrence, T. S. (2015). Molecular Pathways: Overcoming Radiation Resistance by Targeting DNA Damage Response Pathways. *Clinical Cancer Research, 21*(13), 2898-2904. doi:10.1158/1078-0432.Ccr-13-3229

Morita-Tokuhiro, S., Ogawa, Y., Yokota, N., Tsuzuki, A., Oda, H., Ishida, N., Aoyama, N., & Nishioka, A. (2016). Development of a Novel Enzyme-Targeting Radiosensitizer (New KORTUC) Using a Gelatin-Based Hydrogel Instead of a Sodium Hyaluronate. *Cancers (Basel), 8*(1). doi:10.3390/cancers8010010

Mukai, H., Watanabe, T., Mitsumori, M., Tsuda, H., Nakamura, S., Masuda, N., Yamamoto, N., Shibata, T., Sato, A., Iwata, H., & Aogi, K. (2013). Final results of a safety and efficacy trial of preoperative sequential chemoradiation therapy for the nonsurgical treatment of early breast cancer: Japan Clinical Oncology Group Study JCOG0306. *Oncology, 85*(6), 336-341. doi:10.1159/000355196

Nimalasena, S., Gothard, L., Anbalagan, S., Allen, S., Sinnett, V., Mohammed, K., Kothari, G., Musallam, A., Lucy, C., Yu, S., Nayamundanda, G., Kirby, A., Ross, G., Sawyer, E., Castell, F., Cleator, S., Locke, I., Tait, D., Westbury, C., Wolstenholme, V., Box, C., Robinson, S. P., Yarnold, J., & Somaiah, N. (2020). Intratumoral Hydrogen Peroxide With Radiation Therapy in Locally Advanced Breast Cancer: Results From a Phase 1 Clinical Trial. *Int J Radiat Oncol Biol Phys*. doi:10.1016/j.ijrobp.2020.06.022

O'Neill, P., & Wardman, P. (2009). Radiation chemistry comes before radiation biology. *Int J Radiat Biol, 85*(1), 9-25. doi:10.1080/09553000802640401

Oehler, C., Dickinson, D. J., Broggini-Tenzer, A., Hofstetter, B., Hollenstein, A., Riesterer, O., Vuong, V., & Pruschy, M. (2007). Current concepts for the combined treatment modality of ionizing radiation with anticancer agents. *Curr Pharm Des, 13*(5), 519-535. doi:10.2174/138161207780162935

Ogawa, Y., Kubota, K., Aoyama, N., Yamanishi, T., Kariya, S., Hamada, N., Nogami, M., Nishioka, A., Onogawa, M., & Miyamura, M. (2015). Non-Surgical Breast-Conserving Treatment (KORTUC-BCT) Using a New Radiosensitization Method (KORTUC II) for Patients with Stage I or II Breast Cancer. *Cancers (Basel), 7*(4), 2277-2289. doi:10.3390/cancers7040891

Ogawa, Y., Kubota, K., Ue, H., Kataoka, Y., Tadokoro, M., Miyatake, K., Tsuzuki, K., Yamanishi, T., Itoh, S., Hitomi, J., Hamada, N., Kariya, S., Fukumoto, M., Nishioka, A., & Inomata, T. (2009). Phase I study of a new radiosensitizer containing hydrogen peroxide and sodium hyaluronate for topical tumor injection: a new enzyme-targeting radiosensitization treatment, Kochi Oxydol-Radiation Therapy for Unresectable Carcinomas, Type II (KORTUC II). *Int J Oncol, 34*(3), 609-618.

Ogawa, Y., Kubota, K., Ue, H., Tadokoro, M., Matsui, R., Yamanishi, T., Hamada, N., Kariya, S., Nishioka, A., Nakajima, H., Tarutani, M., & Sano, S. (2011). Safety and effectiveness of a new enzyme-targeting radiosensitization treatment (KORTUC II) for intratumoral injection for low-LET radioresistant tumors. *Int J Oncol, 39*(3), 553-560. doi:10.3892/ijo.2011.1069

Ogawa, Y., Takahashi, T., Kobayashi, T., Kariya, S., Nishioka, A., Mizobuchi, H., Noguchi, M., Hamasato, S., Tani, T., Seguchi, H., Yoshida, S., & Sonobe, H. (2003). Mechanism of hydrogen peroxide-induced apoptosis of the human osteosarcoma cell line HS-Os-1. *Int J Mol Med, 12*(4), 459-463.

Ogawa, Y., Takahashi, T., Kobayashi, T., Kariya, S., Nishioka, A., Ohnishi, T., Saibara, T., Hamasato, S., Tani, T., Seguchi, H., Yoshida, S., & Sonobe, H. (2003). Apoptotic-resistance of the human osteosarcoma cell line HS-Os-1 to irradiation is converted to apoptotic-susceptibility by hydrogen peroxide: a potent role of hydrogen peroxide as a new radiosensitizer. *Int J Mol Med, 12*(6), 845-850.

Ogawa, Y., Takahashi, T., Kobayashi, T., Toda, M., Nishioka, A., Kariya, S., Seguchi, H., Yamamoto, H., & Yoshida, S. (2003). Comparison of

radiation-induced reactive oxygen species formation in adult articular chondrocytes and that in human peripheral T cells: possible implication in radiosensitivity. *Int J Mol Med, 11*(4), 455-459.

Ogawa, Y., Ue, H., Tsuzuki, K., Tadokoro, M., Miyatake, K., Sasaki, T., Yokota, N., Hamada, N., Kariya, S., Hitomi, J., Nishioka, A., Nakajima, K., Ikeda, M., Sano, S., & Inomata, T. (2008). New radiosensitization treatment (KORTUC I) using hydrogen peroxide solution-soaked gauze bolus for unresectable and superficially exposed neoplasms. *Oncol Rep, 19*(6), 1389-1394.

Prise, K. M., Davies, S., & Michael, B. D. (1989). Cell killing and DNA damage in Chinese hamster V79 cells treated with hydrogen peroxide. *Int J Radiat Biol, 55*(4), 583-592. doi:10.1080/09553008914550631

Prise, K. M., & O'Sullivan, J. M. (2009). Radiation-induced bystander signalling in cancer therapy. *Nature Reviews Cancer, 9*(5), 351-360. doi:10.1038/nrc2603

Sharma, R. A., Plummer, R., Stock, J. K., Greenhalgh, T. A., Ataman, O., Kelly, S., Clay, R., Adams, R. A., Baird, R. D., Billingham, L., Brown, S. R., Buckland, S., Bulbeck, H., Chalmers, A. J., Clack, G., Cranston, A. N., Damstrup, L., Ferraldeschi, R., Forster, M. D., Golec, J., Hagan, R. M., Hall, E., Hanauske, A. R., Harrington, K. J., Haswell, T., Hawkins, M. A., Illidge, T., Jones, H., Kennedy, A. S., McDonald, F., Melcher, T., O'Connor, J. P., Pollard, J. R., Saunders, M. P., Sebag-Montefiore, D., Smitt, M., Staffurth, J., Stratford, I. J., Wedge, S. R., & Group, N. C. A.-P. J. W. (2016). Clinical development of new drug-radiotherapy combinations. *Nat Rev Clin Oncol, 13*(10), 627-642. doi:10.1038/nrclinonc.2016.79

Sies, H. (2017). Hydrogen peroxide as a central redox signaling molecule in physiological oxidative stress: Oxidative eustress. *Redox Biology, 11*, 613-619. doi:10.1016/j.redox.2016.12.035

Steel, G. G., McMillan, T. J., & Peacock, J. H. (1989). The 5Rs of radiobiology. *Int J Radiat Biol, 56*(6), 1045-1048. doi:10.1080/09553008914552491

Steel, G. G., Hill, R. P., & Peckham, M. J. (1978). Combined radiotherapy--chemotherapy of Lewis lung carcinoma. *Int J Radiat Oncol Biol Phys, 4*(1-2), 49-52. doi:10.1016/0360-3016(78)90114-1

Takaoka, T., Shibamoto, Y., Matsuo, M., Sugie, C., Murai, T., Ogawa, Y., Miyakawa, A., Manabe, Y., Kondo, T., Nakajima, K., Okazaki, D., & Tsuchiya, T. (2017). Biological effects of hydrogen peroxide administered intratumorally with or without irradiation in murine tumors. *Cancer Sci, 108*(9), 1787-1792. doi:10.1111/cas.13302

Tokuhiro, S., Ogawa, Y., Tsuzuki, K., Akima, R., Ue, H., Kariya, S., & Nishioka, A. (2010). Development of a novel enzyme-targeting radiosensitizer (KORTUC) containing hydrogen peroxide for intratumoral injection for patients with low linear energy transfer-radioresistant neoplasms. *Oncol Lett, 1*(6), 1025-1028. doi:10.3892/ol.2010.184

Veal, E. A., Day, A. M., & Morgan, B. A. (2007). Hydrogen peroxide sensing and signaling. *Mol Cell, 26*(1), 1-14. doi:10.1016/j.molcel.2007.03.016

Vilema-Enriquez, G., Arroyo, A., Grijalva, M., Amador-Zafra, R. I., & Camacho, J. (2016). Molecular and Cellular Effects of Hydrogen Peroxide on Human Lung Cancer Cells: Potential Therapeutic Implications. *Oxid Med Cell Longev, 2016*, 1908164. doi:10.1155/2016/1908164

Wang, H., Mu, X., He, H., & Zhang, X. D. (2018). Cancer Radiosensitizers. *Trends Pharmacol Sci, 39*(1), 24-48. doi:10.1016/j.tips.2017.11.003

Wardman, P., & Candeias, L. P. (1996). Fenton chemistry: an introduction. *Radiat Res, 145*(5), 523-531.

Chapter 2
Materials and Methods

2 Introduction

The rationale for laboratory research was to gain understanding of mechanisms relevant to the clinical setting. The aim was to understand how H_2O_2 and IR interact, thereby helping to identify factors relevant to treatment scheduling (e.g., timing of H_2O_2 relative to RT), dosing and normal tissue toxicity. Also of interest was potential application to tumour types other than breast cancer, where radiation has a role in management and where improved response to treatment may have implications for clinical practice.

2.1 In vitro experiments

2.1.1 Cell lines

Cell lines were obtained from ATCC (HCT116) or in-house stocks (PC-3 and LICR-LON-HN5). For *in vitro* and *in vivo* experiments, those known to be relatively radioresistant were selected, as the addition of H_2O_2 to RT was expected to lead to increased cytotoxicity compared to RT alone. PC-3 was selected as it had been used in previous publications using H_2O_2 and RT. The features of these cell lines are summarised in Table 2.1 below.

	PC-3	**LICR-LON-HN5**	**HCT116**
Cell origin	prostate adenocarcinoma	squamous cell carcinoma tongue	colorectal adenocarcinoma
Doubling time	24h	34h	21h
Culture media	RPMI	DMEM	DMEM
Use in clonogenic assays	yes*	yes	yes
Spheroid formation	with matrigel	yes	yes
Xenografts	yes	yes	yes
P53	mutant	mutant	wild type
Other	androgen insensitive	EGFR gene amplified	TGFβ1 and 2 +ve BRAF wild type

Table 2.1. Summary of cell line characteristics
Features of PC-3, HN5, and HCT116 cell lines relevant to *in vitro* and *in vivo* experiments. *PC-3 forms colonies but demonstrates sensitivity to endotoxin concentration in serum which can affect use in colony survival assays. RPMI- Roswell Park Memorial Institute, DMEM- Dulbecco's Modified Eagle's Medium

2.1.2 Cell Culture

Cells were grown in 75 cm^3 flasks (Corning) and when 70-80% confluent were passaged by rinsing with 10 ml sterile PBS followed by dissociation with TrypLE™ Express (ThermoFisher scientific,12605010). Trypsinised cells were resuspended with culture media as indicated in the table above and supplemented with 10% foetal bovine serum (Pan-Biotech, P04-96650). Flasks were incubated at 37°C in humidified air containing 5% CO_2.

2.1.3 Cryopreservation and Thawing

Once obtained, each cell line was cryopreserved to maintain an ongoing stock. Exponentially growing cells that had reached 70%-80% were trypsinised and resuspended in medium, then centrifuged at 300 xg for 5 minutes. The resultant cell pellet was resuspended in freezing mixture comprising 10% DMSO (Sigma-Aldrich, D8418) and 90% complete medium, and transferred in 1 ml (at an approximate concentration of 1-2 x 10^6 cells/ml) aliquots to cryovials (Thermo Scientific. Nunc, 363401) and transferred to a -80°C freezer, and the following day transferred to liquid nitrogen.

2.1.4 STR profiling and Mycoplasma testing

DNA was extracted from cells growing in culture (DNeasy blood and tissue kit, Quiagen, 69504) and used for cell line authentication and mycoplasma testing. Cell lines were authenticated by short tandem repeat (STR) profiling using a GenePrint 10 kit (Promega, Southampton, UK) followed by analysis on a 3730xl DNA analyser (Applied Biosystems, Warrington, UK) to confirm identity. Mycoplasma infection was excluded using PCR analysis (performed by Surrey Diagnostics Ltd, Guildford, UK).

2.1.5 2D GI_{50} and 3D GI_{50}

The initial aim was to determine the effect of H_2O_2 alone on tumour cell viability in both 2D and 3D *in vitro* systems. These results were used to inform further calculations of the H_2O_2 concentration(s) to use in combination with IR in colony survival and spheroid growth kinetic assays.

2.1.6 2D GI_{50} (SRB) method

On Day 1 2-3000* cells/100 μl medium (*dependent on cell line) were seeded into the inner 60 wells of a flat-bottomed 96-well plate. 200 μl PBS was added to the outer wells to limit evaporation from the inner wells. On day 2, serial dilutions of H_2O_2 (Sigma-Aldrich, H1009) in medium were prepared and 100 μl/well added at twice the intended final concentration (range 0-8 mM). Control wells were treated with medium alone. Cells were incubated at 37°C, 5% CO_2 for 72 hours. Growth medium was discarded, and cells fixed by adding 100 μl/well 10% (v/v) TCA in water. Plates were incubated at room temperature for 30 minutes, then gently washed in tap water to remove the fixative and allowed to air dry. Cells were stained with 100 μl/well 0.4% (w/v) sulforhodamine B (Sigma Aldrich, 230162) in 1% (v/v) acetic acid, for 1 hour. Stain was washed off briefly in tap water and then three times in 1% acetic acid. Plates were dried and the stain eluted by adding 100μl/well 10 mM Tris pH 10. Absorbance at 564 nm was read on a FLUOstar Omega plate reader (BMG Labtech).

2.1.7 2D GI_{50} (CTG®) method

Cells were seeded, and H_2O_2 added as described in the SRB assay method above. On day 5, 100 μl was removed from each well and 100 μl of CellTiter-Glo® (CTG; Promega, G9242) was added. 3 wells were selected as blanks and contained 100 μl normal medium and 100 μl CTG reagent. Plates were placed on a mechanical shaker (in the dark) for 20 minutes at room temperature, and the contents transferred to a black, flat-bottomed plate. Plates were read on a FLUOstar Optima luminescence plate reader.

2.1.8 Irradiation

For colony survival assays and 3D spheroid growth assays, IR was generated using an x-ray tube (HPZ-160-11, Varian medical systems) mounted in an x-ray cabinet (Xstrahl). The irradiating parameters were established at 160 kV (operating voltage) and 11.3 mA (operating current), using a broad filament and 1mm aluminium filter. Samples were positioned at an FSD (focus to skin distance) of 40 cm and irradiated at room temperature. They were placed within a region previously determined to receive homogenous dose (± 5%).

2.1.9 Clonogenic survival assay

Clonogenic assays represent the gold standard *in vitro* method for demonstrating loss of reproductive integrity following radiation-based treatment (Citrin & Mitchell, 2014; Franken, Rodermond, Stap, Haveman, & van Bree, 2006). This allows generation of a cell survival curve describing the relationship between the dose of IR+/-drug and the proportion of clonogenic surviving cells (Munshi, Hobbs, & Meyn, 2005). Prior to starting, the plating efficiency of each cell line was determined, and cells were seeded to yield at least 100 colonies per well of a 6-well plate for control, non-irradiated cells. For the purposes of this assay, a colony was defined as such if it comprised at least 50 cells.

2.1.10 Clonogenic assay: Method

Cells were grown in 80 cm^3 flasks in their respective media. Once in the exponential phase of growth (70-80% confluence), cells were trypsinised to form a single cell suspension. Cells were counted manually using a haemocytometer to determine the number of cells per ml, and serial dilutions were performed according to prior calculations of seeding density. Triplicate wells were used for each seeding density and treatment. The corresponding number of cells (in 2 ml medium) were added to each well in 6-well plates. Plates were transferred to an incubator for 4-6 hours, to allow for cells to adhere (confirmed by microscopic examination).

For radiation treatments, a further 2 ml growth medium was added to each well of the plates receiving IR alone. Cells were then irradiated, as described above, and returned to the incubator. For H_2O_2 treatment, a further 2 ml medium containing H_2O_2 at double the final concentration was added to each well. For combination treatments, H_2O_2 was added 30 minutes prior to IR. On day 10-14, plates were viewed using a standard inverted light microscope, to confirm sufficiently large colonies had formed in the control plate. Colonies were fixed with 1.5 ml ice-cold methanol (stored at -20°C) per well and incubated for 20 minutes at 4°C. Methanol was removed to a separate waste pot, and 1 ml/well 0.5% gentian violet (Sigma-Aldrich, 49144) was added to stain the colonies prior to counting. Plates were incubated for 10 minutes at room temperature. Plates were rinsed 3 times with tap water and air-dried. Stained colonies were counted, and plating efficiency (PE) defined as: (number of colonies counted ÷ number of

cells plated) x 100. The surviving fraction (SF) was calculated using the formula: (PE of treated sample ÷ PE of control) x 100 (Munshi et al., 2005).

2.1.11 Clonogenic assay cell seeding numbers

The number of cells seeded (per well of a 6-well plate) for clonogenic assays comparing IR and H_2O_2 + IR is summarised in Table 2.2.

	Number of cells seeded	
IR Dose (Gy)	**HCT116**	**HN5**
0	500	125
2	1000	250
4	5000	500
6	10000	1250
8	20000	2500
10	40000	10000

Table 2.2. Seeding densities used for clonogenic assay with HCT116 and HN5 (number of cells per well of a 6-well plate)

2.2 3D spheroid growth assays

Spheroid growth is a more physiological model of tumour growth *in vivo* than the growth of standard 2D monolayer cultures. The main differences relate to the formation of nutrient and oxygen gradients, as well as cell-cell interactions, gene expression profiles and extracellular matrix deposition more in keeping with features of tumours *in vivo* (Vinci et al., 2012).

Cells growing in 2D in the exponential phase of growth were trypsinised and counted. 300 cells/200 μl medium was seeded into the inner 60 wells of a 96-well ULA plate (Corning, NY, USA) using a multichannel pipette. This was according to prior calculations for number of cells required to give rise to spheroid of 300-500 μm diameter 4 days post seeding. The shape of each well enables the formation of spheroids which are reproducible in size, and without requirement for coating (Vinci et al., 2012).

200 μl PBS was added to the outer wells. On day 4, spheroids were imaged using a Celigo™ automated imaging cytometer (Nexcelom Biosciences, Lawrence, Mass., USA) then treated with 0.6 mM H_2O_2, 3Gy single dose IR, or a combination. In the case of combined treatment H_2O_2 was added 30 minutes prior

to irradiation. Spheroids were imaged every 3 days to monitor growth (days 4-23), and medium refreshed by replacing 100 μl with normal medium.

2.2.1 Data processing

96-well plates were scanned (by selecting 1/16 field of view/well) to measure spheroid diameter by image auto segmentation. Data were transferred to a spreadsheet and spheroid radius calculated to determine volume using the formula: volume = $4/3\pi r^3$ (r= radius). Mean spheroid volume was calculated according to treatment group and at 3 days intervals and plotted to generate a growth curve.

2.2.2 3D GI_{50} method

300-2000 cells/100μl medium was seeded into the inner 60 wells of an ultralow attachment (ULA) 96-well plate (#7007, Corning), with sterile PBS added to the outer wells. On day 4, 100 μl H_2O_2 at double the intended final concentration was added to the corresponding wells (range 0-8 mM), and the plate returned to the incubator. On day 7, spheroid viability was measured as per **2D GI_{50} (CTG) method** above.

2.2.3 Spheroid staining

The ability of PI to enter a cell depends on loss of membrane integrity; therefore, it does not stain live or early apoptotic cells, both of which have an intact cell membrane. In cells undergoing late apoptosis and necrosis, PI is able to traverse the membranes and result in detectable fluorescence (Rieger, Nelson, Konowalchuk, & Barreda, 2011).

Cells were seeded as detailed in **section 2.2 Spheroid growth assays**. On day 4, spheroids were imaged using the Celigo cytometer prior to treatment, and autocontoured to measure diameter. They were treated according to the following groups: control, 0.6 mM H_2O_2 alone, 3 Gy alone, 0.6 mM H_2O_2 + 3 Gy IR. Irradiation was delivered using the Xstrahl cell irradiator. Propidium Iodide (Sigma-Aldrich, P4170) was added to the inner 60 wells of the plate (to achieve a final concentration 1 μg/ml in each well). This concentration of PI was demonstrated by a colleague (Dr Sarah Brüningk) not to interfere with normal cell proliferation. Growth medium and PI were replenished every 3 days. The plate

was returned to the incubator and images acquired under fluorescence and brightfield settings at successive timepoints (days 1, 3, 5, 7, 9) post treatment.

2.2.4 3D spheroid viability (CellTiter-Glo®) method

This is as described in earlier section **3D GI_{50}: Method**. Spheroid viability was measured on Day 7, 11 and 23 in a cohort treated with 0.6 mM $H_2O_2 \pm$ 3Gy IR.

2.2.5 Statistical Analysis

Standard errors were calculated from the data generated. Unless specified, each data point represents the mean $\pm$ the standard error from three independent experiments performed in triplicate.

2.3 *In vivo* experiments

Prior to commencing work with laboratory animals, a personal licence (PIL) was obtained from the Home Office, following the requisite training and assessment. All experiments adhered to Home Office rules; taking into consideration the 3 R's of replacement, refinement and reduction, and animal welfare (Workman et al., 2010).

2.3.1 Identification of a xenograft model

HCT116 was selected for *in vivo* experiments, based partly on prior results obtained from 3D spheroids, and due to its ability to form tumours readily in nude mice.

For *in vivo* experiments Foxn1^{nu} nude mice were selected as a model. These animals have a homozygous mutation of the Foxn1 gene which renders them hairless and athymic. This makes them ideal hosts for rapidly growing human tumour cell lines, and for generation of subcutaneous tumours.

2.3.2 Preparation of cells for *in vivo* inoculation

Cells were cultured in 175 cm^2 flasks (Corning). Once in the exponential growth phase (70-80% confluent, cells were trypsinised and counted in a haemocytometer. The total number of cells required was calculated according to the number of animals to be inoculated (for HCT116 this required 3 x 10^6 cells

per mouse). The correct number of cells were placed in a centrifuge tube and spun for 5 minutes at 1500 rpm at 4˚C. The supernatant was discarded. The resulting cell pellet was resuspended in the exact volume of HBSS (Hank's balanced salt solution), adjusting this for the volume occupied by the cell pellet itself. Cells were placed in a 7 ml polypropylene bijou container, which was placed on ice to preserve cell viability. The required number of cells (in 100 μl HBSS) was injected subcutaneously into the right flank of each mouse using a 25-gauge needle. Aseptic technique was used, and inoculation was performed within a laminar flow hood.

2.3.3 Animal and tumour monitoring

Following inoculation, the weight and health status of the mice were monitored every 3 days, and tumour growth monitored by calliper measurement (3 orthogonal diameters: *d*1, *d*2, *d*3). Tumour volume was calculated using the formula: *volume* = $\pi/6$ *x d1 x d2 x d3*. Mice were treated once the tumour volume reached 400 mm^3 or approached the project licence limits (mean of length and width of 12 mm, or 15 mm longest diameter). If the animal displayed signs of overt suffering or adverse signs (e.g. hunched posture, reluctance to move, dehydration, weight loss ≥15% in 48 hours), they were sacrificed using the schedule 1 method of cervical dislocation.

2.3.4 Tumour preservation and sectioning

Following sacrifice of the animal, tumours were excised immediately and cryopreserved whole by being placed on liquid nitrogen, and then transferred into a -80°C freezer until ready for sectioning.

Sectioning was performed by Ruth Riisnaes, Senior Scientific Officer, ICR. Tumours were sectioned using a cryotome (set at -22°C) after being embedded in OCT (optimum cutting temperature) compound. Specimens were allowed time to equilibrate to the temperature of the cryostat prior to sectioning. 8-10 μm sections were obtained and placed onto polylysine coated slides (Superfrost, VWR, 631-0108). At least 5 good quality (minimal folds and tears) sequential sections were obtained from each tumour. Slides were stored in a -20°C freezer until required for staining.

2.4 Immunohistochemistry

Pimonidazole (Hypoxyprobe, HP2-200), EF5 (Sigma-Aldrich, SML1961) and CCI-103F (Hypoxyprobe, HP4-100) were used to quantify the temporal and spatial variation in hypoxia within xenograft tumours following treatment.

2.4.1 Dual marker hypoxia staining

Dual staining techniques were employed to determine whether a treatment or intervention resulted in a change in hypoxia in xenograft tumours. A baseline marker was administered to the mouse (via intraperitoneal injection) prior to the intervention, followed by a second marker prior to sacrifice and tumour retrieval. A mismatch between the observed staining patterns would be indicative of the change in hypoxia resulting from a given treatment. Table 2.3 summaries the specific concentrations and injected volumes for each marker.

Hypoxia marker	Concentration (intraperitoneal injection)	Volume (25g mouse)
Pimonidazole	20 mg/ml	0.08 ml
EF5	3 mg/ml	0.25 ml
CCI-103F	20 mg/ml	0.1 ml

Table 2.3. Summary of relative concentrations and volumes required for *in vivo* injection of hypoxia markers

2.4.2 Pimonidazole

Using an Immedge hydrophobic barrier pen (Fisher Scientific), a line was drawn around the tissue section (previously fixed by placing in acetone for 5 minutes). 100 μl blocking solution (2% bovine serum albumin (BSA) and 5% goat serum (Sigma-Aldrich G9023) in PBS) was added and incubated at room temperature for 1 hour, to prevent non-specific binding of antibodies to tissue. The slide was tapped to remove blocking solution, and 100 μl secondary antibody (0.5% FITC-conjugated mouse anti-pimonidazole antibody (Hypoxyprobe HP2-100kit) (1:50 dilution) made up in blocking solution) was added. Slides were incubated in the dark overnight at 4°C. Slides were washed for 3 x 5 minutes in 0.1% PBS-Tween (made by adding 500 μl Tween 20 to 500 ml PBS) and then imaged to detect fluorescence.

2.4.3 EF5

Sections were incubated with 100 μl blocking solution (10% non-fat dry milk solution in PBS, 5% goat serum, 2% BSA, 0.1% Tween20 PBS) and incubated overnight in the dark at 4°C. After tapping off the blocking solution, slides were rinsed in 0.1% Tween20 PBS. 100 μl anti-EF5 antibody (ELK3-51 Cyanine 3 conjugate (Sigma-Aldrich EF5011) made up to 75 μg/ml with EF5 antibody dilution buffer) was added to the section and incubated in the dark at 4°C for 6 hours. After tipping off the antibody solution, slides were washed for 3 x 45 minutes in Tween20 PBS prior to imaging.

2.4.4 CCI-103F

Sections were incubated with 100 μl blocking solution (2% BSA, 5% goat serum in PBS). After tapping to remove the block, sections were incubated with 100 μl rabbit anti-CCI-103F (anti-F6) antibody (1:100 dilution made by adding 10 μl of anti-CCI-103F to 1 ml of block) overnight at 4°C. Slides were washed with PBS Tween (3 x 5 minutes). 100 μl Alexa Fluor 594-conjugated secondary antibody (Abcam, ab150116) at 1:200 dilution (5 μl anti-rabbit antibody added to 1 ml blocking solution) was added to the section and incubated at room temperature in the dark for 90 minutes. Slides were washed with PBS Tween (3 x 5 minutes) and kept in the dark prior to imaging.

2.4.5 Hoechst 33342 staining

Hoechst 33342 (Sigma-Aldrich) is a fluorescent DNA/nuclear stain which is also used as a marker of tumour perfusion. It was administered intravenously (10mg/kg) via the tail vein to mice immediately prior to necropsy.

2.4.6 H&E staining

Slides were fixed by placing in ice-cold acetone for 5 minutes, then placed in Gills' haematoxylin (Sigma-Aldrich H9627) for 1 minute. Slides were then rinsed in running tap water for 4 minutes, then placed in 1% acid alcohol for 2 seconds. Sections were rinsed for a further 5 minutes in tap water and placed in eosin (Sigma-Aldrich 318906) for 30 seconds. Sections were dehydrated in 2 changes of 100% alcohol for 30 seconds. Alcohol was removed by immersing in 2 changes of xylene (under fume hood) for 30 seconds. A cover slip was placed over the section using DPX mountant (Sigma-Aldrich 44581) prior to imaging.

2.4.7 Microscopy

Imaging was performed using CellSens imaging software (Olympus Life Science) attached to an Olympus ProScan II microscope, at 4x magnification. H&E sections were imaged using brightfield settings. Hoechst (460-490 nm), pimonidazole (518 nm), EF5 (570 nm) and CCI-103F (617 nm) were imaged with fluorescence microscopy, with sections immersed in PBS to prevent drying. Composite fluorescence images were stitched from individually imaged microscopic sections.

2.5 Oxygen challenge experiment in HCT116 xenografts

Prior to investigating the effect of intratumoural H_2O_2 on tumour hypoxia, a preliminary experiment was performed to establish whether hypoxia in HCT116 tumours could be perturbed.

CCI-103F (80 mg/kg IP in 10% DMSO/90% peanut oil mixed thoroughly for 1 hour before (Hypoxyprobe-F6 HP4-100 kit)) was administered via the intraperitoneal (IP) route to record tumour hypoxia at baseline. 2 hours were allowed for full bioreduction of the compound. Following intraperitoneal anaesthesia (80 mg/kg ketamine and 10 mg/kg xylazine in combination), high flow oxygen (2 litres/min) was administered to each mouse via a nose cone. 15 minutes following the commencement of high oxygen breathing, pimonidazole (60 mg/kg in normal saline (Hypoxyprobe HP-100 mg)) was administered via the IP route. High oxygen breathing was continued for a further 45 minutes, to allow for bioreduction of pimonidazole within the tumour, prior to the mouse being sacrificed by cervical dislocation. Tumours were immediately excised and cryopreserved in liquid nitrogen.

2.5.1 Effect of intratumoural H_2O_2 injection on tumour hypoxia

Subcutaneous HCT116 tumours (right flank) were grown in 12 mice. They were randomly assigned to 2 groups: Group 1 (n=6): Control and Group 2 (n=6): Intratumoural KORTUC. KORTUC was made by mixing 0.4 ml 3% H_2O_2 (in sterile vials) in a syringe pre-loaded with 20 mg/2 ml sodium hyaluronate. This resulted in a 2.4 ml solution of 0.5% H_2O_2 ready for intratumoural injection. Treatment was delivered as outlined in the schedule in Table 2.4.

No. Mice	Treatment arm	Sequence						
3	Control	CCI-103F	2 hr	Intratumoural sodium hyaluronate	1 hr	Pimonidazole	45 mins	Necropsy
3	Control	CCI-103F	2 hr	No injection	1 hr	Pimonidazole	45 mins	Necropsy
6	KORTUC	CCI-103F	2 hr	Intratumoural KORTUC	1 hr	Pimonidazole	45 mins	Necropsy

Table 2.4. Sequence of hypoxia marker administration relative to intratumoural injection in control vs. KORTUC treatment groups *in vivo*

Intratumoural injections were performed under anaesthesia (intraperitoneal ketamine/zylazine) and under ultrasound imaging to ensure drug delivery within the tumour as shown in Fig 2.1. Ultrasound imaging was performed by Nigel Bush, Senior Scientific Officer, ICR. Lubricating gel was applied to the eyes of the animal once anesthetized, to prevent corneal drying and ulceration. The anaesthetized mouse was immobilized on a heated platform and positioned so that the flank tumour was visible and easily accessible for injection. The animal was secured in position. The needle and syringe containing the solution for IT injection was attached to a movable clamp, and the needle (bevel up) gradually advanced into the centre of the tumour. The plunger was depressed as soon as the needle was visualized in the centre of the tumour on US.

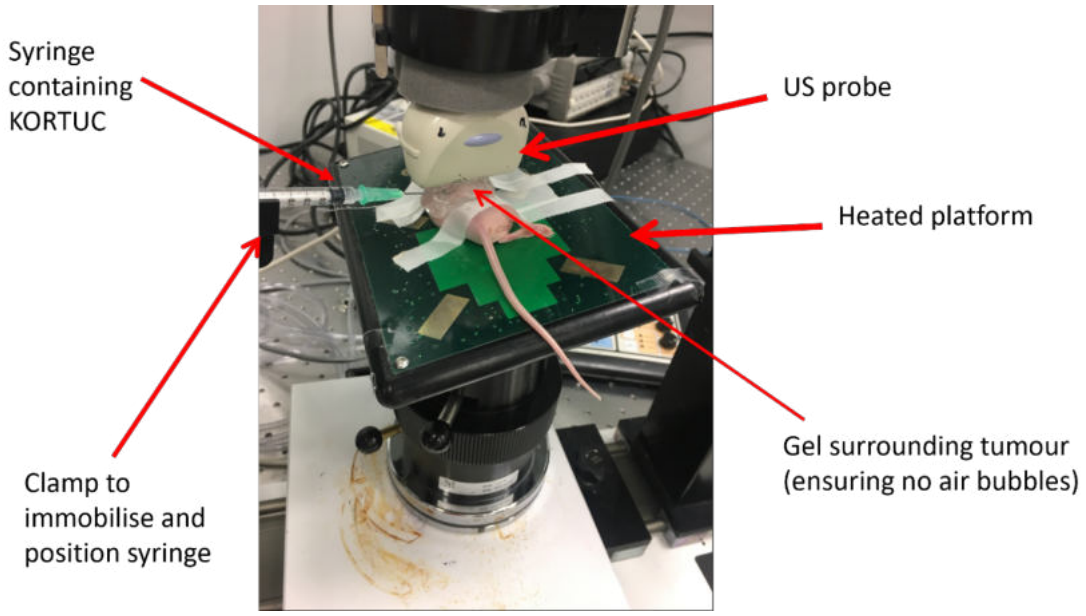

Figure 2.1 Practical set-up for intratumoural KORTUC injection in vivo with US imaging Anaesthetised mouse immobilised on a heated platform with US probe applied over flank tumour. KORTUC in syringe attached to moveable clamp, used to deliver intratumoural injection under US guidance.

When tumours had reached 400 mm^3 size, CCI-103F was injected intraperitoneally (80 mg/kg in 10% DMSO/ 90% peanut oil mixed thoroughly for 1 hour before), to obtain a record of tumour hypoxia at baseline. 2 hours were allowed for full bioreduction. Prior to intratumoural injection, mice were anaesthetised with intraperitoneal ketamine/xylazine mixture (0.1 ml per 10 g weight of mouse). Sodium hyaluronate/ KORTUC was injected intratumourally under ultrasound guidance. The dose of sodium hyaluronate/ KORTUC was 2 ml/kg (i.e. 0.05 ml for a 25 g mouse). 1 hour following IT KORTUC injection, pimonidazole (60 mg/kg) was administered via the intraperitoneal route. Mice were sacrificed 45 minutes after receiving pimonidazole, and the tumours excised and cryopreserved.

References

Citrin, D. E., & Mitchell, J. B. (2014). Altering the response to radiation: sensitizers and protectors. *Semin Oncol, 41*(6), 848-859. doi:10.1053/j.seminoncol.2014.09.013

Franken, N. A., Rodermond, H. M., Stap, J., Haveman, J., & van Bree, C. (2006). Clonogenic assay of cells in vitro. *Nat Protoc, 1*(5), 2315-2319. doi:10.1038/nprot.2006.339

Munshi, A., Hobbs, M., & Meyn, R. E. (2005). Clonogenic cell survival assay. *Methods Mol Med, 110*, 21-28. doi:10.1385/1-59259-869-2:021

Rieger, A. M., Nelson, K. L., Konowalchuk, J. D., & Barreda, D. R. (2011). Modified annexin V/propidium iodide apoptosis assay for accurate assessment of cell death. *J Vis Exp*(50). doi:10.3791/2597

Vinci, M., Gowan, S., Boxall, F., Patterson, L., Zimmermann, M., Court, W., Lomas, C., Mendiola, M., Hardisson, D., & Eccles, S. A. (2012). Advances in establishment and analysis of three-dimensional tumor spheroid-based functional assays for target validation and drug evaluation. *BMC Biol, 10*, 29. doi:10.1186/1741-7007-10-29

Workman, P., Aboagye, E. O., Balkwill, F., Balmain, A., Bruder, G., Chaplin, D. J., Double, J. A., Everitt, J., Farningham, D. A. H., Glennie, M. J., Kelland, L. R., Robinson, V., Stratford, I. J., Tozer, G. M., Watson, S., Wedge, S. R., Eccles, S. A., Navaratnam, V., Ryder, S., & Inst, N. C. R. (2010). Guidelines for the welfare and use of animals in cancer research. *British Journal of Cancer, 102*(11), 1555-1577. doi:10.1038/sj.bjc.6605642

Chapter 3

Effect of the combination of H_2O_2 + IR *in vitro*: results in 2D and 3D experimental systems

3 Introduction

It is well described in the literature that H_2O_2 applied to cultured cells can induce oxidative stress. The original description of radiation sensitisation by H_2O_2 involved a human osteosarcoma cell line Hs-Os1 (Ogawa, Takahashi, et al., 2004). Following a single 30 Gy IR dose, only minimal oxidative DNA damage or cell killing was detectable (by fluorescence of ROS-sensitive dichlorodihydrofluorescein diacetate (H_2DCFA) (Ogawa, Takahashi, Kobayashi, et al., 2003). It was discovered that the radioresistance of Hs-Os-1 cells and of normal chondrocytes was overcome by adding 0.1 mM H_2O_2 to the culture medium 4 hours before IR (Ogawa, Takahashi, Kobayashi, et al., 2003a). This finding was reproduced in the prostate cancer cell line PC-3, where apoptosis was observed in 4.9 % cells 48 hours after 10 Gy alone, 1.9 % after 0.1 mM H_2O_2 alone and 28.4% cells after exposure to both agents (Kariya et al., 2009). Interestingly, the high sensitivity of PC-3 cells and of normal chondrocytes to IR + H_2O_2 was completely abrogated by ammonium chloride (NH_4Cl) in the culture medium, a compound known to increase lysosomal pH and to inactivate lysosomal hydrolases (Kariya et al., 2009).

H_2O_2 + IR also demonstrated enhanced cytotoxicity (by lysosomal apoptosis) in the melanoma cell line MeWo (HTB-65). The effect of 0.05 mM H_2O_2 administered 24 hours prior to IR was investigated in a clonogenic assay. In comparison to the control group, there was decreased colony formation in MeWo cells treated with H_2O_2 alone, and further inhibition of colony growth following H_2O_2 + IR in combination (Yujiang Fang et al., 2013). Prior publications on the combined effect of H_2O_2 and IR are restricted to a small number of cell lines, and aside from the MeWo/HTB-65 cell line, have not been tested in a clonogenic survival assay.

The aim here was to determine the effect of H_2O_2 on cell survival in the selected cell lines, prior to investigating whether combination with IR resulted in enhanced

cytotoxicity. A systematic approach was adopted, starting with traditional 2D monolayer cultures, and then proceeding to 3D models.

3.1 Assays to determine the cytotoxic effects of H_2O_2 (GI_{50})

3.1.1 Sulforhodamine B (SRB) assay

GI_{50} is defined as the concentration of drug required to cause 50% growth inhibition of cells compared to untreated controls (Brooks et al., 2019). An illustrative example of the variation in SRB staining pattern with increasing dose of H_2O_2 in HCT116 cells is shown in Figure 3.1.

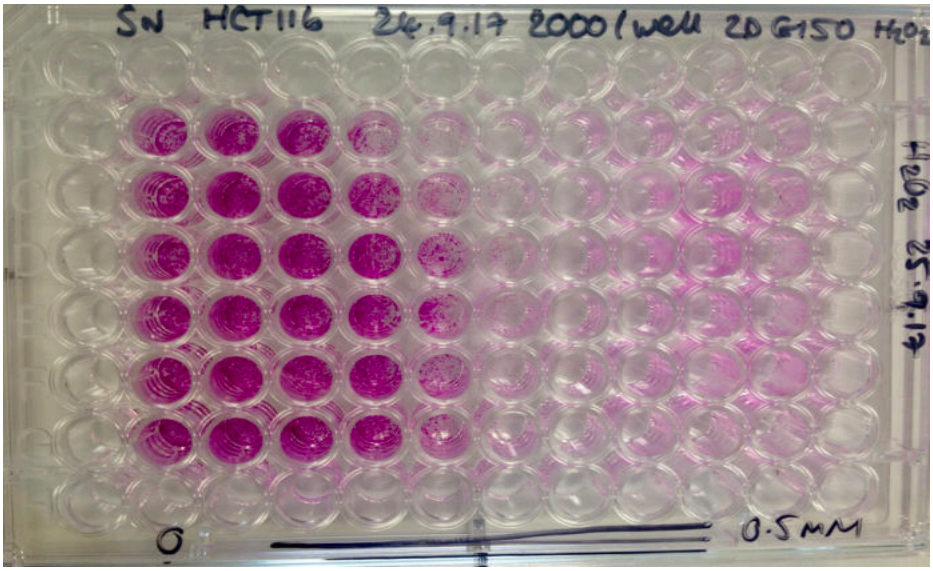

Figure 3.1 96-well plate used for 2D GI50 assay (HCT116 cells) showing reduced SRB staining pattern with increasing concentration of H_2O_2 from left to right (0-0.5 mM)

The results of the SRB assay showed that PC-3, HCT116 and HN5 cells exhibited differing sensitivities to H_2O_2 as shown in Figure 3.2. Of the 3 cell lines tested, PC-3 was the most sensitive with a GI_{50} value of 0.002 mM, compared to 0.01 mM for HCT116 and HN5.

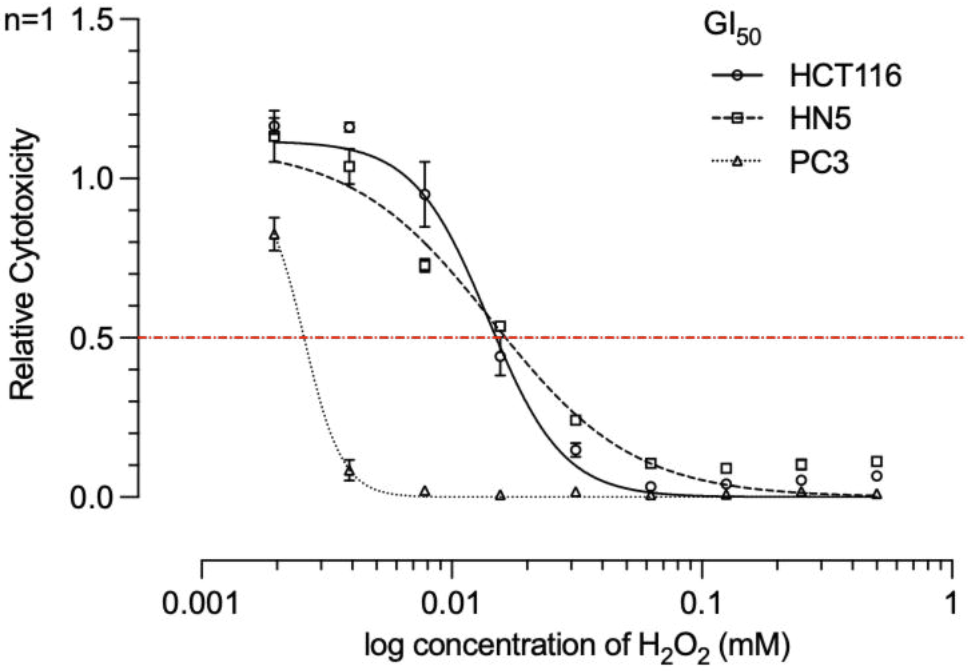

Figure 3.2 Results of SRB assays showing total protein mass (related to cell number) for PC-3, HCT116 and HN5 cell lines exposed to increasing concentrations of H_2O_2. PC-3 cells demonstrated approximately 10-fold greater sensitivity to H_2O_2 than HCT116 and HN5 cell lines. Each data point is the average of 6 measurements. Dotted line indicates H_2O_2 concentration which corresponds to GI_{50} for each cell line. Error bars represent SEM, n=2.

3.1.2 CellTiter-Glo® assay

An alternative method of measuring GI_{50} was used to verify the previous results, using CellTiter-Glo® in place of SRB, the former measuring luminescence rather than fluorescence. Although the results were concordant for both HCT116 and HN5 cells (Figure 3.3), the absolute values were at least 30-fold greater than that obtained with the SRB assay.

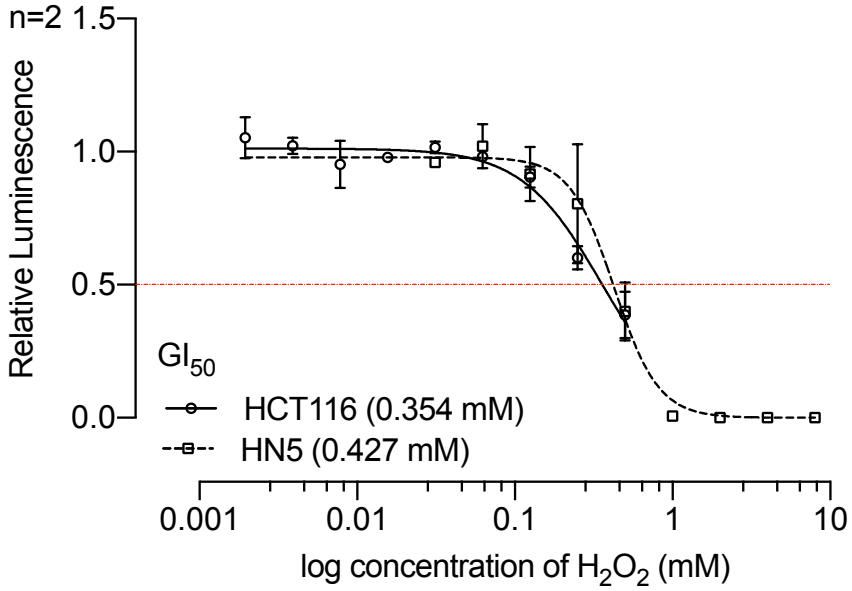

Figure 3.3. 2D GI50 results for HCT116 (0.35 mM) and HN5 (0.43 mM) cell lines obtained using the CellTiter-Glo® assay. Each data point is the average of 6 measurements. Dotted line indicates H_2O_2 concentration which corresponds to GI_{50} for each cell line. Error bars represent SEM, n=2

3.1.3 3D GI_{50}

3D spheroids are physiologically more representative of tumours *in vivo*, due to the existence of gradients of oxygen, nutrients, and pH. They bridge the gap between *in vitro* and *in vivo* models due to their structures having an outer proliferating layer, and an inner quiescent core. Gene expression profiles also differ between 2D and 3D cultures, the latter more closely resembling tumours *in vivo* (Edmondson, Broglie, Adcock, & Yang, 2014). In addition, the molecular processes involved in signal transduction and the DNA damage response vary significantly between 2D and 3D cultured cells (Eke, Hehlgans, Zong, & Cordes, 2015; Storch et al., 2010).

3.1.4 PC-3

Attempts to form spheroids using PC-3 cells were unsuccessful (n=3); they formed loosely cohesive masses with irregular outlines, making it difficult to contour on the image cytometer (Figure 3.4). Therefore, 3D spheroids were not further pursued with this cell line. Similar findings of formation of irregular aggregates with PC-3 cells have been reported and hypothesised to be related

to the absence of E-cadherin expression (Jantti et al., 2018; Kalaydina et al., 2019).

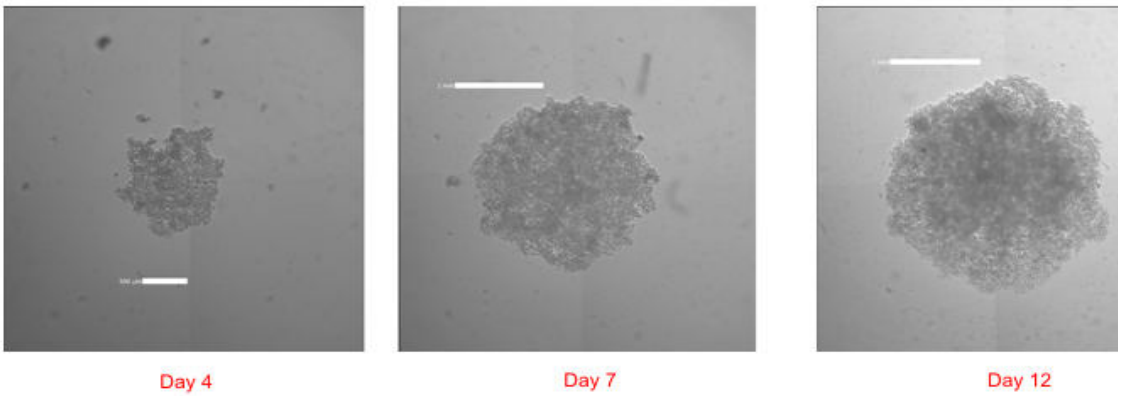

Figure 3.4 PC-3 spheroids on Day 4, 7 and 12 post seeding showing loosely compact structures with irregular borders. White bar represents scale bar (500 μm).

3.1.5 HCT116 and LICR-LON-HN5

3D GI_{50} results were obtained in the HCT116 and HN5 cell lines as summarized in Figure 3. 5.

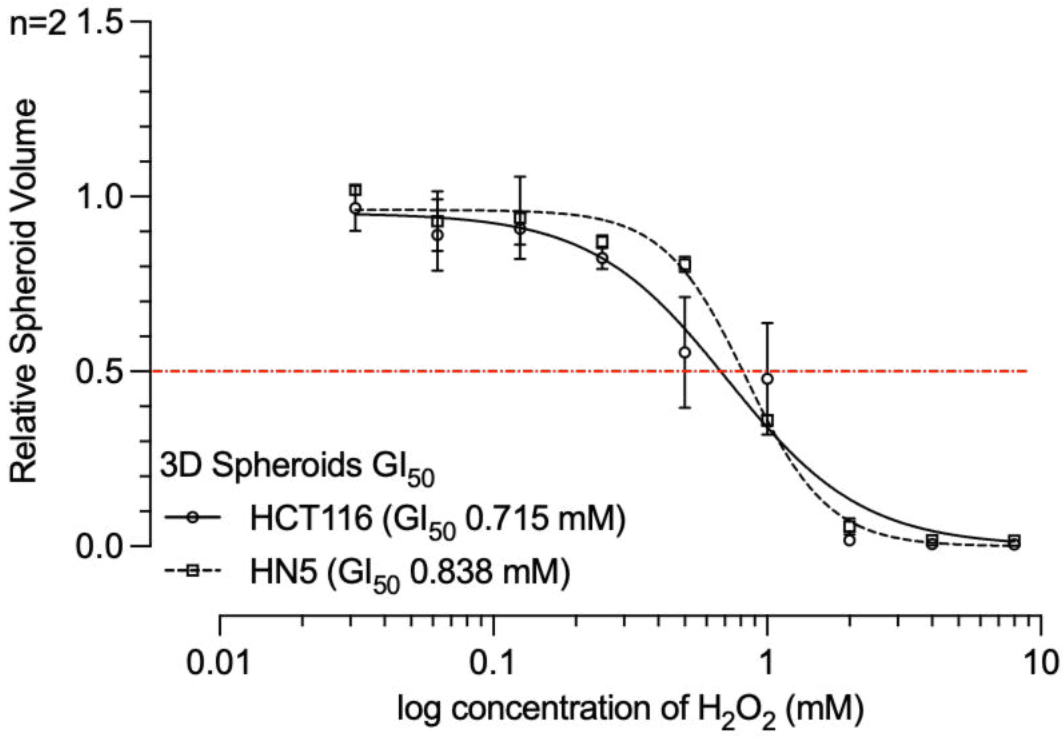

Figure 3.5 GI_{50} results (using CTG assay) for spheroids post H_2O_2 treatment in HCT116 and HN5 cell lines. The 3D GI_{50} for HCT116 = 0.72 mM and for HN5 = 0.84 mM. Each data point is the average from n=2 individual experiments. Dotted line indicates H_2O_2 concentration which corresponds to GI_{50} for each cell line. Error bars represent SEM.

3.2 Clonogenic survival assays do not demonstrate sensitisation or enhancement of IR effect by H_2O_2

3.2.1 Clonogenic GI_{50}

The aim was to determine the effect of H_2O_2 exposure on the ability to form colonies, by treating cells with a range of concentrations and measuring the resulting colonies after 10-14 days. Subsequently, a wider range of doses were tested to calculate a "clonogenic GI_{50}"; the dose of drug required to inhibit colony numbers by 50%. This highlighted that measuring the effect of H_2O_2 in 2D monolayer cultures versus the effect on reproductive capability of single cells can yield differing results. The latter method was chosen to determine the H_2O_2 dose to use in combination with IR in a clonogenic survival assay. Figure 3.6 shows the clonogenic GI_{50} values obtained for HCT116 (0.11 mM) and HN5 (0.30 mM) cells, indicating that the former was more sensitive to H_2O_2 in this assay. This contrasts with the 2D GI_{50} results, where results from two separate assays yielded very similar results between these 2 cell lines.

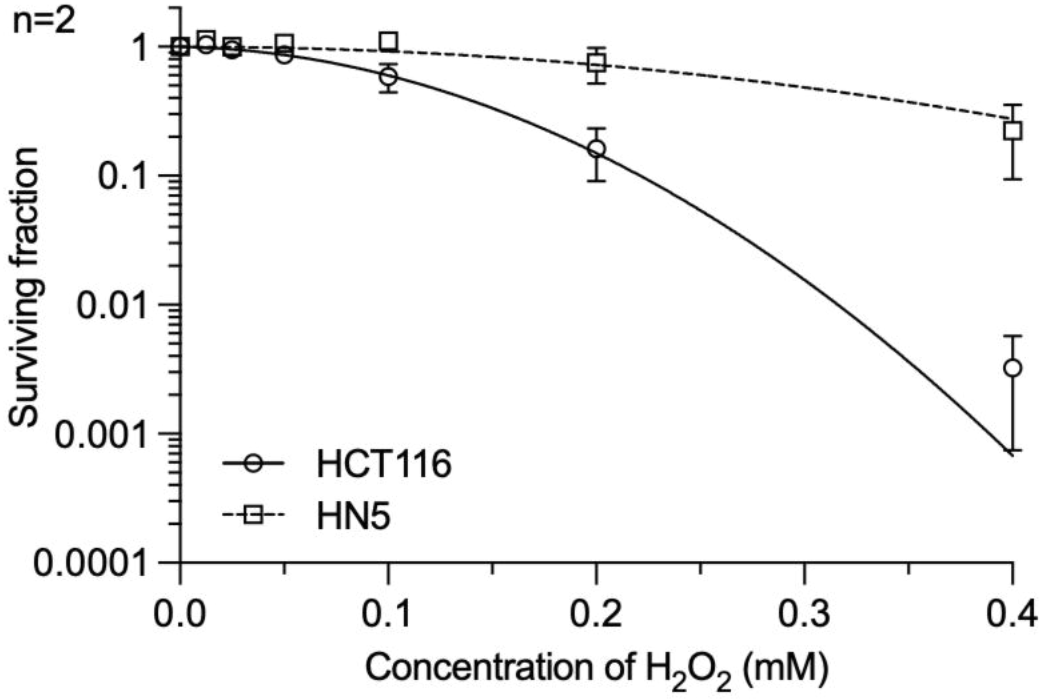

Figure 3.6 Clonogenic GI_{50} results. HCT116 = 0.117 mM, HN5 = 0.295 mM. Non-cytotoxic 0.05 mM H_2O_2 was selected for use in subsequent clonogenic assays testing for a sensitising effect of H_2O_2 on IR response. Each data point represents the average result, error bars represent SEM, n=2

3.2.2 GI_{50} summary

Table 3.1 gives a summary of the overall GI_{50} measurements according to the assay used and cell line. It illustrates the variation in measurements according to the assay used, and the differences between 2D and 3D *in vitro* systems.

Cell line	SRB assay 2D GI_{50} (mM)	CellTiter Glo® assay 2D GI_{50} (mM)	Clonogenic GI_{50} (mM)	3D GI_{50} (mM) (Spheroids)
PC-3	0.002	–	–	–
HCT116	0.01	0.35	0.12	0.72
LICR-LON-HN5	0.01	0.43	0.30	0.84

Table 3.1 Summary of GI_{50} measurements for PC-3, HCT116 and LICR-LON-HN5 cell lines when treated with H2O2. PC-3 is more sensitive than HCT116 and HN5 according to the SRB assay. In 2D assays, HCT116 and HN5 have similar values, whereas in 3D spheroids HN5 is more sensitive.

3.2.3 H_2O_2 + IR in clonogenic survival assays

3.2.4 PC-3

Replicate experiments were conducted with PC-3 cells to determine clonogenic survival following IR alone and H_2O_2 + IR. However, the colonies formed were heterogeneous: whilst some colonies were tight, others had gaps between the cells resulting in a more dispersed appearance. Alternative methods were utilised, such as using gelatin-coated 6-well plates. However, similar problems were encountered in forming colonies with this cell line. The colonies did not stain well, and counts were therefore inaccurate; hence it was decided that the PC-3 cell stock was unsuitable for use in a clonogenic assay.

3.2.5 HCT116 and LICR-LON-HN5

It was important to select a dose of H_2O_2 (and IR) at which a degree of clonogenic survival was retained, so that the combined effect of H_2O_2 followed by IR could be quantified. Two doses of H_2O_2 were selected; a *sensitising* dose defined as one which does not exert any cytotoxic effect when given alone, and an *enhancing* dose which does have a cytotoxic effect both when given alone, and in combination with IR. For both HN5 and HCT116 cell lines 0.05 mM was used for the *sensitising* dose, and 0.1 mM for the *enhancing* dose. Figures 3.7 and 3.8 show the composite clonogenic survival curves for HN5 and HCT116 respectively, comparing IR alone to H_2O_2 + IR.

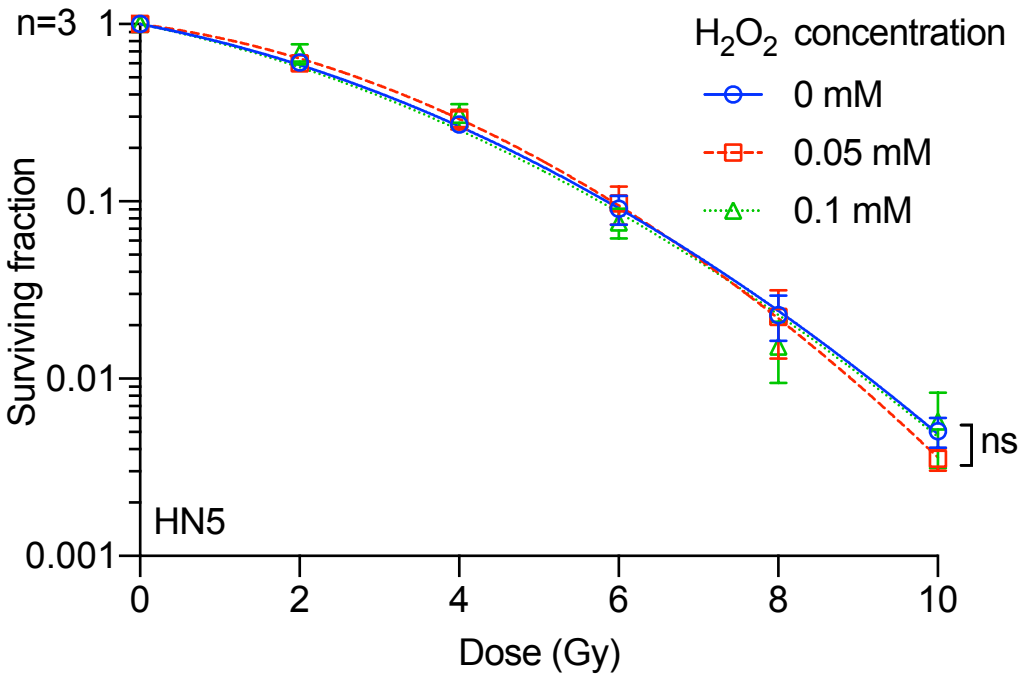

Figure 3.7 Clonogenic survival curves comparing IR alone with H_2O_2 + IR (0.05 and 0.1mM) H_2O_2 was added 30 minutes prior to IR. Results shown are from n=3 replicates for the HN5 cell line and demonstrate no evidence of sensitisation by H_2O_2 using single IR doses of up to 10Gy. ns - non-significant

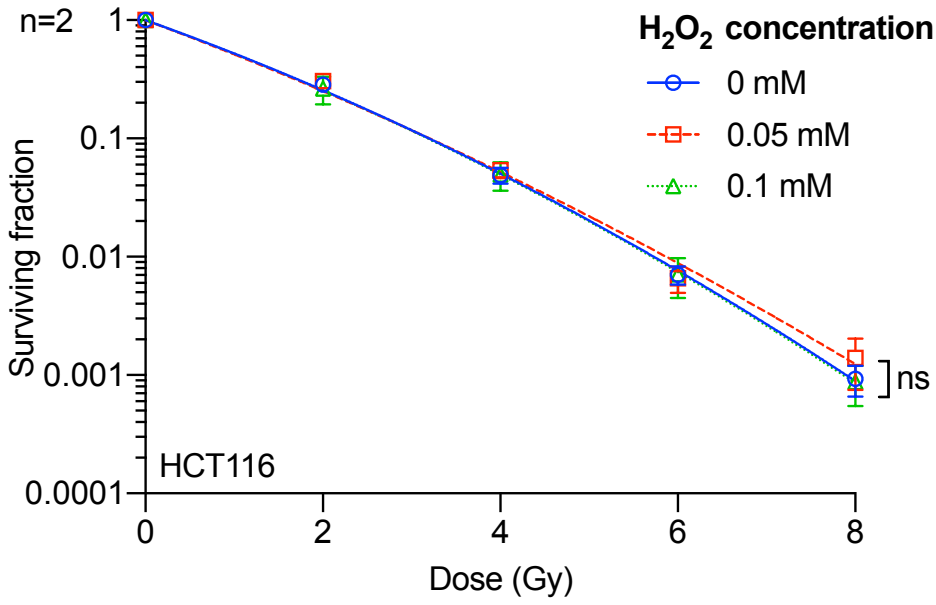

Figure 3.8 Clonogenic survival curves comparing IR alone with H_2O_2 + IR (0.05 and 0.1mM) H_2O_2 was added 30 minutes prior to IR. Results shown are from n=2 replicates for the HCT116 cell line and demonstrate no evidence of supra-additive cytotoxicity by H_2O_2 using single IR doses of up to 8Gy. ns - non-significant

Results were consistent between 2-3 replicates and between both HN5 and HCT116 cell lines. The raw and adjusted data for these experiments are pro6-well plates treated with 0.1 mM H_2O_2 resulted in a reduction in colony numbers, but when combined with IR and the results normalised to 100% at the 0 Gy level, there was no evidence of any supra-additive effect. Therefore, this suggests that the overall outcome of treatment with H_2O_2 and IR results from independent additive effects of both agents.

3.3 Combination treatment with H_2O_2 and IR results in 3D spheroid growth delay greater than with each agent alone

Growth of HCT116 spheroids was inhibited by H_2O_2 + IR, as evidenced by a decrease in spheroid diameter compared to other treatment groups, and this was noticeable from Day 5 post treatment. The difference in size at Day 15 post treatment is illustrated in Figure 3.9.

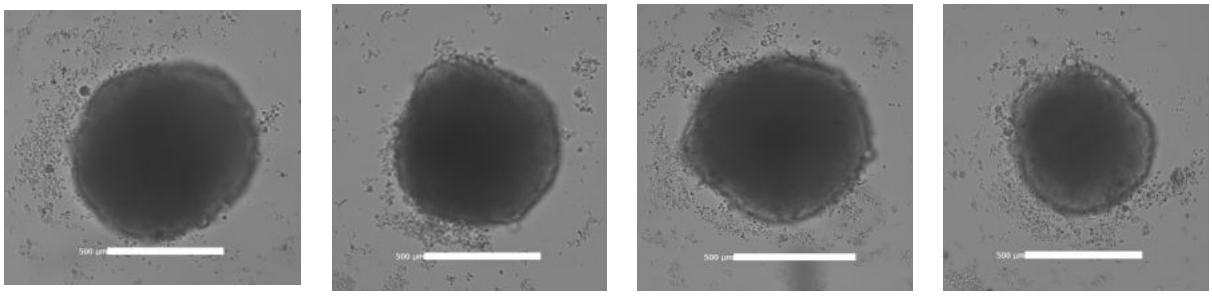

Figure 3.9 HCT116 spheroids at Day 15 post-treatment. Brightfield images obtained using the Celigo imaging cytometer showing comparatively smaller spheroids treated with H_2O_2 + IR than other treatment groups. Scale bar shown in white (500 μm).

Growth delay curves (up to 23 days post-treatment) showed increased growth inhibition in spheroids treated with combination H_2O_2 + IR compared to H_2O_2 or IR alone. This is shown in Figure 3.10. Comparing spheroid volumes in the IR vs. H_2O_2 + IR groups at all timepoints, there was a significant (p=0.01) difference between the two groups on days 15 and 19.

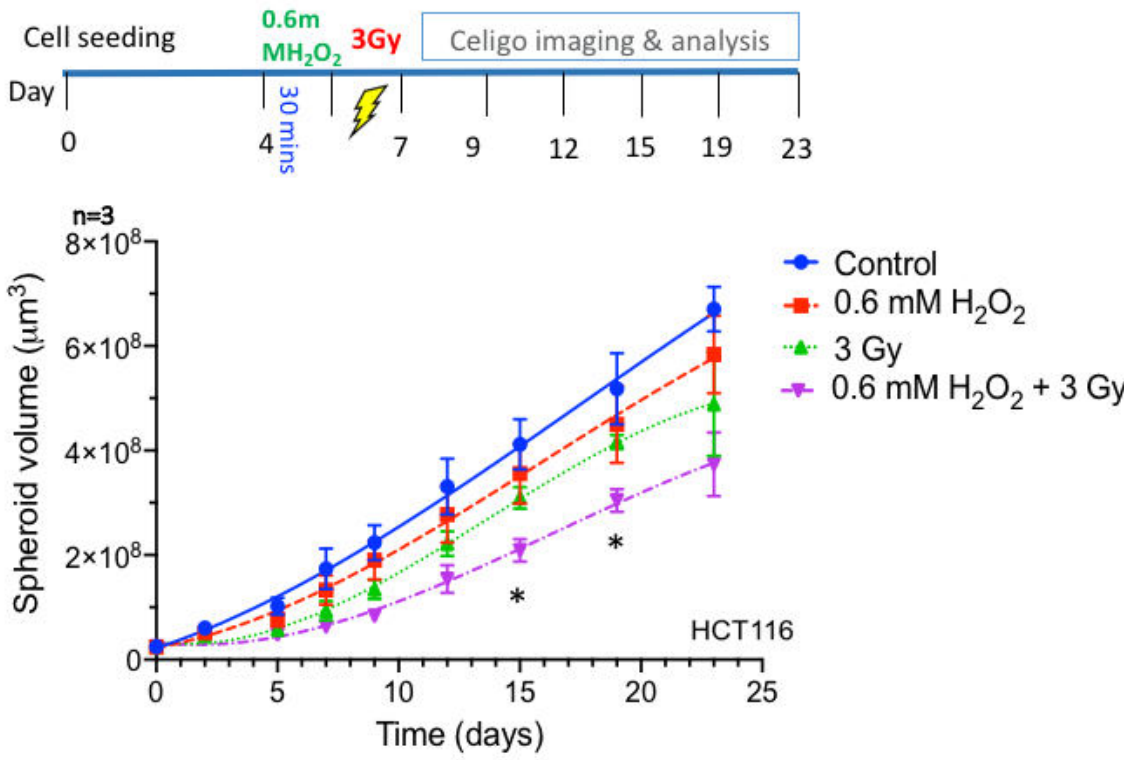

Figure 3.10 Combined treatment with $H2O_2$ and IR in HCT116 spheroids leads to growth delay compared with drug or IR alone (H_2O_2 administered prior to IR). Experimental schema and spheroid growth curves showing growth kinetics up to 23 days post treatment. In the combination treatment group, spheroids were treated with 0.6mM H_2O_2 30 minutes prior to IR, with the drug subsequently left in situ. Student's t-test comparing IR vs. H_2O_2 + IR; * denotes p = 0.01 (Day 15 and 19)

When the treatment schedule was reversed (H_2O_2 administered *after* IR), a similar pattern was seen in the growth kinetics as shown in Figure 3.11. This implies that the growth delay effect of combination treatment is not schedule dependent and supports the 2D data suggesting that both H_2O_2 and IR are contributing independently to the overall effect.

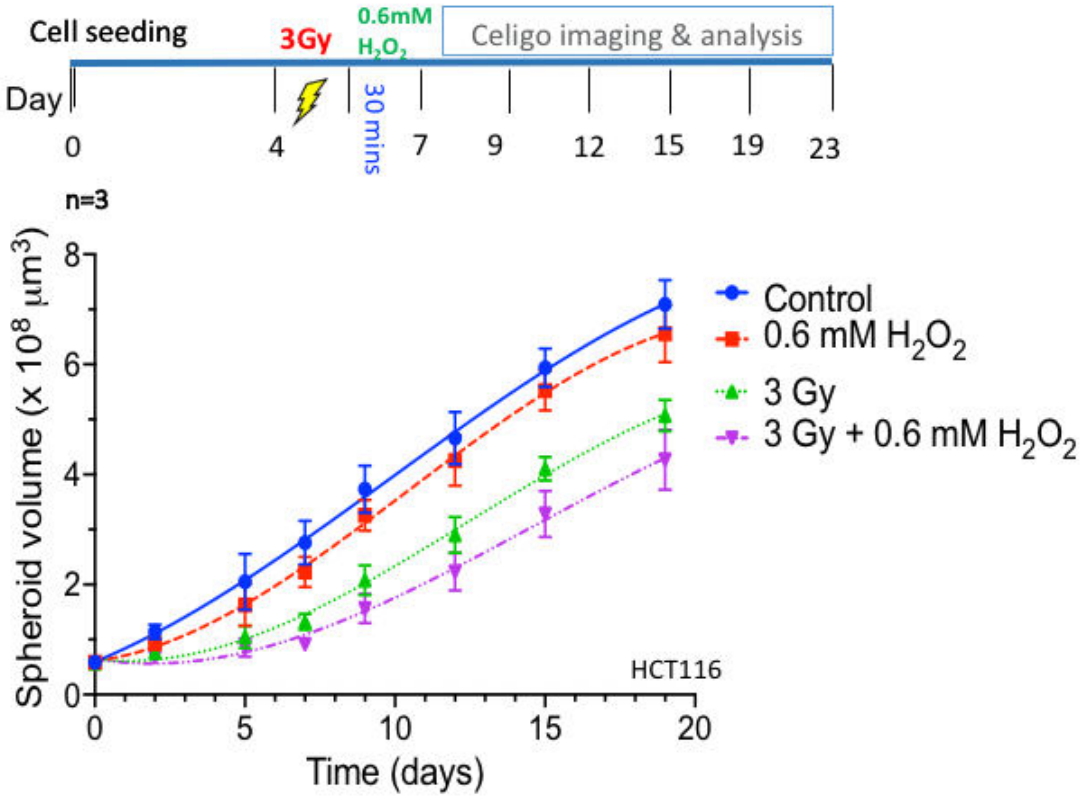

Figure 3.11 Combined treatment with H_2O_2 and IR in HCT116 spheroids leads to growth delay compared with drug or IR alone (H_2O_2 administered after to IR). Experiment schema and spheroid growth curves showing growth kinetics up to 23 days post treatment. In combination treatment group, spheroids were treated with 0.6 mM H_2O_2 30 minutes following IR, with the drug subsequently left in situ.

3.4 HCT116 spheroids treated with H_2O_2+ IR results in reduced viability

3.4.1 Spheroid morphology

Brightfield images of HCT116 spheroids exposed to increasing concentrations of H_2O_2 revealed morphological changes as illustrated in Figure 3.12 below.

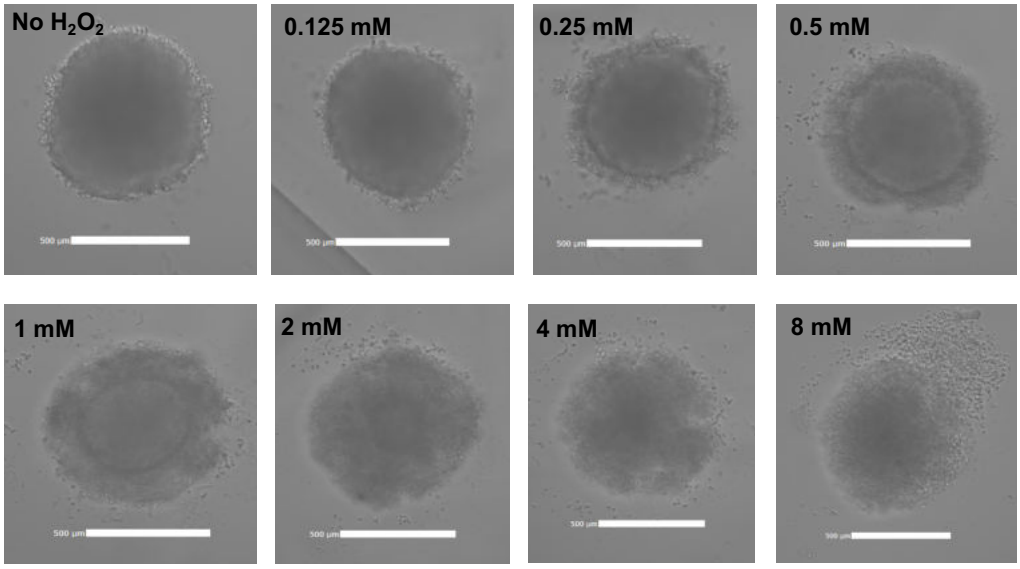

Figure 3.12 HCT116 spheroid morphology 72 hours following treatment with H_2O_2 (0-8 mM).

Compared with the control group, spheroids treated with H_2O_2 exhibited increased shedding of the peripheral cell layer. This pattern of cell shedding appeared to correlate with H_2O_2 concentration, such that following the addition of 8 mM H_2O_2, cell adhesion of the outer layer was perturbed, and a larger proportion of the spheroid architecture disrupted.

3.4.2 Propidium Iodide staining

Figure 3.13 below shows fluorescence images taken on Day 1 post-treatment with H_2O_2 (0-0.8 mM). The images revealed a dose-dependent increase in PI staining. Of note, there was no necrosis demonstrated in the control group, suggesting that the diameter at which a necrotic core formed was not reached (average spheroid diameter on Day 1 = 320 μm). The pattern of fluorescence suggests that the effect of H_2O_2 begins at the spheroid periphery and extends to the core at higher doses. This concurs with the morphological changes observed in Figure 3.12.

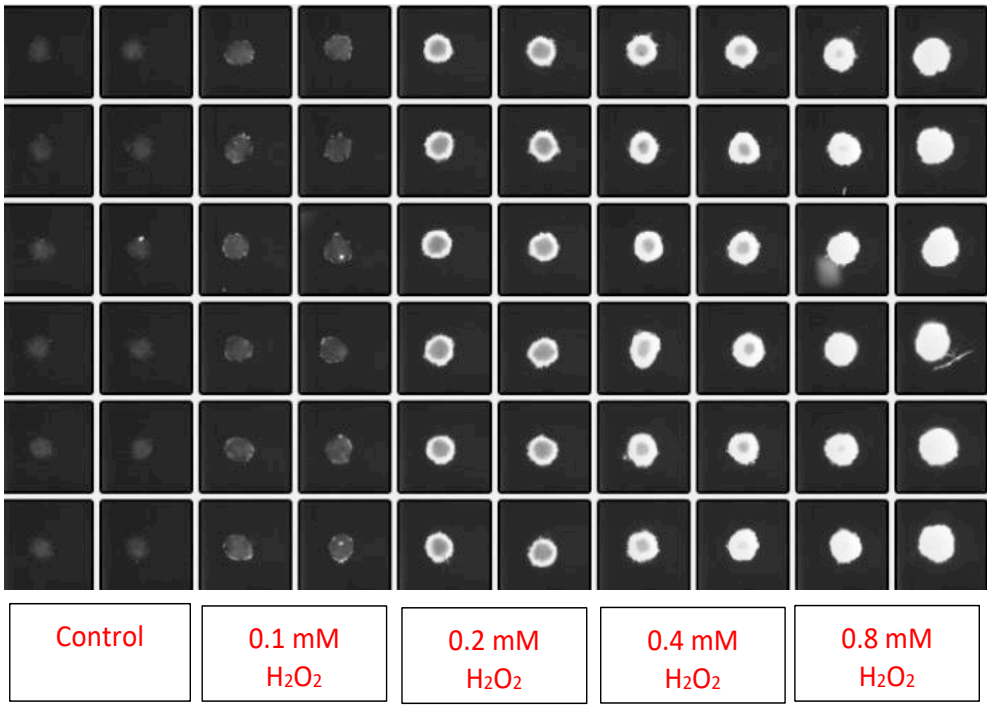

Figure 3.13 Cytometer image of HCT116 spheroids with PI staining on day 1 post-treatment with increasing H_2O_2 concentration. Overview image of 96-well plate showing dose-dependent increase in PI staining. Of note, spheroids in the control group had a viable core, suggesting that the volume at which a necrotic core forms was not reached.

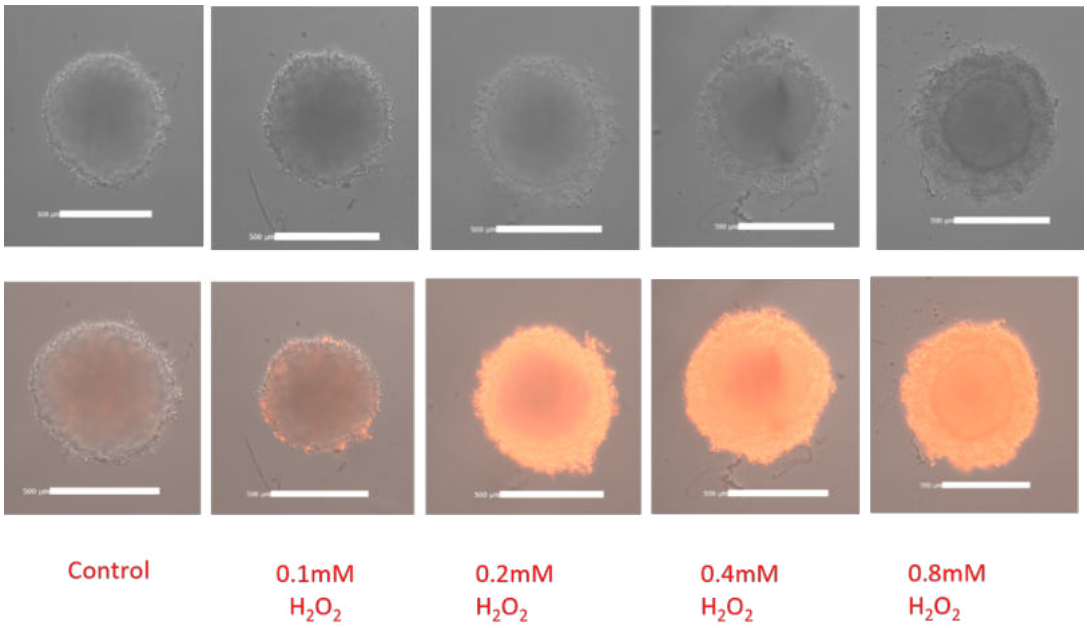

Figure 3.14 Microscope images of HCT116 spheroids treated with 0-0.8 mM H_2O_2 and stained with propidium iodide (PI) at Day 1 post treatment. PI staining (shown in orange) shows minimal effect on spheroid viability when treated with 0.1 mM H_2O_2, but whole spheroid staining at 0.2 mM H_2O_2 and above.

When the pattern of fluorescence was observed (Figure 3.14), there appeared to be a large incremental increase in PI staining between 0.1 mM and 0.2 mM H_2O_2, to "whole spheroid" staining with the latter. On day 5 post treatment, PI staining was visible at the core of all spheroids, including the control group as shown in Figure 3.15 below. This suggested that the core of the spheroid was non-viable. The peripheral cell layer showed increasing fluorescence in a dose-dependent manner.

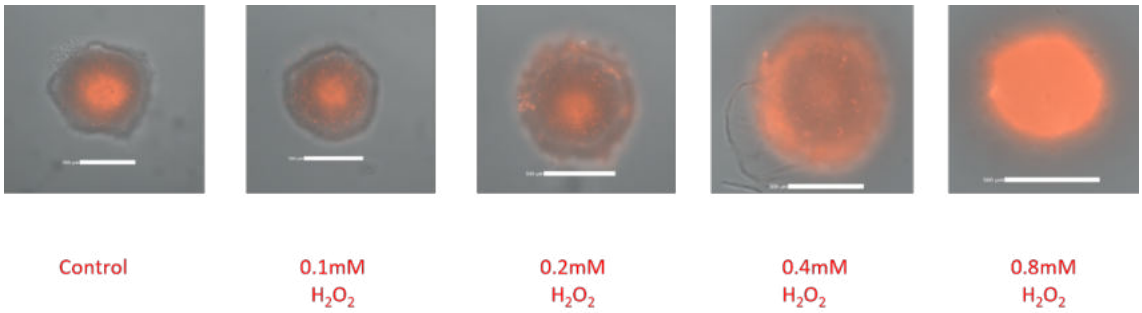

Figure 3.15 Microscope images of HCT116 spheroids treated with 0-0.8 mM H_2O_2 and stained with propidium iodide (PI) at Day 5 post treatment. In the control group, PI staining (shown in orange) revealed a non-viable core formed by Day 5 post treatment (9 days post cell seeding). Following H_2O_2 treatment, there was dose-dependent increase in PI staining.

Only the spheroids exposed to 0.8 mM H_2O_2 exhibited whole spheroid PI staining; at lower doses the staining pattern was concentrated towards the peripheral, more rapidly proliferating cells (aside from the PI-positive core, which was present in all groups). Compared to the control group, spheroids treated with 0.4 mM H_2O_2 exhibited less PI staining of the core. A possible explanation may be reoxygenation by H_2O_2, enabling viable cells at the centre of the spheroid to grow in the days following treatment. This hypothesis is further investigated in Chapter 4 using *in vivo* tumours injected with H_2O_2.

3.4.3 CellTiter-Glo®

Consistently lower viability readings were obtained in H_2O_2+IR treated spheroids compared to control, IR, and H_2O_2 groups (Figure 3.16). The difference in viability between H_2O_2+IR and IR alone, was greatest at D23 (compared to D7 and D11). The effect of "H_2O_2 alone" and "IR alone" on spheroid viability (compared to "control" group) was most marked in the first week post treatment, with the effect becoming less apparent from D11 to D23. This suggests that after the initial impact following treatment, spheroid regrowth occurred such that at later time

points, much of the spheroid was viable. In contrast, the metabolic activity in spheroids treated with H_2O_2+IR remained low in comparison to the other treatment groups.

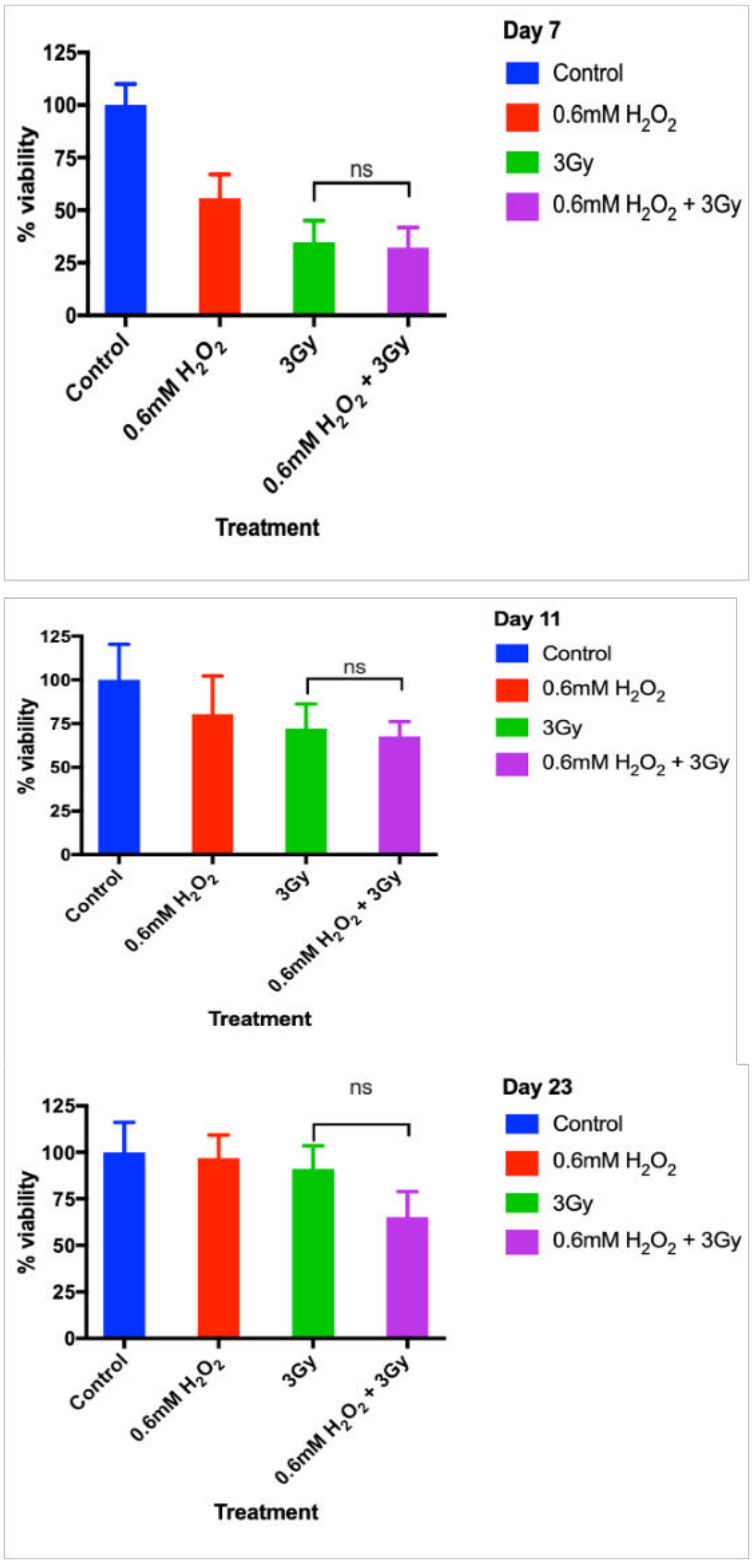

Figure 3.16 HCT116 spheroid viability measured according to treatment group at 7-, 11-, and 23-days post treatment (n=3). Lower viability (measured by CellTiter-Glo®) measurements were seen in spheroids treated with H_2O_2 + IR (compared to control, or either treatment alone) at all timepoints. Differences between groups not statistically significant. Data points represent average values, error bars represent SEM.

3.5 Discussion

It has been demonstrated that the sensitivity to H_2O_2 alone differs between cell lines. An important question is what determines the sensitivity of any given cell to the effects of H_2O_2. It is known that there is considerable variation between cell lines in the concentration of exogenous H_2O_2 required to elicit a specific biological response (Veal et al., 2007). Variation in p53-related gene expression has been demonstrated with different concentrations of H_2O_2. Antioxidant enzyme expression can be induced by low levels of H_2O_2 (hence protecting against ROS damage), whereas higher concentrations promote pro-oxidants which can result in apoptosis (Sablina et al., 2005). In the cell lines tested, PC-3 and HN5 have a p53 mutation, whereas HCT116 is wild type for p53. It is hypothesised that sensitivity to H_2O_2 is largely determined by antioxidant defences (e.g. catalase, glutathione peroxidase, and peroxiredoxins). Such defences by the cell against the deleterious effects of ROS and the multiple resulting signalling pathways are highly regulated (Veal et al., 2007). Therefore, quantification of the expression and activity of these enzymes may be useful to further investigate this.

The clonogenic assay results have not shown evidence of sensitisation or enhancement of IR effect by H_2O_2 but indicate that both agents contribute independently to the overall effect. In previous studies, H_2O_2 alone has been shown to be cytotoxic in terms of clonal survival in the HTB-65 melanoma cell line at supraphysiological concentrations as low as 50 μM (Yujiang Fang et al., 2013). Investigation into the mechanism of action of H_2O_2 in HTB-65 indicates both pro-apoptotic and anti-proliferative effects (Yujiang Fang et al., 2013).

The two methods used to quantify 2D GI_{50} values (SRB and CTG assays) yielded differing absolute values, although there was concordance between HCT116 and HN5 cell lines in each method. It has been shown that different *in vitro* culture methods can affect cell metabolism, proliferation, and overall sensitivity to drug treatments (Hsieh, Chen, Huang, Wang, & Wu, 2015). It is apparent that in 2D experiments, it is not necessarily possible to extrapolate data obtained from one assay to another. The results have demonstrated the importance of

independently testing the effect of H_2O_2 in a clonogenic assay, prior to testing the effect of combined treatment. This "clonogenic GI_{50}" does not necessarily equate to 2D GI_{50} values obtained from a non-clonal, growth inhibition assay. Multiple factors affect dose response, and it is likely that none of the laboratory systems available model the clinical context, which in itself is expected to be highly heterogeneous. An unanswered question is which mode of cell death predominates to account for the aforementioned result. Lysosomal rupture and activation of the intrinsic apoptosis pathway is suggested as the dominant process by *in vitro* studies of human chrondrocytes, T-lymphocytes, and osteosarcoma (Hs-Os-1) cells (Ogawa, Kobayashi, et al., 2004; Ogawa, Takahashi, Kobayashi, et al., 2003a; T. Takahashi et al., 2004)

It is unsurprising that cells are less sensitive to H_2O_2 in 3D than in 2D culture (3D GI_{50}> 2D GI_{50}). Cells in 3D structures have decreased access to drugs when added to the medium, and experience different microenvironments due to nutrient and hypoxic gradients, or phases of the cell cycle (Eke & Cordes, 2011; Kapalczynska et al., 2018). In comparisons of 2D and 3D models, it has been shown that only in 3D culture models where normal tissue density is reproduced is the response to a drug comparable to that of a tumour *in vivo* (Hsieh et al., 2015*)*. The 3D structure of spheroids also influences response to radiation. Compared to 2D monolayer cultures, the 3D architecture impacts upon DNA heterochromatinization, which partially protects DNA against IR-induced DNA double strand breaks (Kapalczynska et al., 2018).

In 3D spheroid models using HCT116 cells, the combination of H_2O_2 and IR demonstrates growth inhibition and reduction in cell viability. This is when compared to either treatment alone, when each are given at doses associated with cytotoxicity. Spheroids are a suitable system for investigating the effects of IR as they demonstrate parameters which can affect IR response, such as hypoxia, variations in cell signalling and proliferation (Al-Ramadan, Mortensen, Carlsson, & Nestor, 2018). To augment these results, it would be useful to perform immunohistochemistry analyses on fixed spheroids to investigate processes including DNA damage and repair and cell death markers.

References

Al-Ramadan, A., Mortensen, A. C., Carlsson, J., & Nestor, M. V. (2018). Analysis of radiation effects in two irradiated tumor spheroid models. *Oncol Lett, 15*(3), 3008-3016. doi:10.3892/ol.2017.7716

Brooks, E. A., Galarza, S., Gencoglu, M. F., Cornelison, R. C., Munson, J. M., & Peyton, S. R. (2019). Applicability of drug response metrics for cancer studies using biomaterials. *Philos Trans R Soc Lond B Biol Sci, 374*(1779), 20180226. doi:10.1098/rstb.2018.0226

Edmondson, R., Broglie, J. J., Adcock, A. F., & Yang, L. (2014). Three-dimensional cell culture systems and their applications in drug discovery and cell-based biosensors. *Assay Drug Dev Technol, 12*(4), 207-218. doi:10.1089/adt.2014.573

Eke, I., & Cordes, N. (2011). Radiobiology goes 3D: how ECM and cell morphology impact on cell survival after irradiation. *Radiother Oncol, 99*(3), 271-278. doi:10.1016/j.radonc.2011.06.007

Eke, I., Hehlgans, S., Zong, Y., & Cordes, N. (2015). Comprehensive analysis of signal transduction in three-dimensional ECM-based tumor cell cultures. *J Biol Methods, 2*(4). doi:10.14440/jbm.2015.96

Fang, Y., Moore, B. J., Bai, Q., Cook, K. M., Herrick, E. J., & Nicholl, M. B. (2013). Hydrogen peroxide enhances radiation-induced apoptosis and inhibition of melanoma cell proliferation. *Anticancer research, 33*(5), 1799-1807.

Hsieh, C. H., Chen, Y. D., Huang, S. F., Wang, H. M., & Wu, M. H. (2015). The effect of primary cancer cell culture models on the results of drug chemosensitivity assays: the application of perfusion microbioreactor system as cell culture vessel. *Biomed Res Int, 2015*, 470283. doi:10.1155/2015/470283

Jantti, M. H., Talman, V., Rasanen, K., Tarvainen, I., Koistinen, H., & Tuominen, R. K. (2018). Anticancer activity of the protein kinase C modulator HMI-1a3 in 2D and 3D cell culture models of androgen-responsive and androgen-unresponsive prostate cancer. *FEBS Open Bio, 8*(5), 817-828. doi:10.1002/2211-5463.12419

Kalaydina, R. V., Zhou, H., Markvicheva, E., Burov, S. V., Zulkernine, F., & Szewczuk, M. R. (2019). Impact of Fucosylation on Self-Assembly of Prostate and Breast Tumor Spheroids by Using Cyclo-RGDfK(TPP) Peptide and Image Object Detection. *Onco Targets Ther, 12*, 11153-11173. doi:10.2147/OTT.S235811

Kapalczynska, M., Kolenda, T., Przybyla, W., Zajaczkowska, M., Teresiak, A., Filas, V., Ibbs, M., Blizniak, R., Luczewski, L., & Lamperska, K. (2018). 2D and 3D cell cultures - a comparison of different types of cancer cell cultures. *Arch Med Sci, 14*(4), 910-919. doi:10.5114/aoms.2016.63743

Kariya, S., Sawada, K., Kobayashi, T., Karashima, T., Shuin, T., Nishioka, A., & Ogawa, Y. (2009). Combination treatment of hydrogen peroxide and X-rays induces apoptosis in human prostate cancer PC-3 cells. *Int J Radiat Oncol Biol Phys, 75*(2), 449-454. doi:10.1016/j.ijrobp.2009.04.092

Ogawa, Y., Kobayashi, T., Nishioka, A., Kariya, S., Ohnishi, T., Hamasato, S., Seguchi, H., & Yoshida, S. (2004). Reactive oxygen species-producing site in radiation and hydrogen peroxide-induced apoptosis of human peripheral T cells: Involvement of lysosomal membrane destabilization. *Int J Mol Med, 13*(5), 655-660.

Ogawa, Y., Takahashi, T., Kobayashi, T., Kariya, S., Nishioka, A., Hamasato, S., Moriki, T., Seguchi, H., Yoshida, S., & Sonobe, H. (2004). Immunocytochemical characteristics of human osteosarcoma cell line HS-Os-1: possible implication in apoptotic resistance against irradiation. *Int J Mol Med, 14*(3), 397-403.

Ogawa, Y., Takahashi, T., Kobayashi, T., Kariya, S., Nishioka, A., Mizobuchi, H., Noguchi, M., Hamasato, S., Tani, T., Seguchi, H., Yoshida, S., & Sonobe, H. (2003). Mechanism of hydrogen peroxide-induced apoptosis of the human osteosarcoma cell line HS-Os-1. *Int J Mol Med, 12*(4), 459-463.

Ogawa, Y., Takahashi, T., Kobayashi, T., Kariya, S., Nishioka, A., Ohnishi, T., Saibara, T., Hamasato, S., Tani, T., Seguchi, H., Yoshida, S., & Sonobe, H. (2003). Apoptotic-resistance of the human osteosarcoma cell line HS-Os-1 to irradiation is converted to apoptotic-susceptibility by hydrogen peroxide: a potent role of hydrogen peroxide as a new radiosensitizer. *Int J Mol Med, 12*(6), 845-850.

Sablina, A. A., Budanov, A. V., Ilyinskaya, G. V., Agapova, L. S., Kravchenko, J. E., & Chumakov, P. M. (2005). The antioxidant function of the p53 tumor suppressor. *Nat Med, 11*(12), 1306-1313. doi:10.1038/nm1320

Storch, K., Eke, I., Borgmann, K., Krause, M., Richter, C., Becker, K., Schrock, E., & Cordes, N. (2010). Three-dimensional cell growth confers radioresistance by chromatin density modification. *Cancer Res, 70*(10), 3925-3934. doi:10.1158/0008-5472.CAN-09-3848

Takahashi, T., Kitaoka, K., Ogawa, Y., Kobayashi, T., Seguchi, H., Tani, T., & Yoshida, S. (2004). Lysosomal dysfunction on hydrogen peroxide-induced apoptosis of osteoarthritic chondrocytes. *Int J Mol Med, 14*(2), 197-200.

Veal, E. A., Day, A. M., & Morgan, B. A. (2007). Hydrogen peroxide sensing and signaling. *Mol Cell, 26*(1), 1-14. doi:10.1016/j.molcel.2007.03.016

Chapter 4

Effect of intratumoural hydrogen peroxide on tumour hypoxia *in vivo*

4 Introduction

In 1955 Thomlinson and Gray first reported that tumours consist of hypoxic as well as oxygenated cells. This was demonstrated by studying histological specimens from human bronchial carcinomas. It was observed that areas of viable tumour surrounded vascular regions, from which oxygen and nutrients are obtained. Necrotic areas were visible in the centre of these tumours, with viable tumour cells found to be within 180 μm from vessels, similar to the diffusion limit of oxygen. Cells beyond this distance were unable to survive, and therefore necrotic (Thomlinson & Gray, 1955). This led to the phenomenon of the "oxygen effect". It was demonstrated that approximately 2.5-3 times the dose of radiation is required for the same effect in hypoxic cells (whether normal or malignant) compared to their normoxic counterparts (Alper & Howard-Flanders, 1956; Gray, Conger, Ebert, Hornsey, & Scott, 1953).

Tumour hypoxia occurs due to an imbalance between oxygen supply and consumption, and generally refers to tissue oxygen levels less than 5-10 mmHg (compared to 40-60 mmHg in healthy tissues) (Challapalli, Carroll, & Aboagye, 2017). This is often the result of an inadequate and disorganised vasculature combined with rapid cellular proliferation, leading to oxygen demand outstripping oxygen supply.

Hypoxia exerts a multitude of effects upon processes such as vasculogenesis, invasiveness, metastasis, cell death resistance, metabolism, and gene instability. This occurs via stabilisation of HIF-1, which is a transcription factor for numerous target genes (Wilson & Hay, 2011). Genotypes favouring survival are selected for (e.g. TP53 mutations), and pro-survival gene expression leads to the inhibition of apoptosis. Hypoxia also leads to increased tyrosine kinase signalling, angiogenesis, and epithelial-to-mesenchymal transition, whilst suppressing immune reactivity (Wilson & Hay, 2011).

There is substantial evidence for the presence of inter- and intratumoural hypoxia across many solid cancers (Horsman & Overgaard, 2016). The majority of solid tumours, even as small as 1-3 mm in diameter, can contain hypoxic fractions of up to 30% (Moulder & Rockwell, 1984). Consequently micro-regional areas exist

within the tumour that are glucose and energy deplete, with high lactate and acidity levels (Sorensen & Horsman, 2020).

Hypoxia in solid tumours is a negative prognostic indicator as it predicts for disease progression and metastasis and confers resistance to drug and radiation treatments (Shannon, Bouchier-Hayes, Condron, & Toomey, 2003). For example, in a meta-analysis of head and neck cancer patients receiving (chemo)radiotherapy, the hypoxic fraction (measured using Eppendorf electrodes) was adversely associated with loco-regional control and 5-year survival. This was independent of other prognostic indicators (Nordsmark et al., 2005).

4.1 Acute and chronic hypoxia

Chronic hypoxia is defined as a region of tumour that experiences an oxygen partial pressure < 10 mmHg for a prolonged period of time. The hypoxia as described by Thomlinson and Gray is often termed “diffusion-limited hypoxia”. It occurs at the limit of oxygen diffusion between blood vessels and tumour cells (up to 180 μm depending on the oxygen concentration in blood plasma). Chronic hypoxia can last from hours to days, and this is sufficiently long enough to lead to gene expression alterations, such as HIF-1 activation (C. T. Lee, Boss, & Dewhirst, 2014).

Tumour microvasculature also tends to be primitive and disorganised compared to the normal host vasculature (partly as a response to hypoxia), further contributing to the oxygen deficit. In addition to the inefficient vascular organisation, other factors that contribute include variations in red blood cell (RBC) transit through vessels, arterio-venous shunts, and O_2 demand exceeding supply (Rickard, Palmer, & Dewhirst, 2019). Chronic hypoxia can thus result from hypoxaemic hypoxia, due to anaemia, which results in low-oxygen content in the blood supplying the tumour (C. T. Lee et al.).

In 1979, it was hypothesised that acute or perfusion-limited hypoxia may develop due to fluctuations in tumour blood flow. Using a skin-fold window chamber tumour model, Yamaura and Matsuzawa demonstrated that cyclic hypoxia could occur over periods of a few minutes following irradiation (Yamaura & Matsuzawa,

1979). Brown showed that this could also occur on a timescale of several hours using an EMT6 tumour model (Brown, 1979). Acute (intermittent or cycling) hypoxia is therefore a dynamic process, caused by transient variations in tumour perfusion with fluctuations above and below the 10 mmHg pO_2 threshold for hypoxia (Almendros & Gozal, 2018; Chaplin, Trotter, Durand, Olive, & Minchinton, 1989).

Figure 4.1 illustrates the difference between diffusion-limited (chronic) and perfusion-limited (acute) hypoxia.

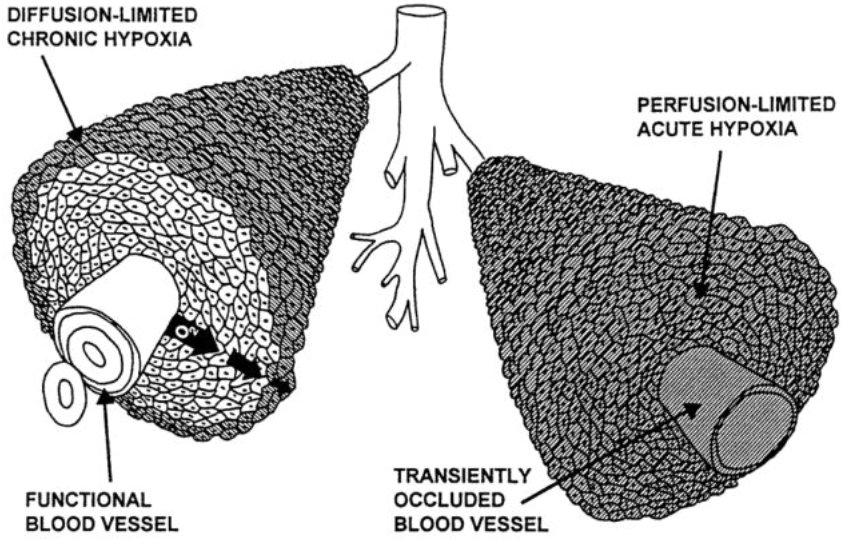

Figure 4.1 Diagrammatic representation of tumour showing the spatial relationship of hypoxic cells to tumour blood vessels. The illustration on the left shows cells growing around a vessel from which oxygen and nutrients are received, and the development of an oxygen gradient with the furthermost cells being chronically hypoxic. In contrast, on the illustration on the right, there is acute hypoxia due to interruption of blood flow through the vessel (Image reproduced from Horsman, 1998)

It is now understood that the tumour microenvironment is in constant flux, with cell subpopulations exposed to constant changes in nutrients and oxygen. Perfusion-limited hypoxia can occur due to intermittent and unstable blood flow within the tumour microvasculature, due to its random and disorganised structure with vessels of variable diameter (Thomlinson, 1977). This is further compounded by the increased metabolic demand of tumour cells. Lanzen et al observed cycling hypoxia occurring up to 130 μm from a microvessel, which is approaching

the diffusion limit of oxygen (Lanzen et al., 2006). Panek et al conducted a study demonstrating that intrinsic susceptibility MRI (IS-MRI) can be used to image cycling oxygenation by measuring changes in paramagnetic deoxyhaemoglobin in xenograft and patient tumours (Panek et al., 2017). These variations occur over minutes to days, are irregular and unpredictable, and contribute to radioresistance (Matsumoto, Yasui, Mitchell, & Krishna, 2010). HIF-1 activation has also been shown to occur as a consequence of cycling hypoxia both *in vitro* and *in vivo*. This upregulation is more pronounced when cells are exposed to cycling hypoxia compared to chronic hypoxia. This may relate to the fact that the process hypoxia-reoxygenation results in free radical formation, which then stabilises HIF-1 (C. T. Lee et al., 2014).

However, the principle that hypoxia can be characterised as either acute or chronic is considered to be over simplistic. There are other parameters that need to be considered, such as nutrient depletion, pH changes and tumour interstitial pressure, which influence radiation response. For example, high interstitial pressure can compromise perfusion of leaky microvasculature (Horsman, Sorensen, Busk, & Siemann, 2021; C. T. Lee et al., 2014).

4.2 Hypoxia and response to radiation

Typically, radiation doses need to be 2.5-3 times higher under hypoxia compared to normoxia, to induce the same level of damage (Berry, Hall, & Cavanagh, 1970; Sorensen & Horsman, 2020). The “oxygen effect” describes the increased sensitivity of cells to IR-induced DNA damage when oxygen concentration increases. For this to occur, oxygen should be present at the time of, or within milliseconds of IR (West & Slevin, 2019). Therefore, the presence of hypoxia in tumours also represents an opportunity for therapeutic strategies to enhance the sensitivity of these resistant cells to treatment and improve patient outcome. Over the last 50 years, considerable effort has been made to identify strategies to abrogate hypoxia-induced radiation resistance. Even with pre-clinical and clinical results showing benefit of several approaches, the only one that has been adopted in clinical practice is the hypoxic cell radiosensitiser Nimorazole, which is used in the treatment of head and neck cancers in Denmark and Norway (Overgaard et al., 1998).

There is compelling evidence that tumour hypoxia represents a significant impediment to the effectiveness of cancer therapy. The biological effect of ionising radiation is influenced by the amount of molecular oxygen present, with cells exhibiting radioresistance under hypoxia.

It is assumed that the mechanism of the oxygen effect occurs at the level of free radicals. Ionising radiation leads to the production of free radicals, which cause DNA strand breaks. These radicals are oxidised by oxygen, rendering the damage permanent. Conversely, in the absence of oxygen, DNA radicals are reduced, thereby restoring DNA to its original structure. Therefore radiation-induced DNA damage is significantly abrogated when molecular oxygen is depleted, leading to the radioresistant phenotype. Furthermore, hypoxia triggers alterations in DNA repair and cell survival pathways, resulting in the cellular radioresistant phenotype. Stabilisation and nuclear translocation of HIF-1α leads to transcription of several genes including VEGF and Glut-1, which enables cells to adapt to hypoxia, and tend towards a more malignant phenotype (Xiang & Semenza, 2019 2010).

4.3 Strategies to manage hypoxia

Numerous attempts have been made to identify means by which tumour hypoxia can be overcome or reversed. Tumour hypoxia may theoretically be abrogated by increasing the oxygen delivery or by decreasing the oxygen consumption rate (OCR) by tumour cells (thereby increasing oxygen retention). Most studies have focused on improving oxygen delivery (Ashton, McKenna, Kunz-Schughart, & Higgins, 2018).

Strategies to increase oxygen delivery tested in phase III clinical trials have included hyperbaric oxygen, carbogen (98% oxygen + 5% carbon dioxide), nitroimidazoles (such as nimorazole and misonidazole), nicotinamide (a vasoactive vitamin B analogue), artificial haemoglobins, haemoglobin modifiers, and hypoxia-activated prodrugs (tirapazamine).

Most have not succeeded due to multifactorial reasons; unacceptable drug toxicity, limited efficacy, practical challenges of treatment administration, and the

absence of predictive biomarkers (Graham & Unger, 2018). An additional setback is the challenge of delivering a drug at an adequate concentration to hypoxic tumour regions which are poorly vascularised (Ashton et al., 2018).

One of the other major drawbacks of prior trials was that prior to patient enrolment, there was no screening to identify tumour hypoxia. In those studies where imaging or biopsy-based methods were used to identify hypoxic tumours, response rates were higher as the trial was able to identify a patient cohort that could benefit (Ashton et al., 2018).

4.3.1 Increasing oxygen delivery

Historically, the main approach to overcoming hypoxia was to increase oxygen delivery to tumours during radiation. Hyperbaric oxygen-breathing, hyperthermia, blood transfusions and erythropoietin administration were employed to enhance tumour oxygenation.

Hyperbaric oxygen therapy involves inhaling 100% oxygen under elevated pressure, resulting in increased systemic oxygen tension. Hyperthermia leads to blood vessel dilatation via local application of heat. Preclinical studies have shown that heating tumours to 43˚C can improve response to radiation, partly attributed to the direct effect of heat, as well as inhibition of DNA repair (Horsman & Overgaard, 2007). Carbogen (consisting of 95% oxygen and 5% carbon dioxide) has also been utilised and combined with nicotinamide (a vasodilator and inhibitor of poly ADP-ribose polymerase I), which has been shown to offset hypoxia. Despite positive effects on local control in preclinical studies, clinical investigation in combination with accelerated radiotherapy have yielded conflicting results (Janssens et al., 2012).

Clinical trials of red blood cell infusion have not been proven to alleviate tumour hypoxia or improve outcomes in patients (Hoff et al., 2011). Furthermore, the combination of erythropoietin (EPO) with radiotherapy for head and neck cancers resulted in a negative impact on locoregional control and survival, likely due to the fact the erythropoietin receptor is also expressed on squamous cell cancer cells, and EPO is also a tumour growth factor (Henke et al., 2003). Additional haemoglobin-related strategies include the use of artificial blood substitutes such

as perfluorocarbons, small particles that have a greater oxygen-carrying capacity than haemoglobin. In contrast to the sigmoidal oxygen dissociation curve, perfluorocarbons exhibit a linear relationship between oxygen partial pressure and oxygen content. They have shown an effect in preclinical studies but have not yet been tested in clinical trials (Horsman et al., 2021; Secomb, Hsu, & Dewhirst, 2004).

Another strategy for counteracting hypoxia is to reduce cellular oxygen consumption rate (OCR) using drugs such as metformin and atovaquone (mitochondrial complex inhibitors). The rationale is that this reduces the oxygen consumption rate, increases the oxygen diffusion distance, and thereby alleviates tumour hypoxia. Mitochondrial complex inhibitors have demonstrated a radiosensitising effect in murine xenograft models, and a recent clinical study demonstrated that atovaquone is able to decrease hypoxia in patients with non-small cell lung cancer (Chevalier et al., 2020; Skwarski et al., 2021).

4.3.2 Hypoxic cell radiosensitisers

Oxygen mimetics work by replacing oxygen in the chemical reactions required to fix radiation-induced DNA damage (Spiegelberg et al., 2019). In the 1970s, it was demonstrated that 2-nitroimidazole compounds, such as misonidazole were selective for hypoxia cells and able to simulate the radiochemical effects of oxygen. Nitroimidazoles are a group of drugs with high electron affinity that mimic the effect of oxygen by reacting with DNA free radicals. Despite an observed oxygen-enhancement ratio (OER) of 1.5-2.0 *in vitro* and *in vivo*, outcomes form clinical trials showed limited clinical benefit, and remain inconclusive (Minsky & Leibel, 1989; Simpson et al., 1989). Effective drug doses were found to cause peripheral neuropathy, the main factor precluding clinical use. A later Danish trial with a similar drug, Nimorazole, demonstrated a benefit in local control and overall survival, and is used in the clinical setting in Denmark (Overgaard et al., 1998). Another drug from this group, Etanidazole, was tested in a clinical trial but did not improve outcomes (D. J. Lee et al., 1995).

4.3.3 Hypoxic cell cytotoxins

One approach to targeting hypoxia is the use of bioreductive prodrugs that are activated by cellular reductases in hypoxic tissue, forming DNA-reactive

cytotoxins (Spiegelberg et al., 2019). The most clinically advanced agent is tirapazamine, which is activated under moderate hypoxia, and forms a free radical that leads to DNA single- and double-strand breaks and base damage (Wang et al., 2018). Tirapazamine showed promising results in early clinical trials, but no benefit was observed in Phase III testing in patients with head and neck and lung cancers treated in combination with radiotherapy and platinum chemotherapy. One showed no survival benefit, and the other was terminated early due to increased mortality in the tirapazamine arm (Choi & Yu, 2015; Rischin et al., 2010; Williamson et al., 2005). Prospective studies are required to identify plasma or imaging biomarkers which may be useful in identifying a subset of patients which may benefit from this drug (Rischin et al., 2010).

Another strategy is the use of small molecule inhibitors of molecular targets involved in hypoxic cell survival. Recent research is focused on the inhibition of the hypoxia-inducible factor 1 (HIF1), the unfolded protein response (UPR) and mTOR pathways. The majority of molecularly targeted agents have been 'repurposed' from other applications, and have low selectivity for hypoxic cells (Wilson & Hay, 2011). Both methods have the limitation of drug penetration of poorly perfused hypoxic tissues.

4.3.4 Radiation-based methods

An alternative strategy to eliminating hypoxic cells is to overcome this with radiation by increasing dose to these areas or "dose painting". The limitation to this approach is accurate identification of such areas, and the fact that tumour hypoxia tends to be dynamic rather than static. PET studies using the tracer [18F] fluoro-misonidazole in head and neck cancer patients have shown variable uptake between scans, although other studies have shown consistent and reproducible uptake over time. In addition, there is uncertainty regarding the degree of radiotherapy dose escalation required to achieve a meaningful effect on response (Horsman & Overgaard, 2016).

4.4 Hypoxia and personalized therapy

Given the emerging techniques available for profiling individual tumours, the successful development of hypoxia-targeted agents will benefit from the potential

to prospectively identify hypoxic tumours. There is a requirement not just to detect, but to quantify hypoxia, as illustrated by a meta-analysis suggesting that outcomes in patients with head and neck cancer undergoing chemoradiotherapy were compromised in those with the most extensive hypoxia (Nordsmark et al., 2005). There is ongoing interest in the development of methods of hypoxia detection, particularly PET and MRI techniques, and serum-based diagnostics (D'Alonzo et al., 2021; Macklin et al., 2020; O'Connor, Robinson, & Waterton, 2019; Wilson & Hay, 2011).

4.5 Hydrogen peroxide and tumour hypoxia

In previously published studies, it was hypothesised that H_2O_2 delivered intratumourally leads to improved tumour oxygenation via the formation of H_2O and O_2 (Tokuhiro et al., 2010). Two studies have demonstrated superior tumour growth inhibition (including near complete responses) in murine tumours treated with intratumoural gel mixture comprising H_2O_2 and sodium hyaluronate, and single dose IR. Both studies involved mice bearing SCCVII tumours allocated to treatment groups including intratumoural H_2O_2 ± sodium hyaluronate ± single or five-fraction IR (Ryo Akima, 2016; Takaoka et al., 2017). Sodium hyaluronate was identified as the most effective agent to combine with H_2O_2 as it increased viscosity and stabilises H_2O_2, ensuring gradual degradation up to 24 hours post-injection. Consequently, due to the catalytic breakdown of H_2O_2 into H_2O and O_2, tumour oxygenation can be preserved for longer than if H_2O_2 was administered alone. In addition, injection of H_2O_2 alone has been shown to cause pain at the injection site in preliminary studies, and this was eliminated by the incorporation of sodium hyaluronate. Although H_2O_2 alone caused modest tumour growth delay, the greatest effect was seen when H_2O_2 and sodium hyaluronate was injected intratumourally immediately prior to IR (dose modifying factor 1.7-2.0) (Ryo Akima, 2016; Takaoka et al., 2017). Investigators used polarographic electrodes to measure tumour oxygenation before and after intratumoural H_2O_2 + sodium hyaluronate injection in murine SCCVII tumours. It was demonstrated that the oxygen partial pressure within the tumour was maintained at 90mmHg (compared to 40 mmHg with PBS injection alone) at up to 24 hours post injection (Tokuhiro et al., 2010).

Although cell culture is an important and necessary process in cancer research and drug discovery, *in vivo* methods enable modelling closer to the clinical context. *In vivo* experiments, by definition are undertaken on live animals, the main advantage being that this is a more physiologically relevant system (Holen, Speirs, Morrissey, & Blyth, 2017). *In vivo* research has to be justified in terms of overall benefit, whilst ensuring that animal welfare is protected and adhering to the 3 R's: reduction, replacement, and refinement. Nevertheless, it is the case that certain research questions are best answered by studying tumours growing *in vivo ("United Kingdom Co-ordinating Committee on Cancer Research (UKCCCR) Guidelines for the Welfare of Animals in Experimental Neoplasia (Second Edition)," 1998)*.

To address the hypothesis that intratumoural H_2O_2 leads to a reduction in tumour hypoxia, it was decided that an *in vivo* model was the most appropriate. Whilst it would be feasible to grow spheroids to a size where hypoxia was demonstrable, treat with H_2O_2 and stain with a hypoxia marker, the method of drug delivery and administered dose would not be directly comparable to the clinical setting. In this study, immunocompromised mice were engrafted with subcutaneous tumours derived from the human colorectal cancer cell line, HCT116. The *Foxn1* nude mouse was selected, as this strain has demonstrated effectiveness in modelling biological processes, as well as genetics and metastatic potential (Szadvari, Krizanova, & Babula, 2016).

4.6 Hypoxia perturbation in the HCT116 xenograft model

The HCT116 cell line was selected as it grows reliably *in vivo* and consistently demonstrates hypoxia. The initial experiment sought to establish whether tumour hypoxia could be altered by administering high flow oxygen to the animal as a "proof of principle". If confirmed, this would support the use of this model in investigating the role of H_2O_2 on tumour hypoxia. Three mice were included in this pilot experiment and the results of dual hypoxia marker staining and corresponding H&E staining of these tumours is illustrated in Figure 4.2.

In all 3 cases, CCI-103F adducts (red) represent the extent and distribution of hypoxia at baseline, and pimonidazole adducts (green) represent tumour hypoxia during hyperoxia. Areas stained yellow reflect overlap of both CCI-103F and pimonidazole adduct formation. The results are consistent between all 3 tumours and demonstrate that overall tumour hypoxia is reduced during hyperoxia (CCI-103F adduct detection is more extensive than for pimonidazole adducts). These results confirmed that hypoxia can be modified via oxygen administration to the animal in the HCT116 xenograft model.

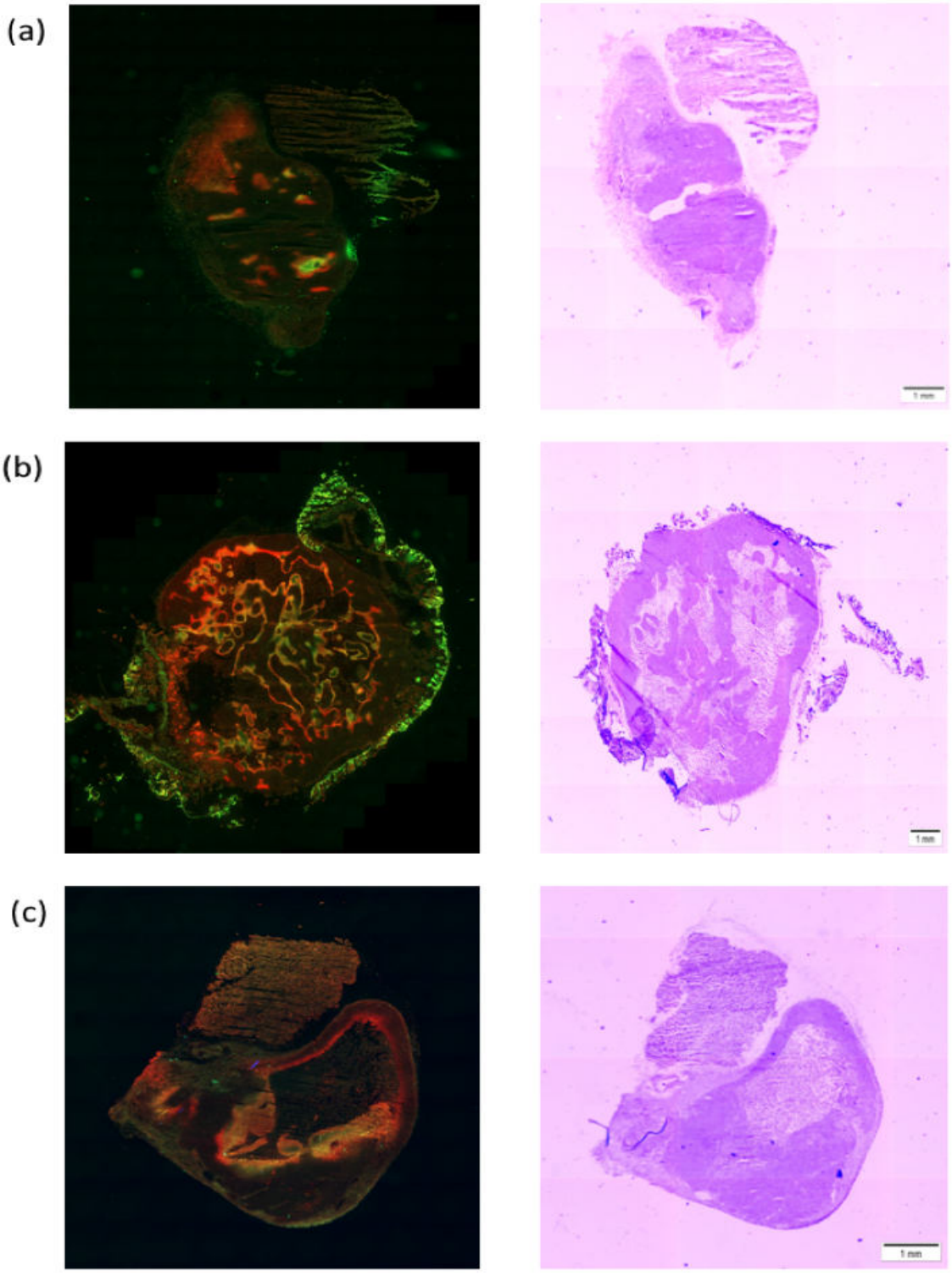

Figure 4.2 Three HCT116 xenografts ((a)-(c)) demonstrating dual hypoxia marker staining, showing CCI-103F adducts (red) at baseline, and pimonidazole adducts (green) during oxygen breathing for 5 minutes. Yellow staining indicates overlap of both CCI-103F and pimonidazole adducts. Corresponding H&E sections are shown in the right hand column (scale bar = 1mm).

4.7 Limitations of dual marker technique with pimonidazole and EF5

The effect of intratumoural H_2O_2 on tumour hypoxia at 3 time points (1, 6 and 24 hours) following injection was investigated. A dual hypoxia marker technique using two different 2-nitroimidazoles (EF5 and pimonidazole) was selected. HCT116 xenografts were treated with intratumoural H_2O_2, each of which was paired with a control tumour (injected with the carrier compound sodium hyaluronate) of approximately equal size.

At each of the 3 timepoints, comparing injected to non-injected tumours, there was no difference observed in the extent of hypoxia present in the xenografts. During the staining and imaging process, it became apparent that there was a degree of "crossover" between the fluorescence emission spectra between EF5 adducts (secondary antibody conjugated to Cyanine 3) and pimonidazole adducts (conjugated to FITC fluorophore), as illustrated in Figure 4.3 below. Therefore, when analysing the composite images, it was not possible to reliably distinguish the EF5 staining pattern from that of pimonidazole.

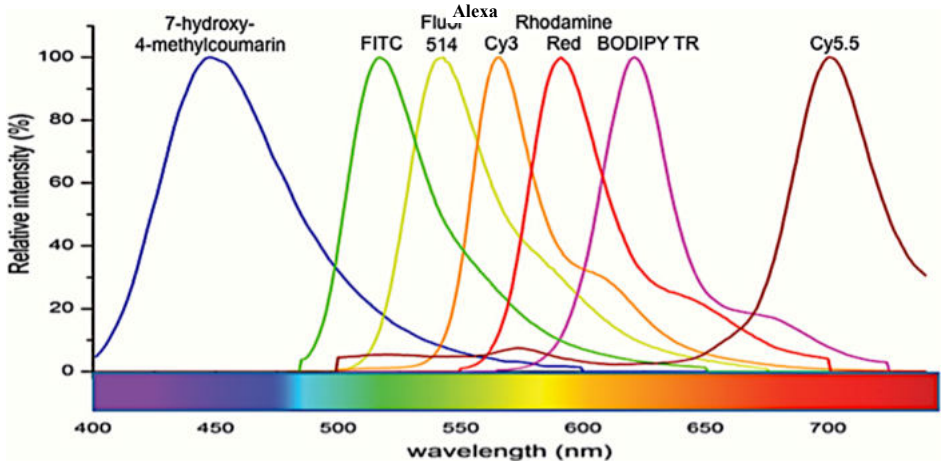

Figure 4.3 Emission spectra of common fluorophores (Chen Y, 2015). Overlap is seen between the wavelengths of FITC (Pimonidazole) in green and Cy3 (EF5) in orange.

Another noticeable feature of the HCT116 xenografts is that there is discernible intertumoural heterogeneity between tumours regarding the extent and pattern of hypoxia staining observed. This finding, combined with the crossover effect of the

fluorophores, limited the accurate comparison of H_2O_2-injected and control tumours in relation to hypoxia quantification.

Figure 4.4 shows a size-matched pair of HCT116 xenograft tumours (a) and (b) with baseline hypoxia (left), followed by administration of a second hypoxia marker 1 hour following injection with H_2O_2 + sodium hyaluronate. Between each pair of xenografts ((a) and (b)), the order of delivery of the hypoxia markers was varied, to remove this as a confounding factor. The composite images (far right column) shows overlap of orange (EF5) adducts and green (pimonidazole) adducts, indicating no change in the extent and pattern of tumour hypoxia following injection. Similarly, Figure 4.5 shows almost exact overlap in EF5 and pimonidazole adduct formation following injection of sodium hyaluronate alone into two xenografts (a) and (b).

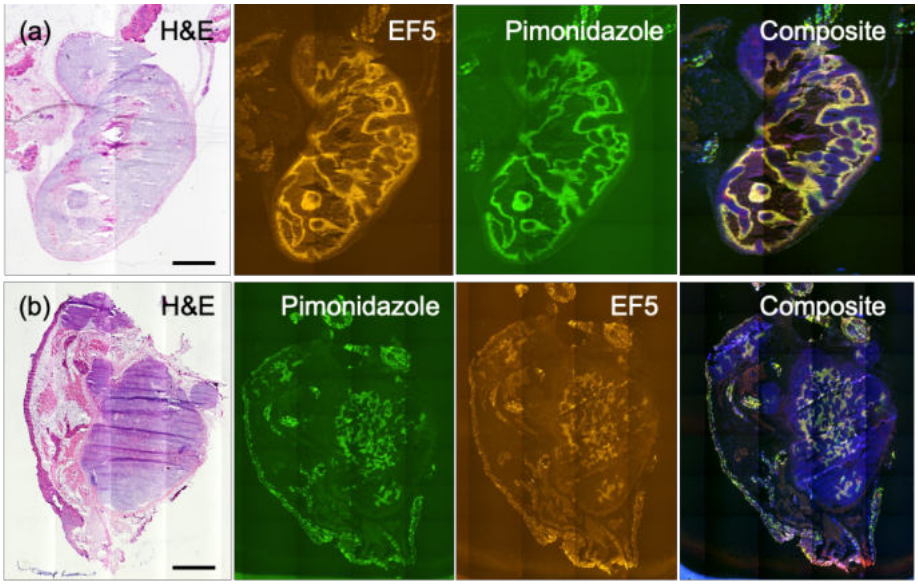

Figure 4.4 Dual marker hypoxia staining of HCT116 tumours injected with H_2O_2 + sodium hyaluronate gel. Representative microscope images of two xenografts (a) and (b) showing H&E, EF5 adducts (orange), pimonidazole adducts (green), and composite fluorescence images. Composite images demonstrate overlap of EF5 and pimonidazole adduct formation (yellow). Scale bar = 2mm

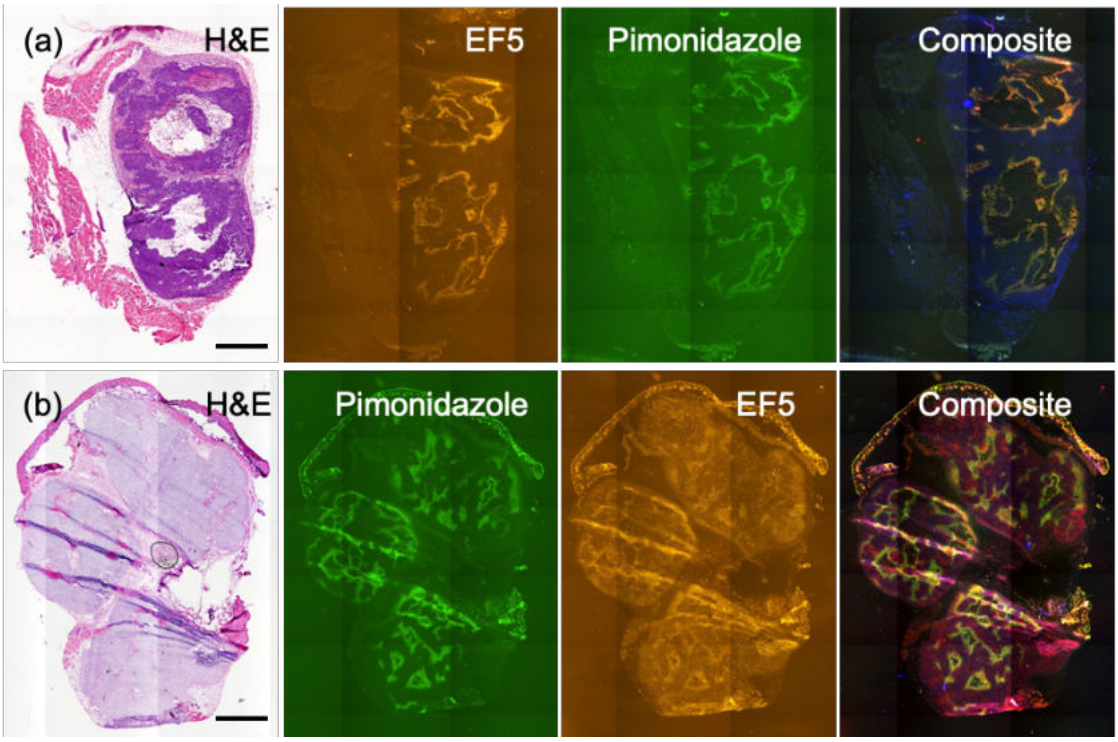

Figure 4.5 Dual marker hypoxia staining of HCT116 tumours injected with sodium hyaluronate. Representative microscope images of two xenografts (a) and (b) showing H&E, EF5 adducts (orange), pimonidazole adducts (green), and composite fluorescence images. Composite images demonstrate overlap of EF5 and pimonidazole adduct formation (yellow). Scale bar = 2mm

Accurate interpretation was not possible due to overlap in the emission spectra, so it was not possible to distinguish whether intratumoural H_2O_2 injection had an impact on hypoxia in these xenografts.

4.8 Effect of intratumoural H_2O_2 on tumour hypoxia up to 24 hours post injection

Given the problems encountered with interpretation of results using a dual hypoxia technique, a refined study was performed in which pairs of mice with HCT116 tumours matched for size were injected either with H_2O_2 + sodium hyaluronate, or sodium hyaluronate alone.

Pimonidazole was administered at three timepoints following intratumoural injection; 1, 6 and 24 hours. Four animals were assigned to each cohort, as detailed in Table 4.1 below.

Timepoint of hypoxia measurements (hours)	No. Mice	Sequence					
1	2	No IT* injection	*1 hr*	Pimonidazole	*1 hr*	IV Hoechst	Necropsy
	2	H_2O_2 + Sodium Hyaluronate	*1 hr*	Pimonidazole	*1 hr*	IV Hoechst	Necropsy
6	2	No IT injection	*6 hrs*	Pimonidazole	*1 hr*	IV Hoechst	Necropsy
	2	H_2O_2 + Sodium Hyaluronate	*6 hrs*	Pimonidazole	*1 hr*	IV Hoechst	Necropsy
24	2	No IT injection	*24 hrs*	Pimonidazole	*1 hr*	IV Hoechst	Necropsy
	2	H_2O_2 + Sodium Hyaluronate	*24 hrs*	Pimonidazole	*1 hr*	IV Hoechst	Necropsy

Table 4.1 Experimental schema for investigation of effect intratumoural H_2O_2 on tumour hypoxia in HCT116 xenograft tumours. Tumours were treated in pairs matched for tumour size (400 mm^3 approx.) with determination of hypoxia at 3 timepoints. *IT= intratumoural

Pimonidazole adducts and Hoechst 33342 uptake (with accompanying H&E images) are shown in representative tumour pairs from the 1-, 6-, and 24-hour cohorts in Figures 4.6- 4.8 respectively.

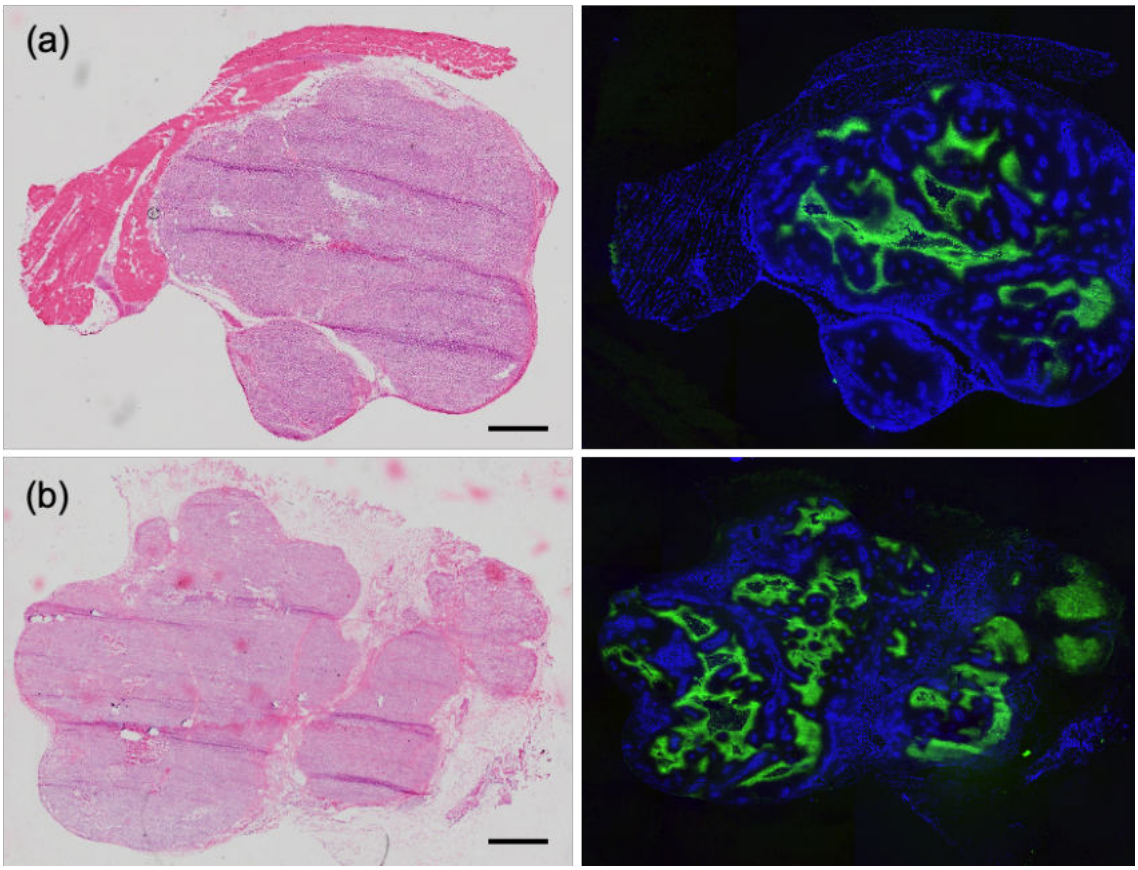

Figure 4.6 Hypoxia staining in HCT116 xenografts (1-hour timepoint) Representative example of H&E sections and accompanying fluorescence images of pimonidazole adducts (green) and Hoechst 33342 uptake (blue) in (a) non-injected control and (b) H_2O_2-injected tumours. Scale bar = 2mm

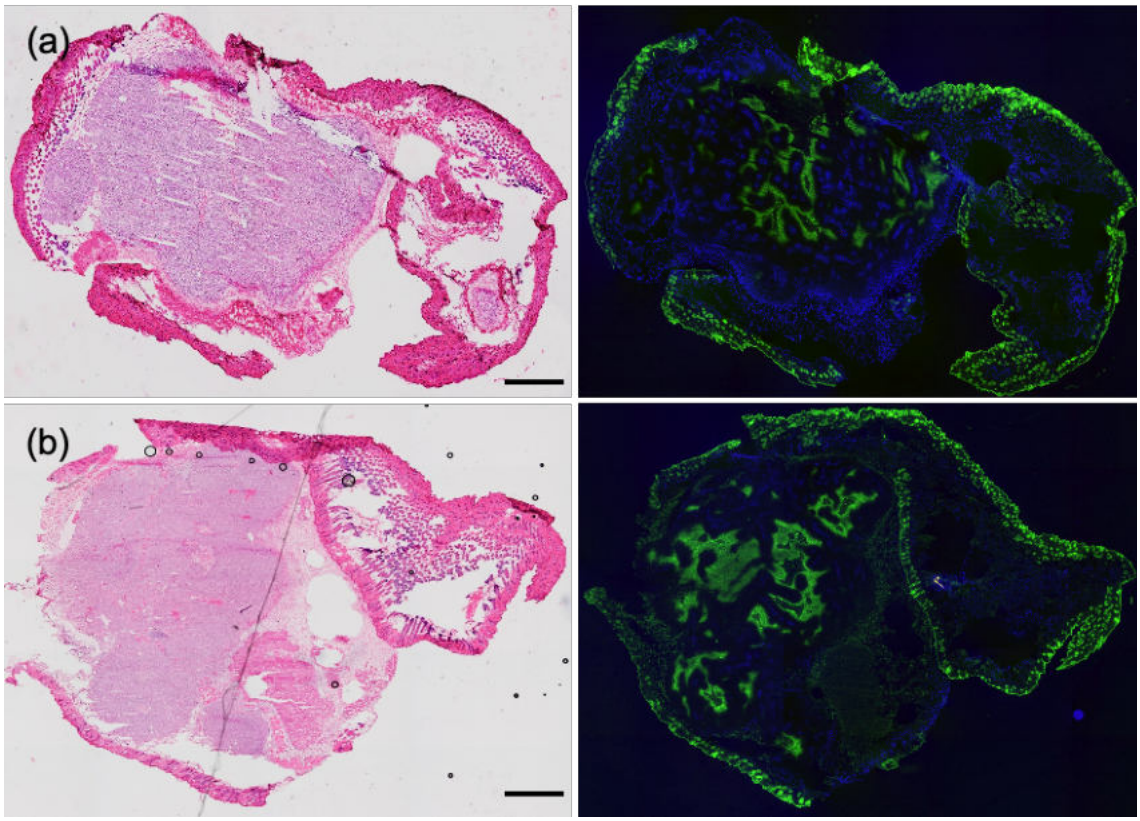

Figure 4.7 Hypoxia staining in HCT116 xenografts (6-hour timepoint) Representative example of H&E sections and accompanying fluorescence images of pimonidazole adducts (green) and Hoechst 33342 uptake (blue) in (a) non-injected control and (b) H_2O_2-injected tumours. Scale bar = 2mm

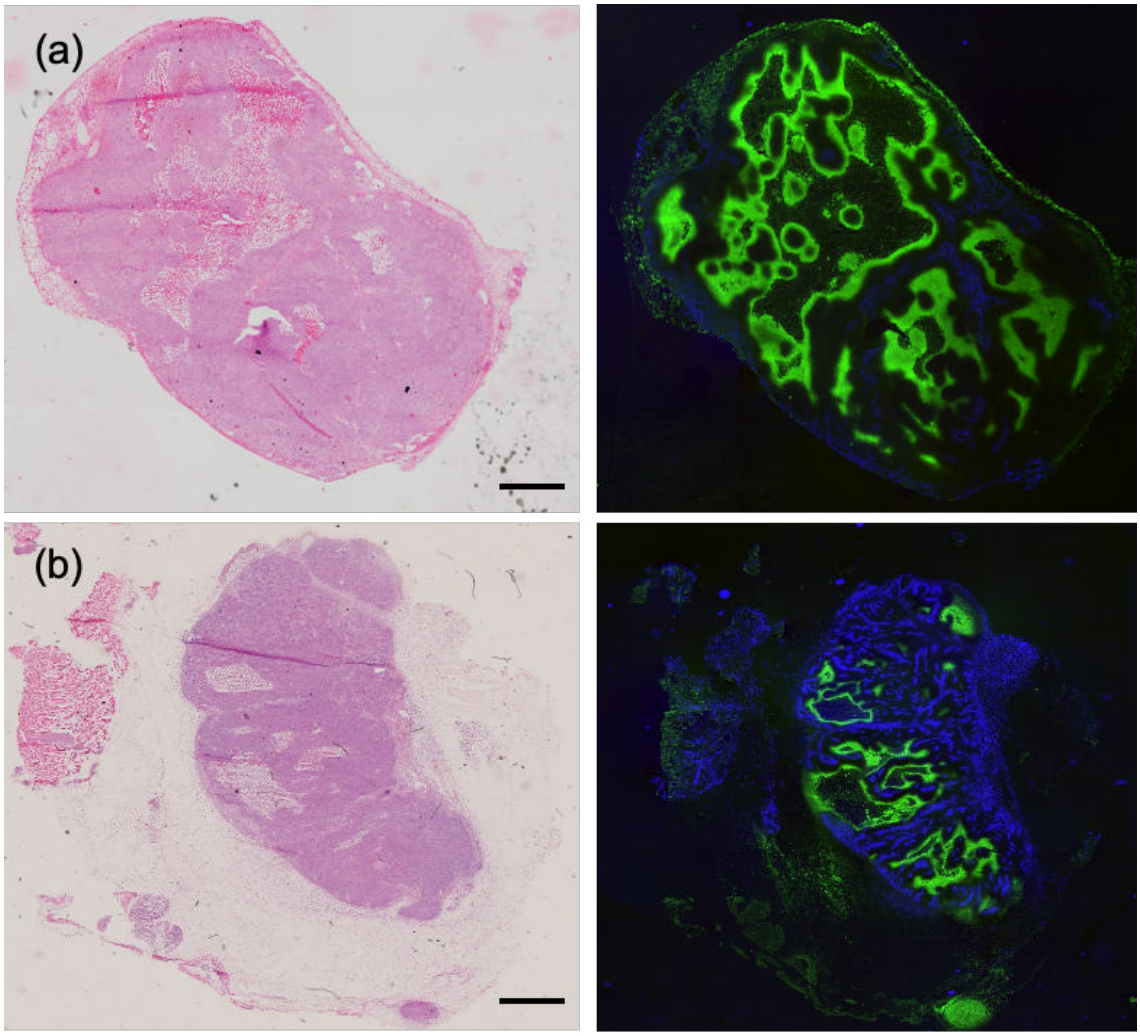

Figure 4.8 Hypoxia staining in HCT116 xenografts (24-hour timepoint). Representative example of H&E sections and accompanying fluorescence images of pimonidazole adducts (green) and Hoechst 33342 uptake (blue) in (a) non-injected control and (b) H_2O_2-injected tumours. Pimonidazole administered 24 hours following intratumoural KORTUC injection. Scale bar = 2mm

Pimonidazole staining was quantified (calculated as percentage of tumour area stained), and the results compared between those injected with H_2O_2 + sodium hyaluronate vs. sodium hyaluronate alone. An example of tumour contouring, with applied thresholds for detection of pimonidazole adducts and Hoechst 33342 uptake is shown in Figure 4.9 (a). The table in Figure 4.9 (b) summarises the percentage staining according, showing no difference in extent of hypoxia (pimonidazole adducts) and perfusion (Hoechst 33342 uptake) in the control versus H_2O_2-injected xenografts.

(a)

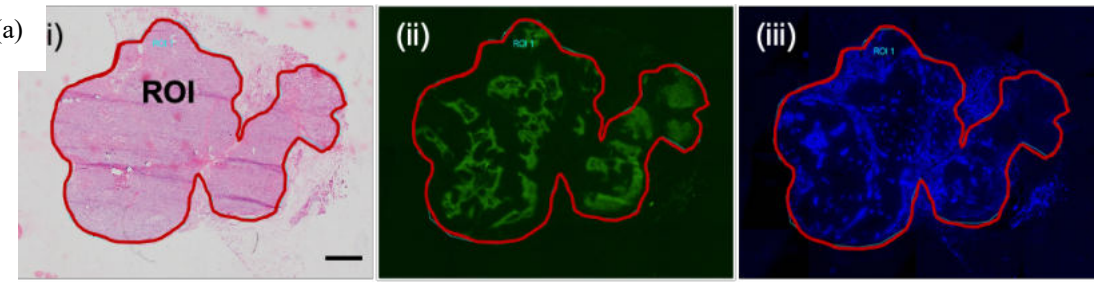

(b)

Pair number (mouse)	Pimonidazole (%)		Hoechst (%)	
	Control	*KORTUC*	*Control*	*KORTUC*
1	23.1	15.3	13.7	12.0
2	18.9	16.8	13.9	N/A
3	22.4	19.9	N/A	10.5
4	16.3	23.8	15.87	N/A
Mean	**20.2**	**18.9**	**13.0**	**14.9**

Figure 4.9 Quantification of pimonidazole adduct formation and Hoechst 33342 uptake (a) Example of (i) H&E staining, and fluorescence images of (ii) pimonidazole adducts and (iii) Hoechst 33342 uptake in an HCT116 xenograft, showing the delineated tumour area used to quantify each histological marker as a percentage of the whole tumour area. Scale bar = 2mm (b) Quantitative summary of the mean pimonidazole adduct formation and Hoechst 33342 uptake (%) in control versus H_2O_2-injected tumours

In view of the small size of the tumours and the resultant uncertainty regarding accurate drug delivery within the tumour, ultrasound (US) guidance was employed to confirm intratumoural injection of H_2O_2 ± sodium hyaluronate. An additional benefit of this method was to allow serial imaging of the resultant oxygen microbubbles following injection, and to record how long they persisted within the tumour.

As outlined in Section 2.2.5, anaesthetised mice were immobilised on a heated platform with an US probe secured in position over the tumour. Intratumoural drug delivery was achieved via a syringe mounted onto a mobile clamp. Once the needle was visualised on the US image entering the centre of the tumour, the drug was delivered over 10-15 seconds.

Figure 4.10 (a) to (e) details in sequence the needle tip entering the tumour, and in the case of H_2O_2 + sodium hyaluronate injection, followed by the formation of microbubbles throughout. On serial images, these microbubbles are seen to gradually disperse, but remained present at up to one-hour post-injection. Further imaging beyond this timepoint was limited by the duration of intraperitoneal anaesthesia used in this study. This injection technique was used to confirm injection in each animal, in the cohort of xenografts discussed in Section 4.9.

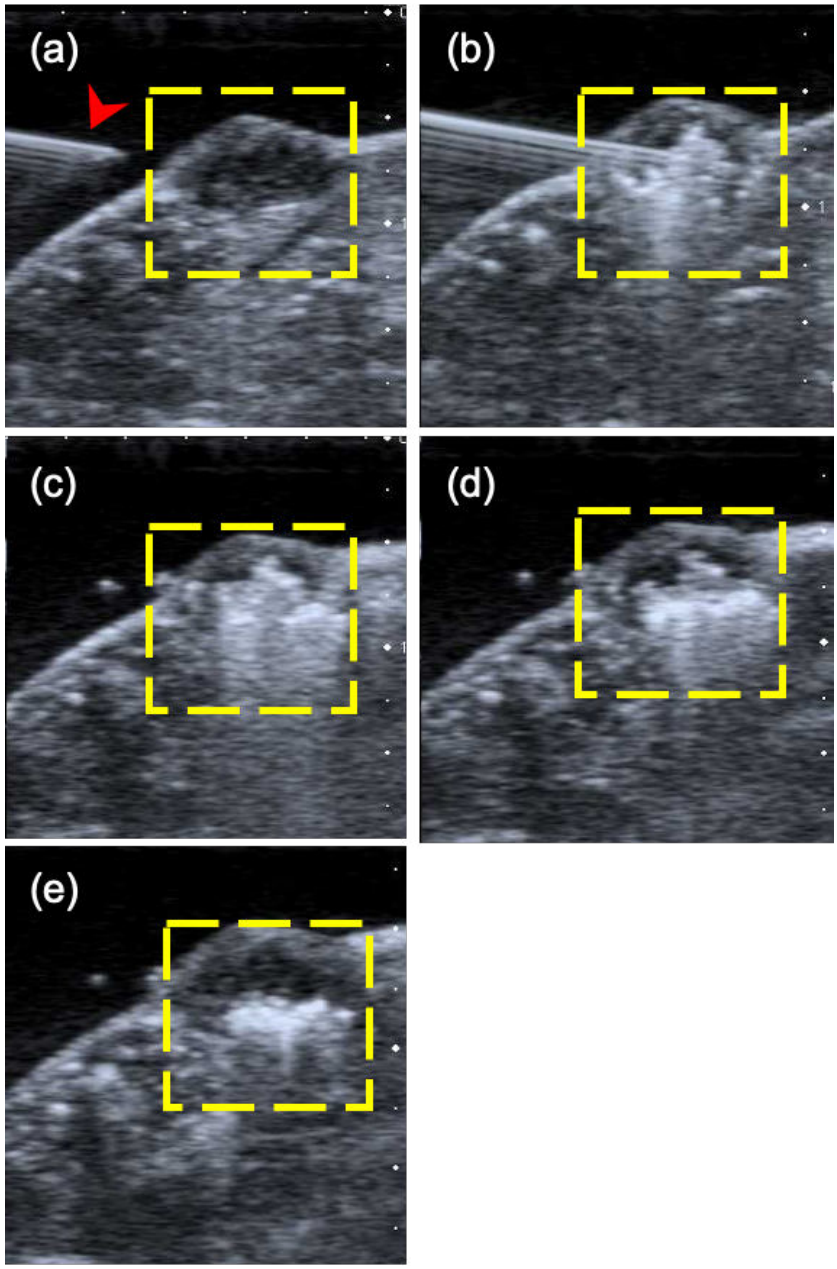

Figure 4.10 Sequence of US images depicting intratumoural KORTUC injection *in vivo*
Images (a) to (e) showing the needle entering the tumour (arrow), and oxygen microbubbles (white) visible within the tumour: (b) during injection and (c) 15 minutes (d) 30 minutes and (e) 1-hour post-injection.

4.9 Changes in tumour hypoxia 1 hour following H_2O_2 injection

Figures 4.11 and 4.12 show that intratumoural H_2O_2 injection leads to an overall reduction in tumour hypoxia in HCT116 xenografts (compared to non-injected controls and tumours injected with sodium hyaluronate) at one-hour post-injection.

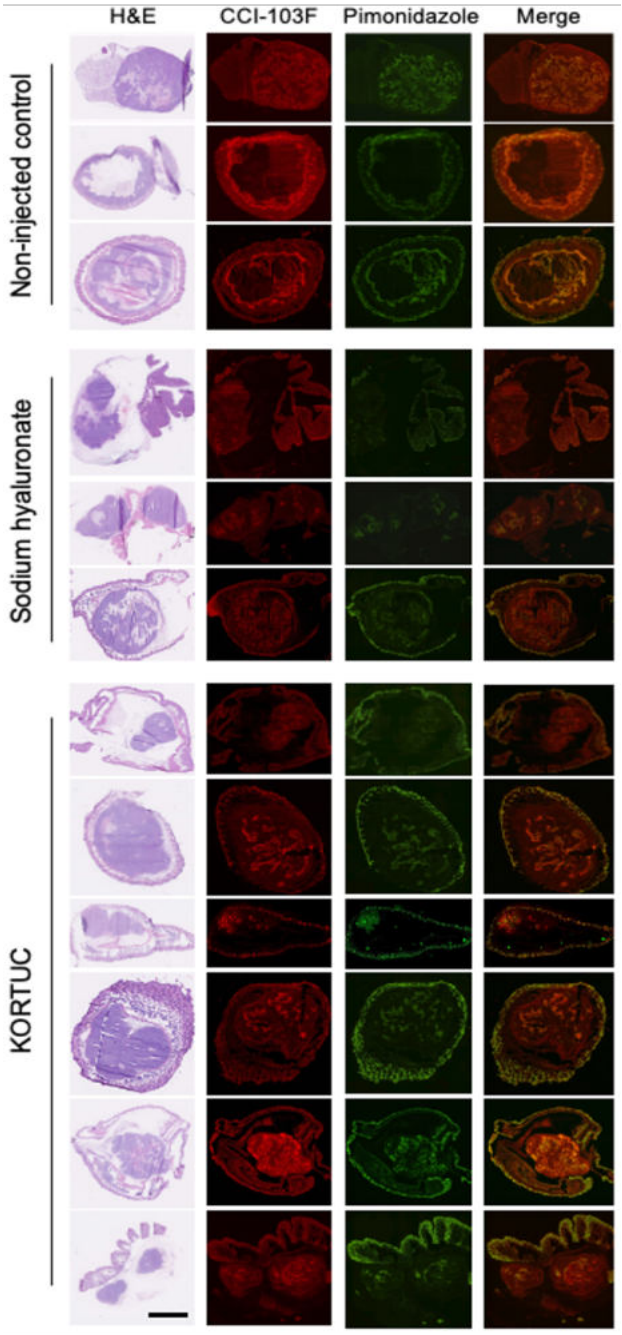

Figure 4.11 Fluorescence microscopy images of dual hypoxia marker staining in HCT116 xenografts
Ostenil = Sodium hyaluronate, KORTUC = H_2O_2 + sodium hyaluronate gel mixture. From left to right, H&E, CCI-103F adducts (red) indicating baseline tumour hypoxia, pimonidazole adducts (green) reflecting hypoxia 1 hour following intratumoural injection, and composite images. Scale bar = 2mm. In the composite images, yellow indicates overlap of both hypoxia markers. Tumours injected with KORTUC exhibit a reduction in hypoxia staining (from baseline) compared to Ostenil/Non-injected controls.

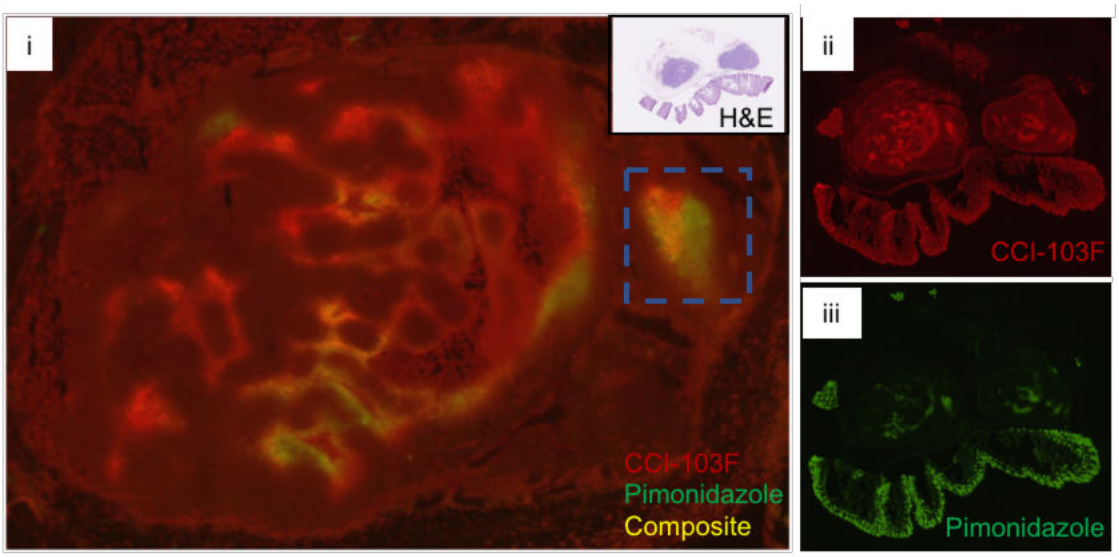

Figure 4.12 Representative fluorescence images demonstrating (i) relatively less hypoxia (green) than at baseline (red), in an HCT116 xenograft following H_2O_2 + sodium hyaluronate (KORTUC) injection. The inset, blue box represents a residual overlapping hypoxic region (yellow) between (ii) CCI-103F and (iii) pimonidazole adducts.

For each xenograft, staining for each hypoxia marker was quantified by first delineating a tumour region of interest (ROI), then using a thresholding technique to objectively quantify the extent of fluorescence (CellSens, Olympus Optical) expressed as a percentage of the tumour area. The method is illustrated in Figure 4.13.

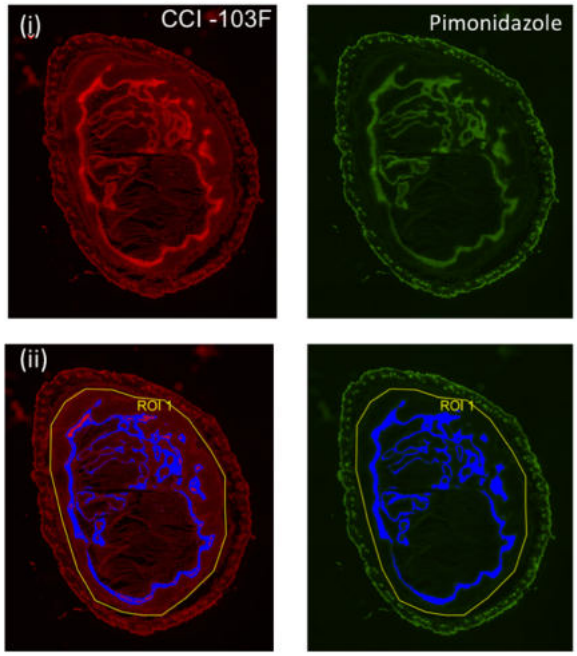

Figure 4.13 Example fluorescence images of CCI-103F and pimonidazole adducts (i), with accompanying regions of interest (ROI) (ii), used to determine percentage staining of each hypoxia marker (delineated in blue).

The quantitative data are shown in Table 4.2. Using Student's paired t-test, a significant (p=0.02) difference in pimonidazole versus CCI-103F adduct formation was found in the KORTUC-injected cohort, with no significant difference in the sodium hyaluronate (ostenil)-injected and non-injected groups (p=0.1 and 0.5 respectively). This result is summarised in Figure 4.14.

	% staining (of whole tumour)	
Tumour	**CCI-103F**	**Pimonidazole**
Non-injected control 1	20.4	15.0
Non-injected control 2	8.0	9.6
Non-injected control 3	12.7	15.0
OSTENIL 1	6.0	3.8
OSTENIL 2	7.7	4.2
OSTENIL 3	13.9	7.4
KORTUC 1	17.0	6.7
KORTUC 2	12.1	6.3
KORTUC 3	4.3	3.2
KORTUC 4	13.9	6.8
KORTUC 5	11.5	6.6
KORTUC 6	7.3	4.3

Table 4.2 Table summarising hypoxia quantification for each xenograft using region of interest (ROI), and according to treatment group. Ostenil = sodium hyaluronate, KORTUC = H_2O_2 + sodium hyaluronate gel mixture.

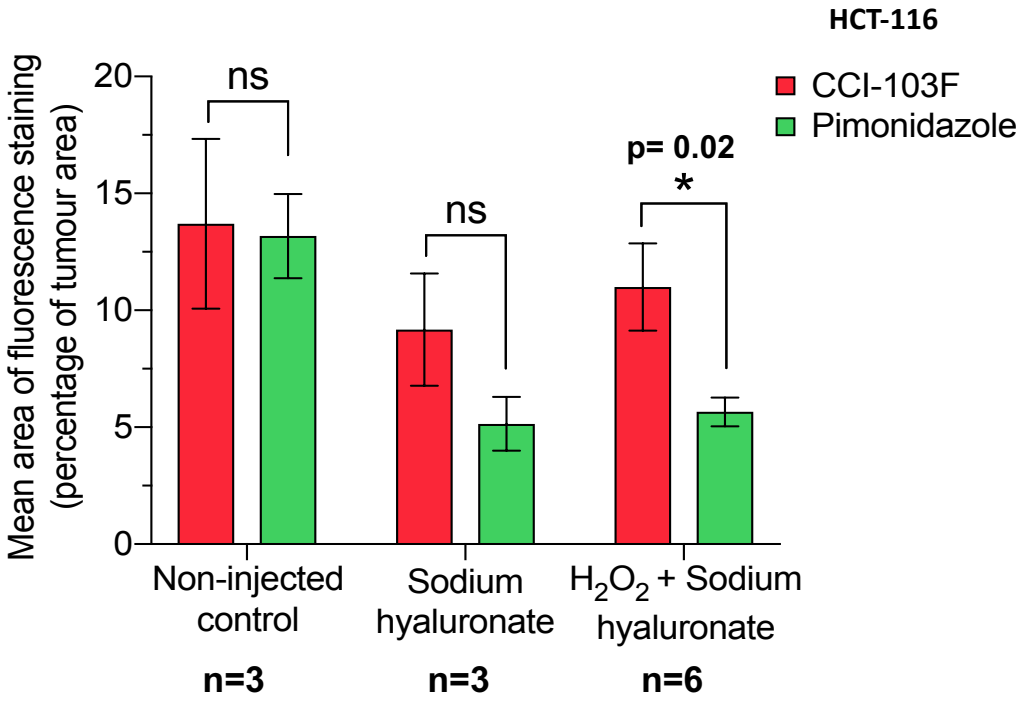

Figure 4.14 Bar graph showing fluorescence intensity values determined from the region of interest (ROI) in images shown in Figure 4.11. Student's paired t-test was performed to determine any statistical significance, 'ns' non-significant; '*' $p < 0.05$. Data are mean ± 1 SEM.

As shown in Table 4.2, hypoxia was also reduced compared to baseline in the Ostenil-injected tumours (n=3), but to a lesser extent than determined with KORTUC.

4.10 Effect of intratumoural H_2O_2 on tumour hypoxia in HN5 xenografts

Having demonstrated that intratumoural H_2O_2 results in a significant reduction in hypoxia adduct formation at 1-hour timepoint post-injection, this was further investigated in a second xenograft model using the HN5 cell line, a model established in our laboratory as forming hypoxic tumours in vivo.

This experiment included a larger cohort of mice treated within the same treatment groups (24 in total; 8 injected with H_2O_2 and 16 controls (either receiving no injection or injected with the control vehicle sodium hyaluronate).

Sections from each tumour are depicted in Figure 4.15 comparing hypoxia adduct formation pre- (CCI-103F) and post-treatment (pimonidazole), with composite images to look for mismatch between the two. Figure 4.16 shows representative tumours from each treatment group, and quantification of CCI-103F compared to pimonidazole adduct formation (Figure 4.16 (b)) revealed a significant reduction in H_2O_2 -injected xenografts compared to the control cohorts, in keeping with findings from HCT116 xenografts.

As observed in the HCT116 cohort, in HN5 tumours injected with sodium hyaluronate alone exhibited a non-significant reduction in percentage tumour hypoxia. It is feasible that sodium hyaluronate alone exerts an individual effect and contributes to the observed overall effect in the H_2O_2-injected tumours, however the mechanism is uncertain.

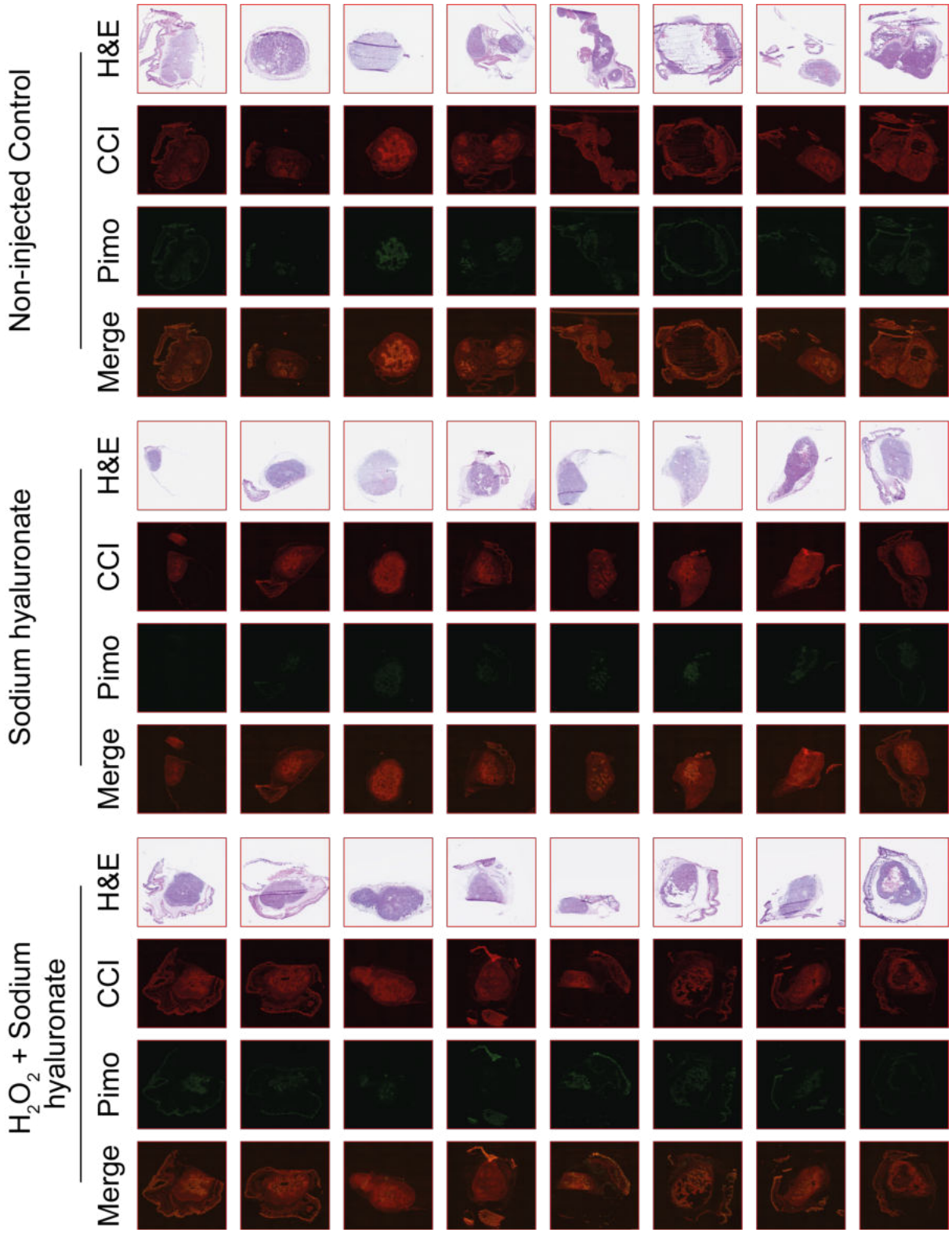

4.15 Fluorescence microscopy images of dual hypoxia marker staining in HN5 xenografts

According to treatment group (left hand column) from top to bottom; H&E, CCI-103F adducts (red) indicating baseline tumour hypoxia, pimonidazole adducts (green) reflecting hypoxia 1 hour following intratumoural injection, and composite images. In the composite images, yellow indicates overlap of both hypoxia markers.

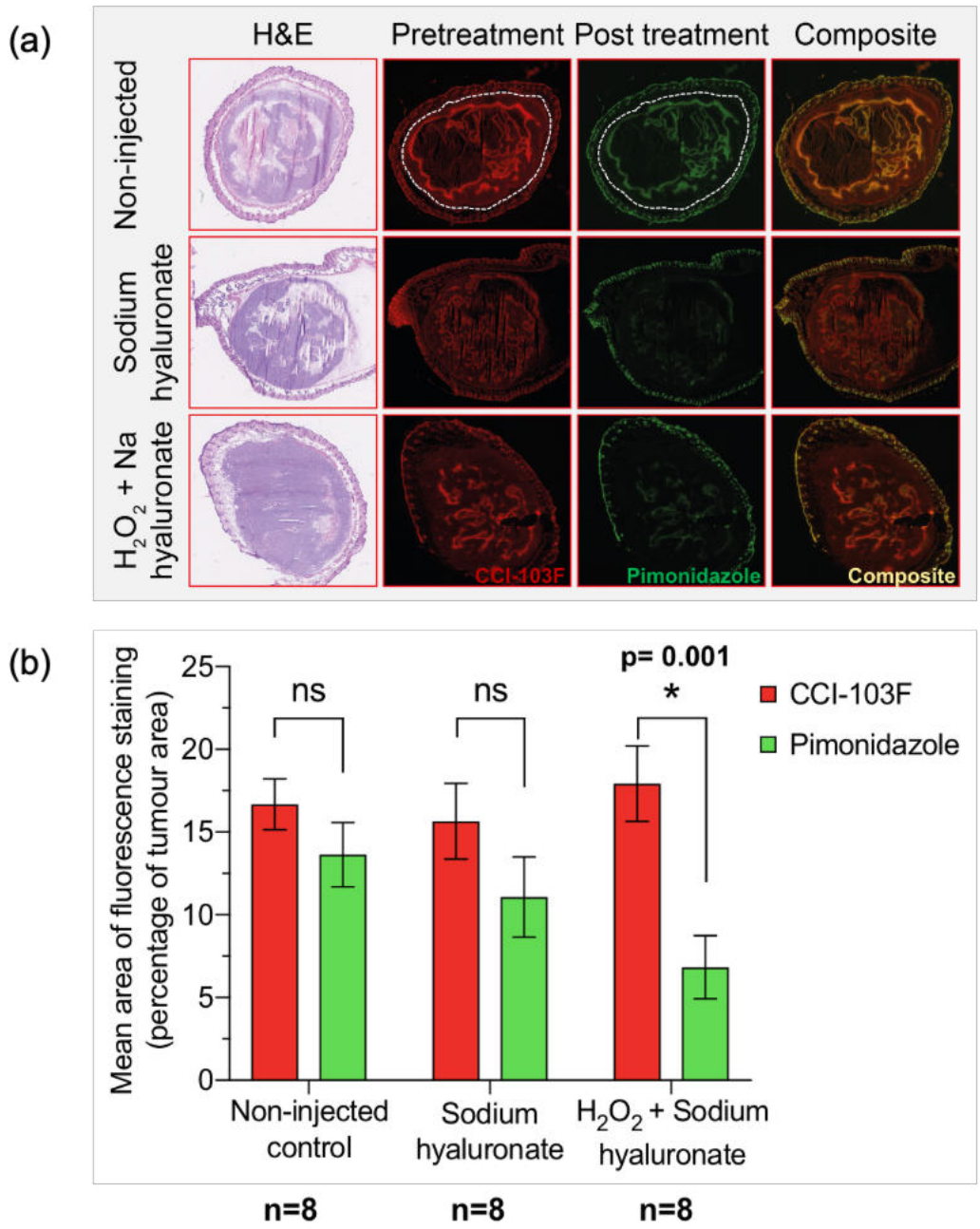

Fig 4.16 (a) representative sections of HN5 xenografts showing H&E images with corresponding fluorescence images, with CCI-103F (red) pre-treatment and pimonidazole (green) post-treatment. Composite images show hypoxia mismatch in H_2O_2 + sodium hyaluronate injected tumours, (b) Mean fluorescence intensity as quantified from the region of interest (ROI).

4.11 Discussion

These *in vivo* studies have highlighted the limitations of measuring hypoxia accurately in xenografts, especially when comparing two treatment cohorts. Although both HCT116 and HN5 consistently yield hypoxic tumours when grown as xenografts in mice, there is considerable intertumoural variation in the amount and pattern of hypoxia observed. Most tumours display a reticular pattern of hypoxia staining, whilst others form a “rim-core” pattern, with a necrotic tumour core. This means that although tumours can be matched for size macroscopically, at the microscopic level the appearances can differ markedly, even with careful and consistent tumour sectioning between samples. However, the experimental findings were consistent between xenografts formed from two cell lines, well-recognised to form hypoxic tumours, and with large enough sample sizes to draw meaningful conclusions.

Injection of H_2O_2 into tumours *in vivo* has been shown to significantly decrease tumour hypoxia at 1 hour following injection, which is relevant to the clinical scheduling of KORTUC injections relative to radiotherapy in the Phase I clinical trial. The observation of an apparent decrease in hypoxia following sodium hyaluronate injection alone is difficult to explain. A possible hypothesis is that it may relate to the viscosity of the compound, thereby impacting upon tumour stiffness and impeding delivery of pimonidazole to the tumour. There is no evidence in published literature to verify this, but hyaluronic acid within the extracellular matrix of some tumour types (e.g. gliomas and pancreatic tumours) has been shown to affect tumour interstitial pressure and stiffness (Jacobetz et al., 2013; Pogoda et al., 2017).

Overall, the main limitation of these findings is that they are demonstrated in only one xenograft model; hence this will need confirmation using at least one other cell line which reliably forms hypoxic tumours *in vivo*. Another useful technique would be to correlate the immunohistochemical findings with real-time imaging of tumours in situ, for example using multispectral opto-acoustic tomography (MSOT) ultrasound or MRI (Challapalli et al., 2017; Ghosh et al., 2020; O'Connor et al., 2019). Both measure changes in oxygenation of haemoglobin and have the advantage that they are non-invasive. This would also enable real-time

recording of temporal and spatial changes in tumour hypoxia. Such imaging techniques could be employed in animal studies, and oxygen-enhanced MRI (OE-MRI) may be useful in longitudinal monitoring of tumour response (although not applicable to assess acute response due to free radical production by H_2O_2 which influences the T1 relaxation time). This has been an important shortcoming in previous trials of hypoxia-alleviating therapies, which may explain why they have not led to changes in clinical practice. Stadlbauer et al used a novel blood oxygenation level dependent (BOLD) MRI approach with vascular architecture mapping (VAM), that could be integrated into standard clinical MRI protocols, to non-invasively assess tumour hypoxia in benign and malignant breast tumours. This approach led to improved characterisation of tumours and the identification of intratumoural heterogeneity (Stadlbauer et al., 2019).

In terms of clinical application, if this method of increasing oxygen delivery to tumours is confirmed to be successful, it has the potential to be utilised in several tumour types. For example, it may be applicable in head and neck tumours, which classically demonstrate hypoxia and are superficially located, and more deeper-seated tumours if injection can be performed under imaging control. In addition, it may be possible to combine this technique of oxygen delivery with brachytherapy treatments which utilises guiding tubes to deliver radiation sources to the tumour.

References

Almendros, I., & Gozal, D. (2018). Intermittent hypoxia and cancer: Undesirable bed partners? *Respir Physiol Neurobiol, 256*, 79-86. doi:10.1016/j.resp.2017.08.008

Alper, T., & Howard-Flanders, P. (1956). Role of oxygen in modifying the radiosensitivity of E. coli B. *Nature, 178*(4540), 978-979. doi:10.1038/178978a0

Ashton, T. M., McKenna, W. G., Kunz-Schughart, L. A., & Higgins, G. S. (2018). Oxidative Phosphorylation as an Emerging Target in Cancer Therapy. *Clin Cancer Res, 24*(11), 2482-2490. doi:10.1158/1078-0432.CCR-17-3070

Berry, R. J., Hall, E. J., & Cavanagh, J. (1970). Radiosensitivity and the oxygen effect for mammalian cells cultured in vitro in stationary phase. *Br J Radiol, 43*(506), 81-90. doi:10.1259/0007-1285-43-506-81

Brown, J. M. (1979). Evidence for acutely hypoxic cells in mouse tumours, and a possible mechanism of reoxygenation. *Br J Radiol, 52*(620), 650-656. doi:10.1259/0007-1285-52-620-650

Challapalli, A., Carroll, L., & Aboagye, E. O. (2017). Molecular mechanisms of hypoxia in cancer. *Clin Transl Imaging, 5*(3), 225-253. doi:10.1007/s40336-017-0231-1

Chaplin, D. J., Trotter, M. J., Durand, R. E., Olive, P. L., & Minchinton, A. I. (1989). Evidence for intermittent radiobiological hypoxia in experimental tumour systems. *Biomed Biochim Acta, 48*(2-3), S255-259.

Chen Y, T. K., Keillor JW. (2015). Fluorogenic protein labelling: a review of photophysical

quench mechanisms and principles of fluorogen design. *Canadian Journal of Chemistry, 93*, 389-398. doi:http://dx.doi.org/10.1139/cjc-2014-0405

Chevalier, B., Pasquier, D., Lartigau, E. F., Chargari, C., Schernberg, A., Jannin, A., Mirabel, X., Vantyghem, M. C., & Escande, A. (2020). Metformin: (future) best friend of the radiation oncologist? *Radiother Oncol, 151*, 95-105. doi:10.1016/j.radonc.2020.06.030

D'Alonzo, R. A., Gill, S., Rowshanfarzad, P., Keam, S., MacKinnon, K. M., Cook, A. M., & Ebert, M. A. (2021). In vivo noninvasive preclinical tumor hypoxia imaging methods: a review. *Int J Radiat Biol, 97*(5), 593-631. doi:10.1080/09553002.2021.1900943

Ghosh, P., Guo, Y., Ashrafi, A., Chen, J., Dey, S., Zhong, S., Liu, J., Campbell, J., Konduri, P. C., Gerberich, J., Garrossian, M., Mason, R. P., Zhang, L., & Liu, L. (2020). Oxygen-Enhanced Optoacoustic Tomography Reveals the Effectiveness of Targeting Heme and Oxidative Phosphorylation at Normalizing Tumor Vascular Oxygenation. *Cancer Res, 80*(17), 3542-3555. doi:10.1158/0008-5472.CAN-19-3247

Graham, K., & Unger, E. (2018). Overcoming tumor hypoxia as a barrier to radiotherapy, chemotherapy and immunotherapy in cancer treatment. *Int J Nanomedicine, 13*, 6049-6058. doi:10.2147/IJN.S140462

Gray, L. H., Conger, A. D., Ebert, M., Hornsey, S., & Scott, O. C. (1953). The concentration of oxygen dissolved in tissues at the time of irradiation as a factor in radiotherapy. *Br J Radiol, 26*(312), 638-648. doi:10.1259/0007-1285-26-312-638

Henke, M., Laszig, R., Rube, C., Schafer, U., Haase, K. D., Schilcher, B., Mose, S., Beer, K. T., Burger, U., Dougherty, C., & Frommhold, H. (2003). Erythropoietin to treat head and neck cancer patients with anaemia undergoing radiotherapy: randomised, double-blind, placebo-controlled trial. *Lancet, 362*(9392), 1255-1260. doi:10.1016/S0140-6736(03)14567-9

Hoff, C. M., Lassen, P., Eriksen, J. G., Hansen, H. S., Specht, L., Overgaard, M., Grau, C., Johansen, J., Bentzen, J., Andersen, L., Evensen, J. F., & Overgaard, J. (2011). Does transfusion improve the outcome for HNSCC patients treated with radiotherapy? - results from the randomized DAHANCA 5 and 7 trials. *Acta Oncol, 50*(7), 1006-1014. doi:10.3109/0284186X.2011.592650

Holen, I., Speirs, V., Morrissey, B., & Blyth, K. (2017). In vivo models in breast cancer research: progress, challenges and future directions. *Dis Model Mech, 10*(4), 359-371. doi:10.1242/dmm.028274

Horsman, M. R., & Overgaard, J. (2007). Hyperthermia: a potent enhancer of radiotherapy. *Clin Oncol (R Coll Radiol), 19*(6), 418-426. doi:10.1016/j.clon.2007.03.015

Horsman, M. R., & Overgaard, J. (2016). The impact of hypoxia and its modification of the outcome of radiotherapy. *J Radiat Res, 57 Suppl 1*, i90-i98. doi:10.1093/jrr/rrw007

Horsman, M. R., Sorensen, B. S., Busk, M., & Siemann, D. W. (2021). Therapeutic Modification of Hypoxia. *Clin Oncol (R Coll Radiol), 33*(11), e492-e509. doi:10.1016/j.clon.2021.08.014

Jacobetz, M. A., Chan, D. S., Neesse, A., Bapiro, T. E., Cook, N., Frese, K. K., Feig, C., Nakagawa, T., Caldwell, M. E., Zecchini, H. I., Lolkema, M. P., Jiang, P., Kultti, A., Thompson, C. B., Maneval, D. C., Jodrell, D. I., Frost, G. I., Shepard, H. M., Skepper, J. N., & Tuveson, D. A. (2013). Hyaluronan impairs vascular function and drug delivery in a mouse model of pancreatic cancer. *Gut, 62*(1), 112-120. doi:10.1136/gutjnl-2012-302529

Janssens, G. O., Rademakers, S. E., Terhaard, C. H., Doornaert, P. A., Bijl, H. P., van den Ende, P., Chin, A., Marres, H. A., de Bree, R., van der Kogel, A. J., Hoogsteen, I. J., Bussink, J., Span, P. N., & Kaanders, J. H. (2012). Accelerated radiotherapy with carbogen and nicotinamide for laryngeal

cancer: results of a phase III randomized trial. *J Clin Oncol, 30*(15), 1777-1783. doi:10.1200/JCO.2011.35.9315

Lanzen, J., Braun, R. D., Klitzman, B., Brizel, D., Secomb, T. W., & Dewhirst, M. W. (2006). Direct demonstration of instabilities in oxygen concentrations within the extravascular compartment of an experimental tumor. *Cancer Res, 66*(4), 2219-2223. doi:10.1158/0008-5472.CAN-03-2958

Lee, C. T., Boss, M. K., & Dewhirst, M. W. (2014). Imaging tumor hypoxia to advance radiation oncology. *Antioxid Redox Signal, 21*(2), 313-337. doi:10.1089/ars.2013.5759

Lee, D. J., Cosmatos, D., Marcial, V. A., Fu, K. K., Rotman, M., Cooper, J. S., Ortiz, H. G., Beitler, J. J., Abrams, R. A., Curran, W. J., & et al. (1995). Results of an RTOG phase III trial (RTOG 85-27) comparing radiotherapy plus etanidazole with radiotherapy alone for locally advanced head and neck carcinomas. *Int J Radiat Oncol Biol Phys, 32*(3), 567-576. doi:10.1016/0360-3016(95)00150-W

Macklin, P. S., Yamamoto, A., Browning, L., Hofer, M., Adam, J., & Pugh, C. W. (2020). Recent advances in the biology of tumour hypoxia with relevance to diagnostic practice and tissue-based research. *J Pathol, 250*(5), 593-611. doi:10.1002/path.5402

Matsumoto, S., Yasui, H., Mitchell, J. B., & Krishna, M. C. (2010). Imaging cycling tumor hypoxia. *Cancer Res, 70*(24), 10019-10023. doi:10.1158/0008-5472.CAN-10-2821

Minsky, B. D., & Leibel, S. A. (1989). The treatment of hepatic metastases from colorectal cancer with radiation therapy alone or combined with chemotherapy or misonidazole. *Cancer Treat Rev, 16*(4), 213-219. doi:10.1016/0305-7372(89)90042-x

Moulder, J. E., & Rockwell, S. (1984). Hypoxic fractions of solid tumors: experimental techniques, methods of analysis, and a survey of existing

data. *Int J Radiat Oncol Biol Phys, 10*(5), 695-712. doi:10.1016/0360-3016(84)90301-8

Nordsmark, M., Bentzen, S. M., Rudat, V., Brizel, D., Lartigau, E., Stadler, P., Becker, A., Adam, M., Molls, M., Dunst, J., Terris, D. J., & Overgaard, J. (2005). Prognostic value of tumor oxygenation in 397 head and neck tumors after primary radiation therapy. An international multi-center study. *Radiother Oncol, 77*(1), 18-24. doi:10.1016/j.radonc.2005.06.038

O'Connor, J. P. B., Robinson, S. P., & Waterton, J. C. (2019). Imaging tumour hypoxia with oxygen-enhanced MRI and BOLD MRI. *Br J Radiol, 92*(1095), 20180642. doi:10.1259/bjr.20180642

Overgaard, J., Hansen, H. S., Overgaard, M., Bastholt, L., Berthelsen, A., Specht, L., Lindelov, B., & Jorgensen, K. (1998). A randomized double-blind phase III study of nimorazole as a hypoxic radiosensitizer of primary radiotherapy in supraglottic larynx and pharynx carcinoma. Results of the Danish Head and Neck Cancer Study (DAHANCA) Protocol 5-85. *Radiother Oncol, 46*(2), 135-146.

Panek, R., Welsh, L., Baker, L. C. J., Schmidt, M. A., Wong, K. H., Riddell, A. M., Koh, D. M., Dunlop, A., McQuaid, D., d'Arcy, J. A., Bhide, S. A., Harrington, K. J., Nutting, C. M., Hopkinson, G., Richardson, C., Box, C., Eccles, S. A., Leach, M. O., Robinson, S. P., & Newbold, K. L. (2017). Noninvasive Imaging of Cycling Hypoxia in Head and Neck Cancer Using Intrinsic Susceptibility MRI. *Clin Cancer Res, 23*(15), 4233-4241. doi:10.1158/1078-0432.CCR-16-1209

Pogoda, K., Bucki, R., Byfield, F. J., Cruz, K., Lee, T., Marcinkiewicz, C., & Janmey, P. A. (2017). Soft Substrates Containing Hyaluronan Mimic the Effects of Increased Stiffness on Morphology, Motility, and Proliferation of Glioma Cells. *Biomacromolecules, 18*(10), 3040-3051. doi:10.1021/acs.biomac.7b00324

Rickard, A. G., Palmer, G. M., & Dewhirst, M. W. (2019). Clinical and Pre-clinical Methods for Quantifying Tumor Hypoxia. *Adv Exp Med Biol, 1136*, 19-41. doi:10.1007/978-3-030-12734-3_2

Rischin, D., Peters, L. J., O'Sullivan, B., Giralt, J., Fisher, R., Yuen, K., Trotti, A., Bernier, J., Bourhis, J., Ringash, J., Henke, M., & Kenny, L. (2010). Tirapazamine, cisplatin, and radiation versus cisplatin and radiation for advanced squamous cell carcinoma of the head and neck (TROG 02.02, HeadSTART): a phase III trial of the Trans-Tasman Radiation Oncology Group. *J Clin Oncol, 28*(18), 2989-2995. doi:10.1200/JCO.2009.27.4449

Ryo Akima, Y. O., Shiho Morita-Tokuhiro, Akira Tsuzuki, Shin Yaogawa, Shinji Kariya, Norihiko Hamada, Akihito Nishioka, Shinichiro Masunaga, Koji Ono. (2016). New Enzyme-Targeting Radiosensitizer (KORTUC) Containing Hydrogen Peroxide & Sodium Hyaluronate for Intra-Tumoral Injection Using Mice Transplanted with SCC VII Tumor. *International Journal of Cancer and Clinical Research, 3*(2), 1-6.

Secomb, T. W., Hsu, R., & Dewhirst, M. W. (2004). Synergistic effects of hyperoxic gas breathing and reduced oxygen consumption on tumor oxygenation: a theoretical model. *Int J Radiat Oncol Biol Phys, 59*(2), 572-578. doi:10.1016/j.ijrobp.2004.01.039

Shannon, A. M., Bouchier-Hayes, D. J., Condron, C. M., & Toomey, D. (2003). Tumour hypoxia, chemotherapeutic resistance and hypoxia-related therapies. *Cancer Treat Rev, 29*(4), 297-307. doi:10.1016/s0305-7372(03)00003-3

Simpson, J. R., Bauer, M., Perez, C. A., Wasserman, T. H., Emami, B., Doggett, R. L., Byhardt, R. W., Phillips, T. L., & Mowry, P. A. (1989). Radiation therapy alone or combined with misonidazole in the treatment of locally advanced non-oat cell lung cancer: report of an RTOG prospective randomized trial. *Int J Radiat Oncol Biol Phys, 16*(6), 1483-1491. doi:10.1016/0360-3016(89)90953-x

Skwarski, M., McGowan, D. R., Belcher, E., Di Chiara, F., Stavroulias, D., McCole, M., Derham, J. L., Chu, K. Y., Teoh, E., Chauhan, J., O'Reilly, D., Harris, B. H. L., Macklin, P. S., Bull, J. A., Green, M., Rodriguez-Berriguete, G., Prevo, R., Folkes, L. K., Campo, L., Ferencz, P., Croal, P. L., Flight, H., Qi, C., Holmes, J., O'Connor, J. P. B., Gleeson, F. V., McKenna, W. G., Harris, A. L., Bulte, D., Buffa, F. M., Macpherson, R. E., & Higgins, G. S. (2021). Mitochondrial Inhibitor Atovaquone Increases Tumor Oxygenation and Inhibits Hypoxic Gene Expression in Patients with Non-Small Cell Lung Cancer. *Clin Cancer Res, 27*(9), 2459-2469. doi:10.1158/1078-0432.CCR-20-4128

Sorensen, B. S., & Horsman, M. R. (2020). Tumor Hypoxia: Impact on Radiation Therapy and Molecular Pathways. *Front Oncol, 10*, 562. doi:10.3389/fonc.2020.00562

Spiegelberg, L., Houben, R., Niemans, R., de Ruysscher, D., Yaromina, A., Theys, J., Guise, C. P., Smaill, J. B., Patterson, A. V., Lambin, P., & Dubois, L. J. (2019). Hypoxia-activated prodrugs and (lack of) clinical progress: The need for hypoxia-based biomarker patient selection in phase III clinical trials. *Clin Transl Radiat Oncol, 15*, 62-69. doi:10.1016/j.ctro.2019.01.005

Stadlbauer, A., Zimmermann, M., Bennani-Baiti, B., Helbich, T. H., Baltzer, P., Clauser, P., Kapetas, P., Bago-Horvath, Z., & Pinker, K. (2019). Development of a Non-invasive Assessment of Hypoxia and Neovascularization with Magnetic Resonance Imaging in Benign and Malignant Breast Tumors: Initial Results. *Mol Imaging Biol, 21*(4), 758-770. doi:10.1007/s11307-018-1298-4

Szadvari, I., Krizanova, O., & Babula, P. (2016). Athymic nude mice as an experimental model for cancer treatment. *Physiol Res, 65*(Suppl 4), S441-S453. doi:10.33549/physiolres.933526

Takaoka, T., Shibamoto, Y., Matsuo, M., Sugie, C., Murai, T., Ogawa, Y., Miyakawa, A., Manabe, Y., Kondo, T., Nakajima, K., Okazaki, D., &

Tsuchiya, T. (2017). Biological effects of hydrogen peroxide administered intratumorally with or without irradiation in murine tumors. *Cancer Sci, 108*(9), 1787-1792. doi:10.1111/cas.13302

Thomlinson, R. H. (1977). Hypoxia and tumours. *J Clin Pathol Suppl (R Coll Pathol), 11*, 105-113. doi:10.1136/jcp.s3-11.1.105

Thomlinson, R. H., & Gray, L. H. (1955). The histological structure of some human lung cancers and the possible implications for radiotherapy. *Br J Cancer, 9*(4), 539-549. doi:10.1038/bjc.1955.55

Tokuhiro, S., Ogawa, Y., Tsuzuki, K., Akima, R., Ue, H., Kariya, S., & Nishioka, A. (2010). Development of a novel enzyme-targeting radiosensitizer (KORTUC) containing hydrogen peroxide for intratumoral injection for patients with low linear energy transfer-radioresistant neoplasms. *Oncol Lett, 1*(6), 1025-1028. doi:10.3892/ol.2010.184

United Kingdom Co-ordinating Committee on Cancer Research (UKCCCR) Guidelines for the Welfare of Animals in Experimental Neoplasia (Second Edition). (1998). *Br J Cancer, 77*(1), 1-10. doi:10.1038/bjc.1998.1

Wang, H., Mu, X., He, H., & Zhang, X. D. (2018). Cancer Radiosensitizers. *Trends Pharmacol Sci, 39*(1), 24-48. doi:10.1016/j.tips.2017.11.003

West, C. M., & Slevin, F. (2019). Tumour Hypoxia. *Clin Oncol (R Coll Radiol), 31*(9), 595-599. doi:10.1016/j.clon.2019.06.008

Williamson, S. K., Crowley, J. J., Lara, P. N., Jr., McCoy, J., Lau, D. H., Tucker, R. W., Mills, G. M., Gandara, D. R., & Southwest Oncology Group Trial, S. (2005). Phase III trial of paclitaxel plus carboplatin with or without tirapazamine in advanced non-small-cell lung cancer: Southwest Oncology Group Trial S0003. *J Clin Oncol, 23*(36), 9097-9104. doi:10.1200/JCO.2005.01.3771

Wilson, W. R., & Hay, M. P. (2011). Targeting hypoxia in cancer therapy. *Nat Rev Cancer, 11*(6), 393-410. doi:10.1038/nrc3064

Xiang, L., & Semenza, G. L. (2019). Hypoxia-inducible factors promote breast cancer stem cell specification and maintenance in response to hypoxia or cytotoxic chemotherapy. *Adv Cancer Res, 141*, 175-212. doi:10.1016/bs.acr.2018.11.001

Yamaura, H., & Matsuzawa, T. (1979). Tumor regrowth after irradiation; an experimental approach. *Int J Radiat Biol Relat Stud Phys Chem Med, 35*(3), 201-219. doi:10.1080/09553007914550241

Chapter 5
The KORTUC Phase I clinical trial

5 Introduction

Breast cancer is the most common malignancy and the second most frequent cause of cancer-related death in women, with an estimated incidence of 2 million worldwide (Ginsburg et al., 2017). Approximately 4% of European patients with breast cancer present with locally advanced disease. This figure reaches up to 60% in low-resource countries. Despite treatment advances, the management of locally advanced breast cancer remains a challenge globally, particularly in developing countries (Tryfonidis, Senkus, Cardoso, & Cardoso, 2015). In many regions, women presenting with locally advanced disease have limited access to effective therapies, but in countries including Brazil, Russia, India and China with combined populations of 3 billion, women diagnosed with inoperable locally advanced disease have increasing access to high quality radiotherapy expertise and facilities (Datta, Samiei, & Bodis, 2014).

Locally advanced or recurrent disease in the breast (with or without metastases), is associated with significant morbidity (e.g. ulceration, bleeding, pain) and impacts upon quality of life. Therefore, control of local disease is important in these patients, whose prognosis often extends to years rather than months. In this context, radiotherapy is often limited in its ability to secure local control of large tumour masses by dose constraints imposed by the surrounding healthy tissues, including skin, muscle, and ribcage. In this context, a relatively cost-effective radiation sensitiser which is easy to administer would have a great impact in terms of quality of life and survival.

The UK KORTUC Phase I trial ((NCT02757651) completed recruitment in August 2018, and included 12 patients with breast tumours $\geq$ 3 cm who were treated with intratumoural H_2O_2 in combination with RT. This was the first systematic Phase I trial of intratumoural H_2O_2 in conjunction with UK radiotherapy schedules. The objective was to assess the safety and tolerability of KORTUC, with the aim of subsequent efficacy testing in a randomised Phase II trial.

5.1 Phase I clinical trial

5.1.1 Study design

This non-randomised study involved patients with locally advanced or locally recurrent breast cancer (with or without metastases) in whom RT was indicated for loco-regional disease control. The single centre study was conducted at The Royal Marsden NHS Foundation Trust, London, UK (CCR4502).

Prior to the launch of the Phase I trial, a team of clinicians and radiologists from the Royal Marsden Hospital, visited colleagues in Japan to learn more about the combination treatment of H_2O_2 with radiotherapy in clinical practice. It was also an opportunity to observe the methods involved in the mixing and preparation of the H_2O_2 gel mixure, and the intratumoural injection process.

Approval by a Research Ethics Committee (REC) and the Medicines and Healthcare products Regulatory Agency (MHRA) was obtained prior to trial commencement, and this was in place prior to the start of this MD(Res) research project.

Monitoring was undertaken by the Clinical Trials Unit at The Royal Marsden NHS Foundation Trust. In addition, our colleague Professor Ogawa was able to visit the Royal Marsden Hospital to supervise the treatment of the first patient treated within the UK Phase I trial.

The trial schema is shown in Figure 5.1.

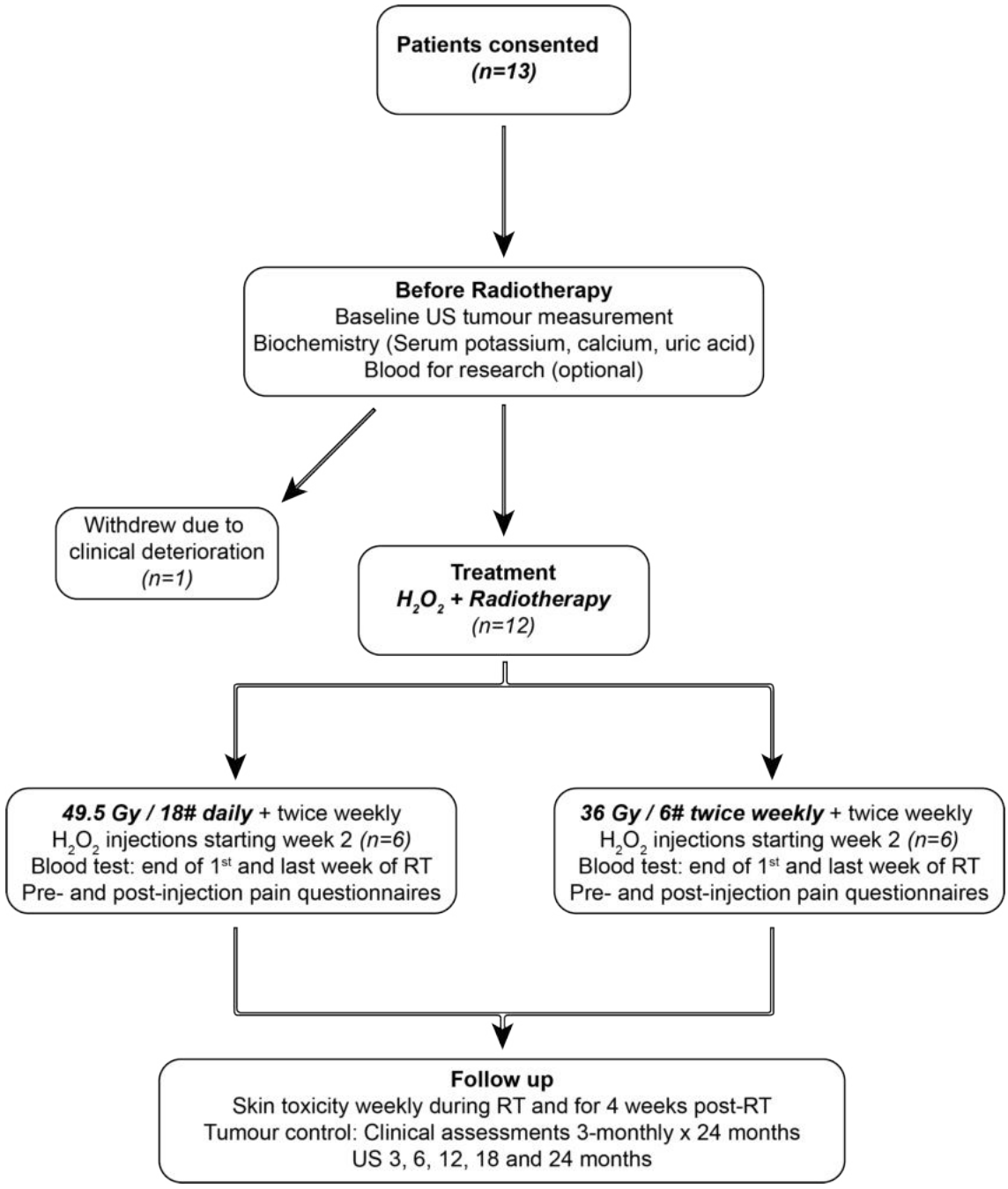

Figure 5.1 Phase I trial schema

A non-randomised study design testing intratumoural H_2O_2 in sodium hyaluronate gel in combination with two radiotherapy fractionation schedules in patients with locally advanced breast cancer, and corresponding follow up schedule. #- radiotherapy fraction; US- ultrasound; RT- radiotherapy.

Eligible patients were over 18 years of age, had histologically confirmed breast cancer, and required breast RT for local control and/or palliation of loco-regional symptoms. They had at least one breast tumour measuring ≥3cm in diameter, and in a superficial location accessible for injection. Any combination of oestrogen receptor (ER), progesterone receptor (PR) and HER2 expression was allowed. Exclusion criteria included prior RT to the breast and concomitant biological therapy other than trastuzumab, pertuzumab and denosumab. Pregnancy was excluded in female patients of child-bearing age. Patients were excluded if the anatomical location of the breast tumour, such as proximity to blood vessels or the brachial plexus, precluded safe access for intratumoural injection. This was to reduce the risk of injection into the vasculature and the theoretical risk of embolism, although this has not been described in the literature in relation to intratumoural H_2O_2 (Ogawa, 2016; Sleigh & Linter, 1985).

5.1.2 Drug formulation

A slow release 0.5% H_2O_2 solution was created by mixing 0.4 ml of 3% H_2O_2 (2.0 ml sterile ampoules supplied by Stockport Pharmaceuticals, UK) with 2.0 ml OSTENIL® (20 mg sodium hyaluronate in a 2.0 ml pre-loaded syringe provided by AAH Pharmaceuticals, UK), the latter licensed for intra-articular injection of arthritic joints (Puhl et al., 1993). Mixing was performed under aseptic conditions, and using 2 syringes connected via a 2-way tap. The low molecular weight of H_2O_2 (34 g/mol) ensured rapid equilibration of drug within the gel. The resulting mixture was a colourless, viscous solution (pH 6.8-7.8) stored at room temperature and remained stable for at least 2 hours following preparation, as determined by viscosity measurements.

Tests were performed by QCNW (Quality Control North West) by preparing a total of 60 syringes of 2.4 mls H_2O_2 gel mixture as described above. Viscosity was measured as an indication of stability of the H_2O_2 and sodium hyaluronate preparation. H_2O_2 concentration was measured by titration, and a suspended level viscometer was used to determine viscosity at 20°C at 0, 2, 4 hours following mixing. This was based on the viscosity decreasing over time, as the H_2O_2 within the mixture was broken down to generate water and oxygen. Results indicated that the H_2O_2 concentration remained stable (at 99% of initial

concentration) throughout the 4-hour time period (Stockport Pharmaceuticals UK).

The gel enabled slow release of H_2O_2 over at least 24 hours, as evidenced by generation of oxygen microbubbles upon injection, a feature that provided a strong rationale for twice-weekly administration during RT (Morita-Tokuhiro et al., 2016). In the trial, the drug and gel were mixed under aseptic conditions using two syringes connected via a 2-way tap. Once made up, each syringe contained 2.4 ml of 0.5% H_2O_2, and the contents of both syringes were required for tumours measuring 30-60 mm in diameter.

5.1.3 Radiotherapy treatment

Six patients received 49.5 Gy in 18 daily fractions of 2.75 Gy, and 6 were treated with 36 Gy in 6 twice-weekly fractions of 6 Gy to the breast ± locoregional lymph nodes. The equivalent RT dose expressed in conventional 2 Gy fractions (EQD_2) was 57 Gy and 65 Gy for these two schedules respectively.

The RT schedule was selected according to the patient's performance status and comorbidities, with fitter patients selected for the daily treatment schedule. RT was delivered using a linear accelerator, with 6-10 MV photons, and 3D-planned using data from a CT planning scan and using standard tangentially opposed fields. Patients were simulated and treated in the supine position on a breast board with both arms abducted. The clinical target volume (CTV) comprised the entire ipsilateral breast, including the deep fascia, but excluding underlying muscle or overlying skin (when not involved with disease). The RT dose was prescribed to the 100% isodose, ensuring the target volume was within the 95%-107% isodose lines. Organs at risk including the heart, lung and contralateral breast were outlined and standard guidelines for dose tolerances followed. A standard treatment verification protocol was used, consisting of daily imaging for the first 3 days, and subsequent weekly imaging. In cases where there was skin involvement by tumour, treatment included 5 mm wax bolus throughout RT to maximise dose to skin, in keeping with

standard practice. In patients treated with 49.5 Gy in 18 fractions, a sequential boost dose to the tumour bed (13.35 Gy in 5 daily fractions using mini-tangential opposed beams or a directly applied electron beam) was allowed, but this needed to be declared at time of trial entry. A tumour bed boost dose increased the EQD_2 to that comparable with 36 Gy in 6 fractions and with dose intensities previously reported in earlier patient cohorts treated with the same drug preparation (Aoyama et al., 2017; Aoyama et al., 2016).

5.1.4 Intratumoural injections of H_2O_2 in sodium hyaluronate gel

Transdermal intratumoural KORTUC injections were administered twice-weekly commencing in the second calendar week of RT. Each patient received 4 to 6 doses in total (median = 5 injections), the smaller number given to patients prescribed 6 fractions. The rationale for starting KORTUC in the second week was to allow for reduction in tumour interstitial pressure during the first week of RT, enabling technically easier and more tolerable injections for the patient. Injections were performed (23-gauge needle) under ultrasound (US) guidance by a trained radiologist or radiographer after 0.5% lignocaine injection to anaesthetise the skin. For tumours measuring 30-60 mm in size, 4.8 ml of 0.5% H_2O_2 in sodium hyaluronate gel was injected at each time point. Three syringes (7.2 ml) were required for tumours >60 mm in size. Uniform and accurate delivery under US guidance via 2-3 differently angled needle tracks was aided by the immediate appearance of oxygen microbubbles as H_2O_2 degraded to oxygen and water within the tumour (Figure 5.2).

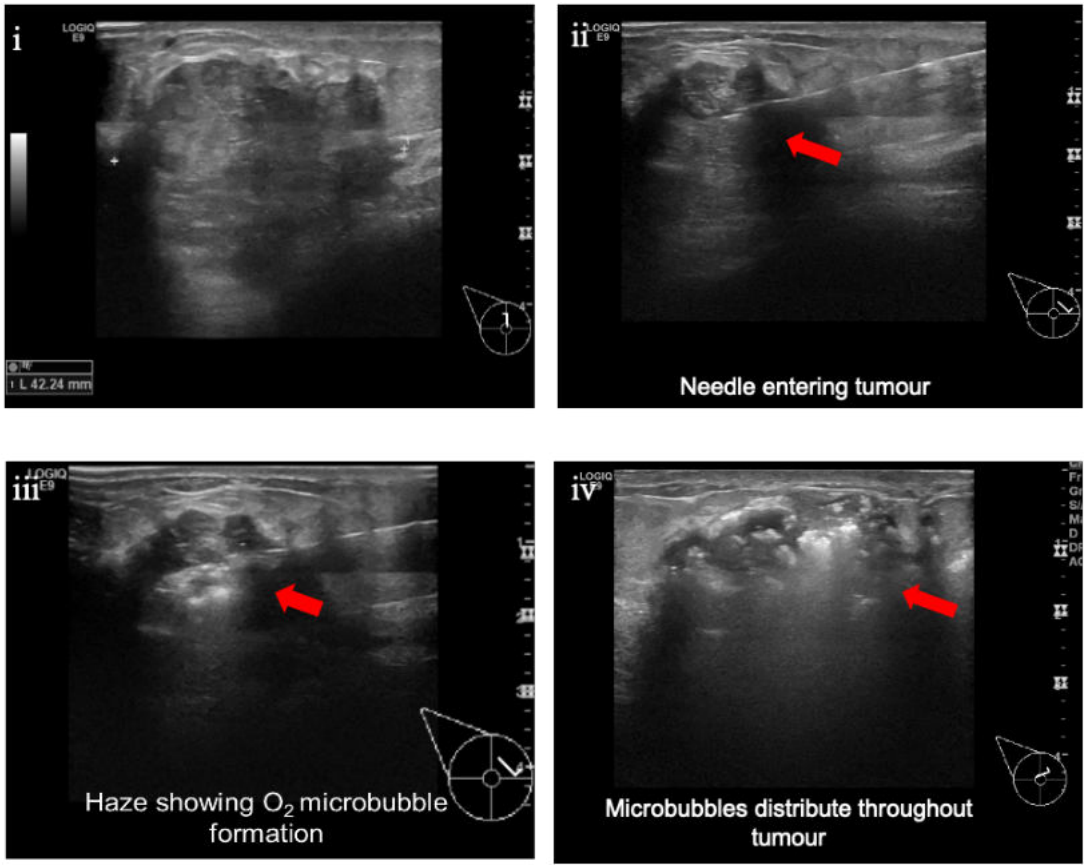

Figure 5.2 Sequence of ultrasound images of a breast tumour showing H_2O_2 administration, red arrow indicating (i) tumour at baseline, (ii) Needle entering under ultrasound guidance (iii), H_2O_2 with sodium hyaluronate gel mixture being injected intratumourally, (iv) breakdown of H_2O_2 with formation of oxygen microbubbles (white) within the tumour.

If any gel tracked back to the skin surface upon withdrawal of the needle it was promptly wiped away with sterile gauze. If patients had >1 distinct tumour in the breast/axilla, the clinician/radiologist was required to clearly document the injected lesion (usually the largest) to aid response assessment. RT was delivered within 1-2 hours after H_2O_2 injection.

5.1.5 Treatment monitoring

Within each RT group (daily or twice-weekly fractions), a minimum gap of 1 week was stipulated between the first and second patient, during which acute toxicity data associated with intratumoural injections (pain, skin toxicity, and tumour lysis) was reviewed by an Independent Data Monitoring Committee (IDMC). Based on predetermined criteria, the second and third patients in each

group and subsequently the fourth, fifth and sixth patients in each group were allowed to be treated concomitantly.

5.1.6 Primary endpoint

This related to the timing, severity and duration of pain post-injection recorded via a self-reported questionnaire completed by patients at home. An 11-point numerical scale ranging from 0 (“no pain”) to 10 (“worst possible pain”) recorded severity and duration prior to and over 24 hours after each H_2O_2 injection (Figure 5.3).

Figure 5.3 Patient self-reported tumour pain scale. Tumour pain refers to pain experienced at the target tumour site during radiotherapy with/without H_2O_2 injections.

Patient-reported scores were used to calculate i) the proportion of patients with pain scores ≥5 points above baseline after any of the intratumoural injections, and ii) the requirement for additional pain medication.

5.1.7 Secondary endpoints

Secondary endpoints included acute RT-induced skin toxicity, serum biochemistry and tumour response. Skin toxicity was assessed weekly in all patients during and for 4 weeks after RT by a member of the clinical team. Standardised proformas recorded the degree of erythema and desquamation of the skin of the breast, according to CTCAE (v4.02) as detailed in Table 5.1. In each of the RT groups, if no more than one of the first 3 patients had a persistent skin toxicity ≥ grade 3 six weeks after RT, the IDMC allowed recruitment to continue for a further 3 patients within that RT schedule. If moist desquamation was seen beyond skin folds, weekly assessments were continued until severity reduced to ≤ grade 1. The proportion of patients with ≥ grade 3 skin toxicity at any time from the start of RT to 4 weeks post-RT, and the worst grade of skin toxicity reported from the start of RT to 4 weeks post

RT were recorded in these cases. However, it was recognised that if cancer infiltrated skin, patients would typically experience ≥ grade 3 skin toxicity after RT alone.

Radiation dermatitis grading (CTCAE)	Criteria
0	No change
1	Faint erythema or dry desquamation
2	Moderate to brisk erythema or patchy moist desquamation, mostly confined to skin folds and creases; moderate edema
3	Confluent moist desquamation, not confined to skin folds; pitting edema
4	Skin necrosis or ulceration of full-thickness dermis; may include bleeding not included by minor trauma or abrasion
5	Death

Table 5.1 Radiation dermatitis grading based on CTCAE v.4.02 criteria

In every patient, routine biochemistry including serum potassium, calcium and uric acid were measured 2 days after the first H_2O_2 dose to rule out tumour lysis prior to proceeding with subsequent doses (Rampello, Fricia, & Malaguarnera, 2006).

Tumour response was assessed at 3-, 6-, and 12-months post-treatment. At each timepoint 3-dimensional US measurements were obtained and the tumour volume calculated on the assumption that breast tumours assume a hemi-ellipsoid shape, as previously demonstrated (Wapnir, Wartenberg, & Greco, 1996). Tumour volumes were compared against pre-treatment measurements with complete response (CR) defined as disappearance of the target lesion.

5.1.8 Statistical considerations

Based on the previously published data, 30-100% patients experienced pain described as no worse than 'mild' (or CTCAE grade 1) and lasting for several hours following injection (Aoyama et al., 2016; Miyatake et al., 2010; Ogawa et al., 2009; Ogawa et al., 2011). A single case of tumour lysis syndrome (mild) was reported in a total of 139 breast cancer patients. Given this knowledge of the safety of H_2O_2 plus RT, the Phase I trial required 12 patients to be recruited. Patients treated with once-daily and twice-weekly fractions of RT were analysed as a single stratum and the study population defined as all patients who registered for the trial and received at least one dose of intratumoural H_2O_2. Tumour volumes were calculated using 3-dimensional measurements obtained from US scans.

5.1.9 Plasma markers

Blood samples were obtained pre-RT and at the end of the first and last weeks of RT. Blood (two 9 ml K3-EDTA tubes) was obtained by venepuncture and processed within 30 minutes. Plasma and buffy coat were isolated by centrifugation at 1600 x g for 10 minutes at room temperature and frozen in aliquots at -80°C. All the plasma samples subsequently underwent one freeze-thaw cycle prior to assay.

5.1.10 ELISA and Luminex assay

The ELISA and Luminex assays were performed by Dr Selva Anbalagan, Higher Scientific Officer, ICR. Frozen plasma samples were thawed on ice and brought to room temperature. They were centrifuged at 10000 x g for 10 minutes and the plasma supernatant assayed either by ELISA or Luminex assay as per manufacturers' protocols. Results were measured against a normal plasma control obtained from a healthy donor (Cambridge Bioscience Ltd). The absorbance for ELISA was obtained using a POLAR star Omega plate reader (BMG LABTECH). The Luminex Human XL Cytokine Discovery Panel (15-plex, #FCSTM18-15, R&D System) was carried out with a minimum of 100 events per bead using a Luminex 200 system with xPONENT v3.1 software (Millipore). The plasma samples were assayed in duplicate wells for individual analytes at their corresponding time-points (pre-RT, end of first week

of -RT and post-H_2O_2 + RT) and the log2 fold change calculated. Further information regarding the ELISA and Luminex analytes, their dilutions and kit details used in this study are provided in Table 5.2.

Target	Assay	Plasma dilutions	Catalogue no	Manufacturer
CD137	ELISA	UD	EHTNFRSF9	Thermo Scientific
CXCL12		1:2	DSA00	R&D Systems
HSP70		1:2	EHHSPA4	Thermo Scientific
PD-1		1:2	BMS2214	Thermo Scientific
RIPK3		1:2	OKCA02138	Aviva Systems Biology
HMGB1		1:100	OKCD04074	Aviva Systems Biology
PD-L1 MIP-1α MIP-1β CXCL-10 GM-CSF GZM-B IFN-γ IL-10 IL-13 IL-1b IL-4 IL-6 TNF-a TRAIL VEGF	Luminex (15-plex)	1:2	FCSTM18-15	R&D Systems
Normal Plasma	ELISA, Luminex	UD or 1:2 or 1:100	PLSSKF2EDE10-XSXX	Cambridge BioScience Ltd

Table 5.2 Overview of 21 plasma markers quantified (with corresponding plasma dilutions) and manufacturer details. UD – undiluted; normal plasma obtained from a healthy volunteer.

5.1.11 Exploratory translational endpoints (post-hoc analysis)

Exploratory analyses of plasma biomarkers of cell death, inflammation, and immune response were conducted to test feasibility of investigating novel mechanisms of action and biomarkers of response in trial patients. This was performed by Dr Sheng Yu (Dept. of Data Science and Modelling, ICR). A linear mixed effect model was used to model the random effect of longitudinal data that the markers generated (Lindstrom & Bates, 1988). The model was built to study the effect of each marker, and to quantify its significance in terms of association with tumour shrinkage over time. The difference between individual and temporal variability was treated as random effect. The impact of each marker was regarded as a fixed effect. The model used was:

Tumour_volume = marker + time + marker: time + random_effect (time)

The ‘:’ colon sign denotes the variation of each plasma marker with time. Each marker was used to fit a mixed model individually with all patient samples and 20 models were fitted in total. A p-value for the coefficient of each marker was calculated to indicate whether the fixed effect had significance (at the 5% level). All graphs were generated using GraphPad Prism v8.1 (Mac OS), GraphPad Software, La Jolla California USA.

5.2 Results

13 patients (11 female, 2 male) were recruited to the study and 12 completed treatment. All patients had locally advanced disease that was deemed not suitable for surgery due to co-existing medical problems/performance status, disease extent, or metastatic disease. 1 patient withdrew due to clinical decline prior to starting radiotherapy.

The mean age was 70 years (median= 77, range= 45-93). 10 patients had ER+/HER2- disease and 2 had triple negative disease. 8/12 patients had distant metastatic disease, and all patients had received at least 1 prior systemic therapy for breast cancer. 3/12 patients had locally recurrent disease within the breast, having previously had breast surgery. The breast tumour size ranged from 30 mm to 164 mm in maximum dimension. During radiotherapy, 7/12 patients continued with concurrent endocrine therapy, and 2/12 with bisphosphonates for bone metastases.

Each patient's demographics, tumour details, and treatment history is summarised in Table 5.3.

Patient	Age	Sex	PS (ECOG*)	Baseline TNM stage	Tumour Phenotype	Prior treatment (no. of lines of therapy)	RT target volume
1	77	F	1	T2N1M1	$ER^{+}/HER2^{-}$	Endocrine (3)	Breast + axillary LN levels I-IV
2	69	F	0	T4N0M1	ER+/HER2-	Endocrine (2)	Breast
3	79	F	3	T4N0M0	ER+/HER2-	Endocrine (3)	Breast
4	80	M	2	T4N0M0	ER+/HER2-	Endocrine (2)	Breast
5	89	F	3	T2N0M0	ER+/HER2-	Endocrine (1)	Breast
6	78	F	2	T4N1M1	ER+/HER2-	Endocrine (2) Chemotherapy (1)	Breast + axillary LN levels I-IV
8	53	M	0	T2N0M1	ER-/HER2-	Surgery Endocrine (3) Chemotherapy (4) RT (contralateral)	Breast
9	53	F	2	T2N1M1	ER+/HER2-	Surgery Endocrine (3) Chemotherapy (2) RT (contralateral)	Breast + axillary LN levels I-IV
10	45	F	0	T4N1M1	ER+/HER2-	Chemotherapy (1)	Breast + axillary LN levels I-IV
11	75	F	3	T4N1M0	ER+/HER2-	Surgery Endocrine (3)	Breast
12	45	F	1	T4N1M1	ER-/HER2-	Chemotherapy (2)	Breast + axillary LN levels I-IV
13	93	F	3	T2N0M0	ER+/HER2-	None	Breast

Table 5.3 Summary of patient demographics, tumour characteristics, previous lines of treatment and RT treatment volumes. *Performance status (Eastern Cooperative Oncology Group) (0= fully active)

5.2.1 Patient compliance

Compliance with KORTUC injections was 100% for all patients. This included one patient with needle phobia, and three who were both frail and wheelchair bound due to comorbidities. All patients received radiotherapy within 2 hours of intratumoural KORTUC injection with one exception where a patient underwent radiotherapy prior to intratumoural injection in error. Results were analysed at a minimum of 12 months follow-up (range 2-24 months) for all patients alive at the time of reporting. 11/12 patients were followed up for at least 12 months. At the time of reporting, 6/12 patients treated in this trial have died, 2 of metastatic breast cancer and 4 of comorbid illnesses unrelated to cancer.

5.2.2 Toxicities

3/12 patients experienced Grade 1 (mild) tumour pain post injection lasting <30 minutes, and 5/12 experienced Grade 2 pain (moderate and limiting activities) according to CTCAE v4.02 (NCI, 2009). The remainder did not report any additional pain.

Median pain duration was 60 minutes with an inter-quartile range of 20-60 minutes. 4/12 patients reported short-lived pain $\geq$5 points above baseline during treatment. One patient had significant breast pain at the outset due to a fungating tumour and was already taking opiate analgesia. 6/12 patients required additional painkillers above what they were taking at baseline. In these cases, management included ensuring compliance with pre-existing painkillers and optimising analgesia +/- anxiolytics for the remainder of their treatment.

Skin toxicity (CTCAE v4.02) was assessed weekly during radiotherapy and 4 weeks following treatment completion. The grading of skin reactions is summarised in Table 5.4 below.

CTCAE skin toxicity grade	No. of pts
0	2
1	1
2	4
3	5 (all of whom treated with bolus)

Table 5.4 Highest grade of skin toxicity experienced by patients in KORTUC Phase I trial according to CTCAE v4.02

As expected, patients who were treated with bolus experienced grade 3 skin toxicity. All resolved to <grade 3 by 4 weeks post-RT. There was no suggestion of enhancement of erythema due to local leakage of H_2O_2. The acute radiation skin toxicity observed in the trial was comparable to that expected with standard RT alone. There were no cases of tumour lysis syndrome.

5.2.3 Radiological responses

US imaging was undertaken at baseline, to record pre-treatment tumour dimensions for comparison with future scans at 3, 6 and 12 months. Table 5.5 below summarises the tumour response measurements post-treatment and corresponding volume reduction. At the last imaging assessment percentage tumour volume reduction was between 50 and 100% as shown in Figure 5.4. All patients in this study have had maintained loco-regional control in the irradiated target lesion at last clinical follow-up (median 10 months, range 2-24 months).

Phase I tumour volume measurement by US (mm)						Clinical assessment
Patients	Baseline	3 months	6 months	9 months	12 months	
1	42x28x37	40x27x30	36x22x25	-	29x16x25*	PR
2	55x30x47	28x9x31	12x8x28	12x11x29	-	PR
3	47x36x30	32x17x25	26x25x17	-	18x14x17	PR
4	29x30x30	17x20x17	22x20x12	18x24x18	-	PR
5	43x17x14	31x9x16	19x8x8	18x7x7	-	CR
6	33x19x41	45x15x28	41x10x24	-	37x15x23	PR
7	-	-	-	-	-	-
8	49x19x48	41x10x33§	21x14x20	-	18x12x11	CR
9	26x24x31	14x8x10	6x5x5	-	16x12x13¶	PR
10	41x14x18	8x6x9	7x3x5	-	0x0x0	CR
11	64x45x65	46x15x34	39x13x33	-	25x4x24	CR
12	164x102x164¥	-	-	-	-	-
13	20x18x40	23x14x25	22x12x19	-	18x17x9	PR

Table 5.5 Tumour volume and clinical response assessment 3-12 months post-treatment PR: Partial Response; CR: Complete Response *H_2O_2 injected tumour showed PR, compared to 2 further breast tumours at non-injected sites which demonstrated stable disease.§Patient had complete metabolic response in breast tumour on PET scan (12 months post-treatment), maintained despite progressive disease outside the breast.¶Tumour dimensions increased at 12 months (vs. 6 months) post treatment; US scan indicates this was due to fibrosis. ¥Sarcomatoid breast tumour, measured on CT due to large size. Rapid progression between baseline and start of RT, but stabilised following RT.

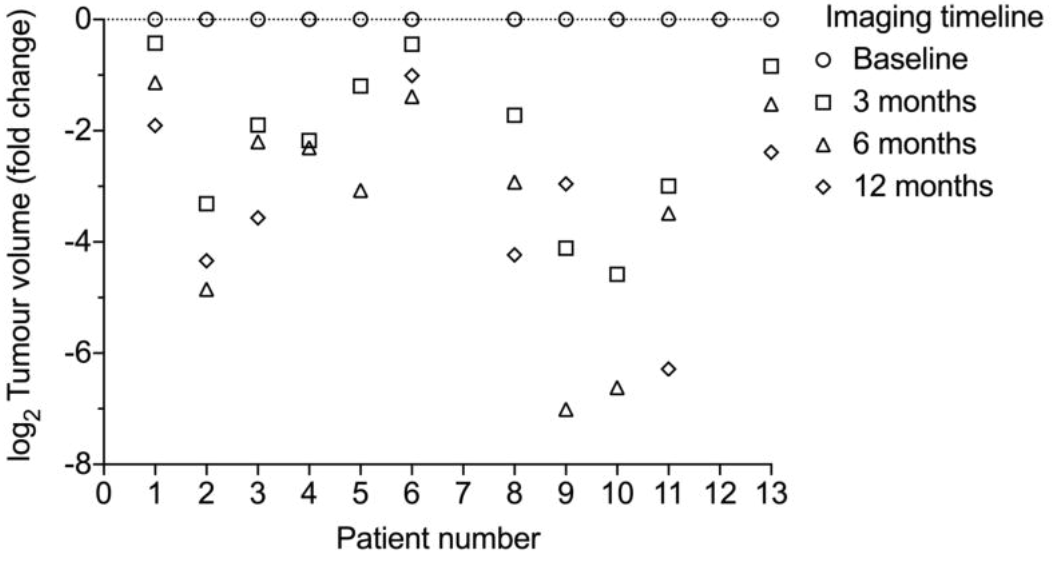

Figure 5.4 Tumour volume (US) of patients enrolled in the Phase I study Scatter plot depicting $\log_2$ transformed tumour volume fold change in individual patients normalized from their baseline tumour measurement for the indicated period of time.

As an illustrative example Figure 5.5 (i) and (ii) shows tumour extent in patient 10 at baseline and 3 months post-treatment. This was a 45-year old female who presented with a large ER+/HER2- fungating tumour of the left breast, with lung metastases at diagnosis. She received first-line chemotherapy with an initial partial response, followed by rapid symptomatic progression in the primary breast tumour. Subsequent to intratumoural KORTUC and RT, there was a complete response on imaging with no detectable disease in the breast at 17 months, despite progressive pulmonary and hepatic metastatic disease.

In terms of tumour response assessment, there were differences in two patients between US and clinical response assessments. In one patient, US measurement between 6 and 12 months reflected an increase in tumour dimensions despite clinical examination showing a good partial response. Radiology review of the US images at 12 months post-treatment indicated changes consistent with fibrosis rather than active tumour. Another patient demonstrated CR on clinical assessment at 12 months, despite US scan suggesting stable disease. A staging PET/CT scan performed concurrently confirmed complete metabolic response in the KORTUC-treated breast tumour.

Figure 5.5 Clinical photographs of patient 10 showing fungating tumour at (i) baseline and (ii) 12 months following treatment with intratumoural KORTUC + RT

5.2.4 Biomarker results (exploratory endpoint)

I am grateful to Dr Selva Anbalagan and Dr Sheng Yu for performing the following work related to blood biomarker measurement and analysis. 11/13 patients consented to provide blood for research. The exploratory target panel for ELISA and Luminex assays comprised 21 markers involved in cell death, immune checkpoint pathways, chemo-attraction, immune regulation, and angiogenesis as shown in Table 5.6 and Figure 5.6.

Pathways	Targets
Cell death	HSP70, HMGB1, RIPK3, GZM-B, IFNγ, IL-1β, TNFα, TRAIL, CXCL10
Immune checkpoint	CD137, PD-1, PD-L1
Chemoattractant	MIP-1α, MIP-1β, CXCL10
Immune regulators	GM-CSF, IFNγ, IL-1β, IL-4, IL-6, IL-10, IL-13, CXCL10, CXCL12
Angiogenesis	VEGF, CXCL12

Table 5.6 Exploratory plasma markers and associated cellular signalling pathways

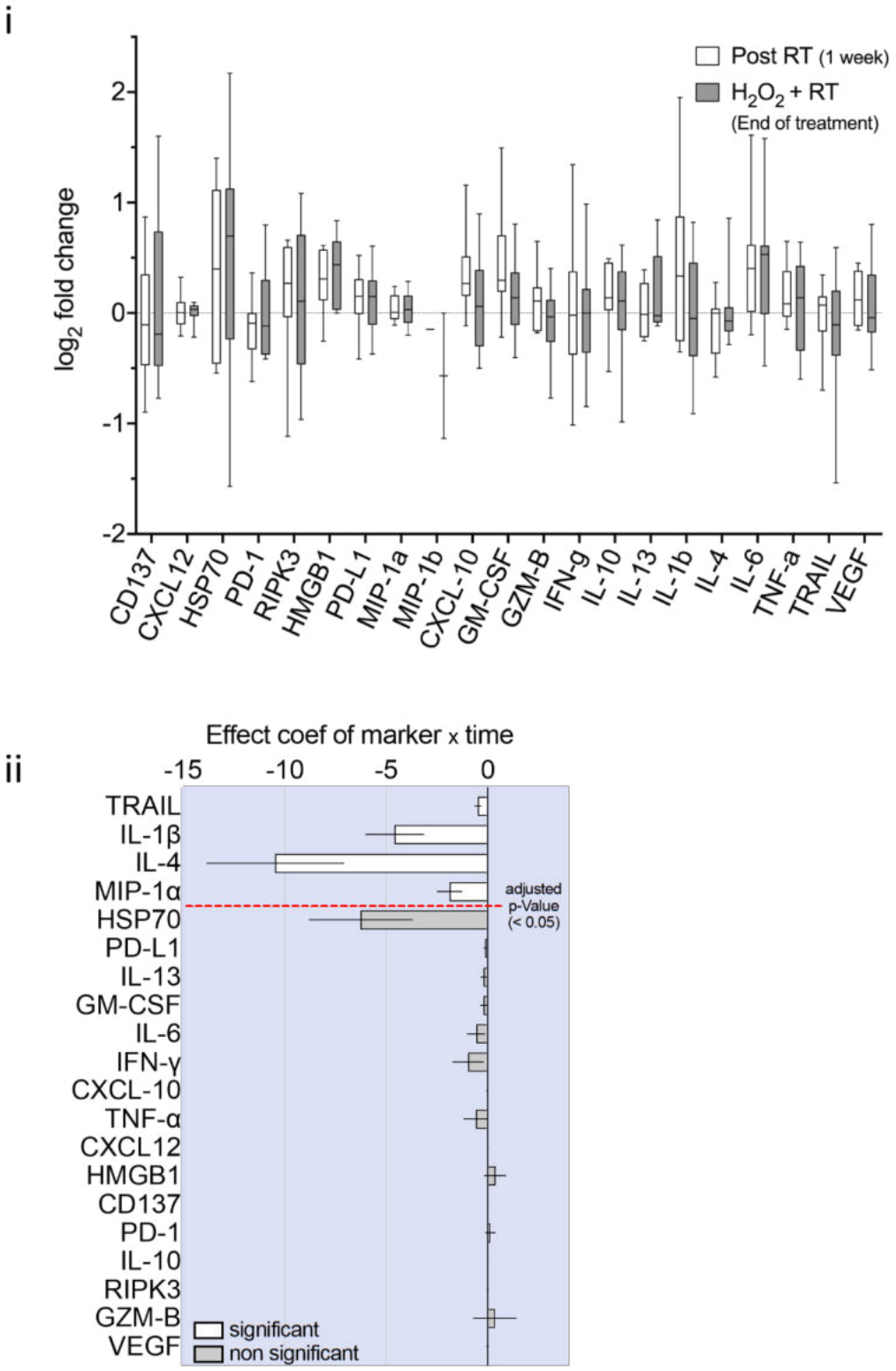

Figure 5.6 Exploratory plasma panel targets and associated pathways (i) Box and whisker plot showing log2 transformed fold change of each of the 21 markers, normalized to baseline expression (ii) Relationship between markers and tumour response, with bars in white showing significant association with tumour shrinkage (multicomparison adjusted P value < 0.05). Negative coefficient reflects positive correlation with tumour shrinkage.

Log2 transformed fold change of each marker normalised to their baseline level expression were plotted for each patient, comparing levels after RT alone (at the end of 1st week of treatment) and at the end of treatment (Figure 5.6 (i)). There was no definite trend in the results comparing RT alone versus RT + KORTUC in this small cohort. However, in general upregulation of markers involved in inflammation, immune modulation, and Damage Associated Molecular Patterns (DAMPs) was noted. A linear mixed effect model was built to study the effect of each marker, and to quantify their significance in terms of association with tumour shrinkage over time. This analysis resulted in four significant associations, suggesting tumour necrosis factor apoptosis-inducing ligand (TRAIL) mediated apoptosis with increased activated T-cell signalling (IL-4, MIP-1α) and macrophage stimulation (IL-1β) (Figure 5.6 (ii)).

5.3 Discussion

The results of the Phase I trial of intratumoural H_2O_2 in sodium hyaluronate gel illustrate the safety and tolerability of KORTUC in combination with breast radiotherapy (RT). The results are consistent with previously published cohort studies from Japan. KORTUC is a feasible and well tolerated treatment for patients with inoperable breast tumours difficult to eradicate with radiotherapy alone. Following IDMC review of the Phase I data, approval was granted for a multicentre Phase II trial comparing radiotherapy alone vs. KORTUC plus radiotherapy in breast cancer. This is currently underway in 6 UK centres, with 2 centres from India due to join. Both the Phase 1 and 2 data will contribute to licensing of the drug if the trial is positive. If effectiveness of KORTUC is demonstrated, this will have implications for breast cancer patients with locally advanced disease, but also in the treatment of other tumour types.

This study has also established that circulating plasma markers can be successfully quantified using the ELISA and Luminex platforms, providing insights into mechanism of cell death following treatment. Radiation induces DNA damage but also has the potential to modulate the immuno-inflammatory axis through the generation of ROS and DAMPs (Galluzzi, Buque, Kepp et al, 2017). Treatment with H_2O_2 has been shown to induce ROS, inflammatory

signaling, DNA damage, senescence, and cell death, informing the choice of 21 markers in our exploratory panel.

The effect of H_2O_2 within the cell is concentration dependent; having a role in signalling and homeostasis at nanomolar concentrations (nM) and triggering cell death at supraphysiogical (mM) concentrations (Gough & Cotter, 2011). The physiological outcome within the cell is modulated by antioxidant enzymes such as catalases, peroxidases and thioredoxin-linked systems (Sena & Chandel, 2012). By affecting protein kinases and phosphatases, H_2O_2 influences a number of signaling cascades including ERK, JNK, MAPK, p38, TNFα, NFκB, IL-1β, IL-6, IL-8, MCP-1 and MIP (Daroui, Desai, Li, Liu, & Liu, 2004; Kwon, Choi, Choi, & Benveniste, 2008; Schreck, Rieber, & Baeuerle, 1991; Takada et al., 2003; A. Takahashi et al., 2005; Tochigi et al., 2013; Zhang, Johnston, Stebler, & Keller, 2001). Several publications have demonstrated apoptosis as the predominant mode of cell death following H_2O_2 treatment, but this is concentration dependent (Clement, Ponton, & Pervaiz, 1998; Ogawa, Takahashi, Kobayashi, et al., 2003; A. Takahashi et al., 2005; Whittemore, Loo, Watt, & Cotman, 1995). The intrinsic mitochondrial pathway is thought to be the predominant mechanism of apoptosis (Tochigi et al., 2013). One study reported apoptosis induction following exposure to H_2O_2 levels <0.4 mM and upregulation of RIP, a gene associated with necrosis, at higher concentrations (Wan, Xiang, Li, & Guo, 2016). Exposure to H_2O_2 can result in increased expression of inflammatory cytokines (Di Marzo, Chisci, & Giovannoni, 2018). IL-1 is a key mediator of T-cell and dendritic cell (DC) function. Increased IL-1α levels occur in cells undergoing necrosis, whereas IL-1β signals towards apoptosis (England, Summersgill, Edye et al, 2014; Hogquist, Nett, Unanue, & Chaplin, 1991). IL-1β was significantly associated with tumour shrinkage in our study. In response to inflammation, receptor interacting protein kinase-3 (RIPK3) regulates cytokines (IL-1β, IL-23 and IL-22) in dendritic cells and initiates necroptosis (Moriwaki et al., 2014; Newton et al., 2014; Orozco & Oberst, 2017; Seifert & Miller, 2017). The active form of IL-1β is derived from pro-IL-1β in a RIPK3-dependent manner, in macrophages and dendritic cells (Moriwaki, Bertin, Gough, & Chan, 2015). In

this study, there was no clear trend in RIPK3 levels, which were either upregulated (4/10) or downregulated (3/10) following RT + KORTUC. IL-4 was also significantly associated with tumour response. One study reported that treating splenic T-cells from Ovalbumin (OVA) immunized mice with H_2O_2, resulted in a significant increase in IL-4 production, a key regulator in humoral and adaptive immunity (Obata, Hoshino, & Toyama, 2006). This is in accordance with another study showing that this occurs via activation of the STAT-6 signaling pathway, contributing to a positive feedback loop between STAT-6 and IL-4 in the predominantly TH2 immune response (Kaplan, Schindler, Smiley, & Grusby, 1996).

In the plasma analysis, a significant association between TRAIL and tumour shrinkage was found. Intracellular ROS such as H_2O_2 are thought to mediate apoptosis triggered by death receptor ligands, such as TRAIL (Tochigi et al., 2013). A study in an astroglial cell line, demonstrated an increase in TRAIL gene expression in cells treated with H_2O_2 in a dose-dependent manner up to a concentration of 0.8 mM (Kwon & Choi, 2006). TRAIL -dependent apoptosis regulates the priming of CD8+ memory T-cells by CD4+ TH1 cells (Janssen et al., 2005). In a study using a murine macrophage cell line (B10R), exposure to H_2O_2 increased the transcription of the chemokines MIP-1α, MIP-1β, MIP-2 and MCP-1 (Jaramillo & Olivier, 2002). MIP-1α and MIP-1β levels also increase during acute inflammation (O'Grady et al., 1999). MIP-1α has been shown to attract CD8+ T cells whereas MIP-1β attracts CD4+ T cells (Taub, Conlon, Lloyd et al, 1993). Interestingly, the expression of MIP-1β was undetectable in 7/10 patients but MIP-1α expression was observed in all the plasma samples, suggesting activation of CD8+ T lymphocytes.

Other markers in the exploratory panel, were not clearly associated with tumour response, and were either up- or down-regulated following RT + KORTUC. The pro-inflammatory markers TNF-α, IL6, and IL-1β were detected, as well as other mediators of inflammation and angiogenesis including IL-6, IL-8 and IL-10, which along with TGF-β is known to regulate T-

cell and macrophage activity to ameliorate the immune response (Showalter et al., 2017).

In summary, the plasma marker analysis suggests an inflammatory/immune response associated with apoptotic cell death, with necrosis possibly contributing in a subset of patients. However, in this small cohort, all of whom received RT + KORTUC, it is difficult to distinguish the contribution from KORTUC over and above that with RT alone. This requires testing in a randomized setting comparing RT alone versus RT + KORTUC. However, the plasma analysis has been valuable in informing the selection of markers to investigate in the subsequent Phase II trial.

References

Clement, M. V., Ponton, A., & Pervaiz, S. (1998). Apoptosis induced by hydrogen peroxide is mediated by decreased superoxide anion concentration and reduction of intracellular milieu. *FEBS Lett, 440*(1-2), 13-18. doi:10.1016/s0014-5793(98)01410-0

Daroui, P., Desai, S. D., Li, T. K., Liu, A. A., & Liu, L. F. (2004). Hydrogen peroxide induces topoisomerase I-mediated DNA damage and cell death. *J Biol Chem, 279*(15), 14587-14594. doi:10.1074/jbc.M311370200

Datta, N. R., Samiei, M., & Bodis, S. (2014). Radiation therapy infrastructure and human resources in low- and middle-income countries: present status and projections for 2020. *Int J Radiat Oncol Biol Phys, 89*(3), 448-457. doi:10.1016/j.ijrobp.2014.03.002

Di Marzo, N., Chisci, E., & Giovannoni, R. (2018). The Role of Hydrogen Peroxide in Redox-Dependent Signaling: Homeostatic and Pathological Responses in Mammalian Cells. *Cells, 7*(10). doi:10.3390/cells7100156

England, H., Summersgill, H. R., Edye, M. E., Rothwell, N. J., & Brough, D. (2014). Release of interleukin-1alpha or interleukin-1beta depends on mechanism of cell death. *J Biol Chem, 289*(23), 15942-15950. doi:10.1074/jbc.M114.557561

Galluzzi, L., Buque, A., Kepp, O., Zitvogel, L., & Kroemer, G. (2017). Immunogenic cell death in cancer and infectious disease. *Nat Rev Immunol, 17*(2), 97-111. doi:10.1038/nri.2016.107

Ginsburg, O., Bray, F., Coleman, M. P., Vanderpuye, V., Eniu, A., Kotha, S. R., Sarker, M., Huong, T. T., Allemani, C., Dvaladze, A., Gralow, J.,

Yeates, K., Taylor, C., Oomman, N., Krishnan, S., Sullivan, R., Kombe, D., Blas, M. M., Parham, G., Kassami, N., & Conteh, L. (2017). The global burden of women's cancers: a grand challenge in global health. *Lancet, 389*(10071), 847-860. doi:10.1016/S0140-6736(16)31392-7

Gough, D. R., & Cotter, T. G. (2011). Hydrogen peroxide: a Jekyll and Hyde signalling molecule. *Cell Death Dis, 2*, e213. doi:10.1038/cddis.2011.96

Hogquist, K. A., Nett, M. A., Unanue, E. R., & Chaplin, D. D. (1991). Interleukin 1 is processed and released during apoptosis. *Proc Natl Acad Sci U S A, 88*(19), 8485-8489. doi:10.1073/pnas.88.19.8485

Janssen, E. M., Droin, N. M., Lemmens, E. E., Pinkoski, M. J., Bensinger, S. J., Ehst, B. D., Griffith, T. S., Green, D. R., & Schoenberger, S. P. (2005). CD4+ T-cell help controls CD8+ T-cell memory via TRAIL-mediated activation-induced cell death. *Nature, 434*(7029), 88-93. doi:10.1038/nature03337

Jaramillo, M., & Olivier, M. (2002). Hydrogen peroxide induces murine macrophage chemokine gene transcription via extracellular signal-regulated kinase- and cyclic adenosine 5'-monophosphate (cAMP)-dependent pathways: involvement of NF-kappa B, activator protein 1, and cAMP response element binding protein. *J Immunol, 169*(12), 7026-7038. doi:10.4049/jimmunol.169.12.7026

Kaplan, M. H., Schindler, U., Smiley, S. T., & Grusby, M. J. (1996). Stat6 is required for mediating responses to IL-4 and for development of Th2 cells. *Immunity, 4*(3), 313-319. doi:10.1016/s1074-7613(00)80439-2

Kwon, D., & Choi, I. H. (2006). Hydrogen peroxide upregulates TNF-related apoptosis-inducing ligand (TRAIL) expression in human astroglial cells, and augments apoptosis of T cells. *Yonsei Med J, 47*(4), 551-557. doi:10.3349/ymj.2006.47.4.551

Kwon, D., Choi, K., Choi, C., & Benveniste, E. N. (2008). Hydrogen peroxide enhances TRAIL-induced cell death through up-regulation of DR5 in human astrocytic cells. *Biochem Biophys Res Commun, 372*(4), 870-874. doi:10.1016/j.bbrc.2008.05.148

Moriwaki, K., Balaji, S., McQuade, T., Malhotra, N., Kang, J., & Chan, F. K. (2014). The necroptosis adaptor RIPK3 promotes injury-induced cytokine expression and tissue repair. *Immunity, 41*(4), 567-578. doi:10.1016/j.immuni.2014.09.016

Moriwaki, K., Bertin, J., Gough, P. J., & Chan, F. K. (2015). A RIPK3-caspase 8 complex mediates atypical pro-IL-1beta processing. *J Immunol, 194*(4), 1938-1944. doi:10.4049/jimmunol.1402167

NCI. (2009). Common Terminology Criteria for Adverse Events (CTCAE). Retrieved from https://evs.nci.nih.gov/ftp1/CTCAE/CTCAE_4.03/Archive/CTCAE_4.02_2009-09-15_QuickReference_5x7.pdf

Newton, K., Dugger, D. L., Wickliffe, K. E., Kapoor, N., de Almagro, M. C., Vucic, D., Komuves, L., Ferrando, R. E., French, D. M., Webster, J., Roose-Girma, M., Warming, S., & Dixit, V. M. (2014). Activity of protein kinase RIPK3 determines whether cells die by necroptosis or apoptosis. *Science, 343*(6177), 1357-1360. doi:10.1126/science.1249361

O'Grady, N. P., Tropea, M., Preas, H. L., 2nd, Reda, D., Vandivier, R. W., Banks, S. M., & Suffredini, A. F. (1999). Detection of macrophage inflammatory protein (MIP)-1alpha and MIP-1beta during experimental endotoxemia and human sepsis. *J Infect Dis, 179*(1), 136-141. doi:10.1086/314559

Obata, F., Hoshino, A., & Toyama, A. (2006). Hydrogen peroxide increases interleukin-12 p40/p70 molecular ratio and induces Th2-predominant

responses in mice. *Scand J Immunol, 63*(2), 125-130. doi:10.1111/j.1365-3083.2005.01718.x

Ogawa, Y., Takahashi, T., Kobayashi, T., Kariya, S., Nishioka, A., Ohnishi, T., Saibara, T., Hamasato, S., Tani, T., Seguchi, H., Yoshida, S., & Sonobe, H. (2003). Apoptotic-resistance of the human osteosarcoma cell line HS-Os-1 to irradiation is converted to apoptotic-susceptibility by hydrogen peroxide: A potent role of hydrogen peroxide as a new radiosensitizer. *Int J Mol Med, 12*(6), 845-850.

Orozco, S., & Oberst, A. (2017). RIPK3 in cell death and inflammation: the good, the bad, and the ugly. *Immunol Rev, 277*(1), 102-112. doi:10.1111/imr.12536

Schreck, R., Rieber, P., & Baeuerle, P. A. (1991). Reactive oxygen intermediates as apparently widely used messengers in the activation of the NF-kappa B transcription factor and HIV-1. *EMBO J, 10*(8), 2247-2258.

Seifert, L., & Miller, G. (2017). Molecular Pathways: The Necrosome-A Target for Cancer Therapy. *Clin Cancer Res, 23*(5), 1132-1136. doi:10.1158/1078-0432.CCR-16-0968

Sena, L. A., & Chandel, N. S. (2012). Physiological roles of mitochondrial reactive oxygen species. *Mol Cell, 48*(2), 158-167. doi:10.1016/j.molcel.2012.09.025

Showalter, A., Limaye, A., Oyer, J. L., Igarashi, R., Kittipatarin, C., Copik, A. J., & Khaled, A. R. (2017). Cytokines in immunogenic cell death: Applications for cancer immunotherapy. *Cytokine, 97*, 123-132. doi:10.1016/j.cyto.2017.05.024

Takada, Y., Mukhopadhyay, A., Kundu, G. C., Mahabeleshwar, G. H., Singh, S., & Aggarwal, B. B. (2003). Hydrogen peroxide activates NF-kappa B

through tyrosine phosphorylation of I kappa B alpha and serine phosphorylation of p65: evidence for the involvement of I kappa B alpha kinase and Syk protein-tyrosine kinase. *J Biol Chem, 278*(26), 24233-24241. doi:10.1074/jbc.M212389200

Takahashi, A., Hanson, M. G., Norell, H. R., Havelka, A. M., Kono, K., Malmberg, K. J., & Kiessling, R. V. (2005). Preferential cell death of CD8+ effector memory (CCR7-CD45RA-) T cells by hydrogen peroxide-induced oxidative stress. *J Immunol, 174*(10), 6080-6087. doi:10.4049/jimmunol.174.10.6080

Taub, D. D., Conlon, K., Lloyd, A. R., Oppenheim, J. J., & Kelvin, D. J. (1993). Preferential migration of activated CD4+ and CD8+ T cells in response to MIP-1 alpha and MIP-1 beta. *Science, 260*(5106), 355-358. doi:10.1126/science.7682337

Tochigi, M., Inoue, T., Suzuki-Karasaki, M., Ochiai, T., Ra, C., & Suzuki-Karasaki, Y. (2013). Hydrogen peroxide induces cell death in human TRAIL-resistant melanoma through intracellular superoxide generation. *Int J Oncol, 42*(3), 863-872. doi:10.3892/ijo.2013.1769

Tryfonidis, K., Senkus, E., Cardoso, M. J., & Cardoso, F. (2015). Management of locally advanced breast cancer-perspectives and future directions. *Nat Rev Clin Oncol, 12*(3), 147-162. doi:10.1038/nrclinonc.2015.13

Wan, C., Xiang, J., Li, Y., & Guo, D. (2016). Differential Gene Expression Patterns in Chicken Cardiomyocytes during Hydrogen Peroxide-Induced Apoptosis. *PLoS One, 11*(1), e0147950. doi:10.1371/journal.pone.0147950

Whittemore, E. R., Loo, D. T., Watt, J. A., & Cotman, C. W. (1995). A detailed analysis of hydrogen peroxide-induced cell death in primary neuronal culture. *Neuroscience, 67*(4), 921-932. doi:10.1016/0306-4522(95)00108-u

Zhang, J., Johnston, G., Stebler, B., & Keller, E. T. (2001). Hydrogen peroxide activates NFkappaB and the interleukin-6 promoter through NFkappaB-inducing kinase. *Antioxid Redox Signal, 3*(3), 493-504. doi:10.1089/15230860152409121

Chapter 6
Discussion

6 Discussion

This research project was prompted by laboratory findings by Ogawa et al. reporting striking sensitisation of radioresistant osteosarcoma and prostate cancer cell lines by a relatively low concentration (0.1 mM) of H_2O_2 added to the medium prior to single dose IR (Ogawa, Takahashi, Kobayashi, et al., 2003). This effect was not solely due to enhanced classical DNA damage as might be expected following radiation. Instead, the treatment triggered permeabilization of the lysosomal membrane, with resultant release of heavy metal ions, followed by mitochondrial membrane disruption and apoptosis (Kariya et al., 2009; Ogawa, Takahashi, Kobayashi, et al., 2003a).

Even more noteworthy were the clinical outcomes from cohort studies which reported durable local control rates of 79-100% at up to 5 years in patients with breast tumours injected with H_2O_2 in combination with radiotherapy (Kariya et al., 2009; Tokuhiro et al., 2010). These results were important, as in patients with locally advanced breast tumours treated with radiotherapy alone at equivalent doses, expected local control rates are between 45-57% at 3 years post-treatment, with lower response rates associated with larger tumours (Arriagada, Mouriesse, Sarrazin, Clark, & Deboer, 1985).

In view of the published response rates, priority was given to investigating the safety and efficacy of the combination of H_2O_2 with radiotherapy (RT) systematically within the context of a trial. In parallel, this prompted further interrogation of mechanisms of action in this research project. The rationale was to identify clinically relevant findings that may impact upon patient selection and treatment delivery. Examples include scheduling and sequencing of H_2O_2 relative to ionising radiation (IR), and identification of tumour features (hypoxia extent, cellular redox state, antioxidant enzyme levels) that are most likely to influence response to this treatment. Also of interest was the concept of oxidative stress as a research strategy, and

potential modulation of intracellular ROS by the combination H_2O_2 and IR (Gorrini, Harris, & Mak, 2013).

Initially the aim of my laboratory research, which I conducted in parallel with the phase I clinical trial, was to independently test the efficacy of the combination of H_2O_2 and IR. If the clinical results could be reproduced in a laboratory model, this would enable further interrogation of the postulated mechanisms at play. Early on during the experiments, it became apparent that this was limited by the sensitivity of tumour cells *in vitro* to H_2O_2 at concentrations at least 100-fold lower (1 mM compared to 150 mM) than injected intratumourally in patients. Results from 2D clonogenic survival assays in 2 different cell lines could not demonstrate sensitisation or enhancement of radiation effect by H_2O_2 (see Chapter 3- *In vitro* results). Instead, this was suggestive of an independent additive effect of the two agents (i.e., without evidence of interaction or synergy between H_2O_2 and RT). Therefore, it was not possible to establish a synergistic or supra-additive effect relevant to the clinical context of H_2O_2 + IR using clonogenic survival.

It was decided to test the treatment effect in 3D spheroids as they more closely approximate to three-dimensional tumours, with the formation of oxygen and nutrient gradients that result in the formation of a hypoxic and necrotic core above approximately 400 μm diameter.

Growth kinetic curves illustrated spheroid growth inhibition following treatment with H_2O_2 administered prior to IR, compared to either agent alone or a control cohort. The magnitude of this *in vitro* response, although small, was in keeping with the effect reported in clinical cohort studies and in the KORTUC Phase I trial, considering the lower relative concentration of H_2O_2 used in this experimental model. Interestingly, the same effect was observed when H_2O_2 was administered following IR, suggesting that both agents are influencing the outcome, and that the timing of H_2O_2 administration relative to

IR may not be critical. This is in contrast with a true synergistic, (greater-than-additive) process where the presence of intratumoural H_2O_2 at the time of IR is imperative.

It was reasoned that several possible mechanisms may be contributing to the overall effect; for example apoptosis induction, oxidative DNA damage, and inhibition of antioxidant enzymes (Ogawa, Takahashi, Kobayashi, et al., 2003; Ogawa et al., 2008; T. Takahashi et al., 2004).

One hypothesis is that intratumoural H_2O_2 leads to reoxygenation of hypoxic tumours, thereby providing a mechanism for interaction between H_2O_2 and RT. In an in vivo study testing intratumoural H_2O_2 and RT, intratumoural oxygen concentration was measured using an IMP-211 electrode (Inter Medical Co Ltd, Japan) at 1- and 24-hour timepoints following injection. This reported that 24 hours following intratumoural injection of H_2O_2 and sodium hyaluronate, the partial pressure of oxygen was approximately 90 mmHg, compared to 40 mmHg in control tumours injected with PBS (Tokuhiro et al., 2010).

The advantage of using an *in vivo* model is that tumour sections maintain the heterogeneity of tumour cell subpopulations, supporting cells and vasculature (Katt, Placone, Wong, Xu, & Searson, 2016). Xenografts are well-placed to investigate reoxygenation as H_2O_2 can be injected directly into the tumour, as in patients. This is not the case in 3D *in vitro* models, where H_2O_2 is added to the medium containing cells/spheroids, and there is uncertainty whether or when the drug reaches the spheroid core for example.

By employing a dual hypoxia marker technique in two separate xenograft models, it was demonstrated that significant tumour reoxygenation occurs at 1 hour following H_2O_2 injection. Importantly, this timepoint was selected to reproduce the clinical scenario, where patients receive radiotherapy within an

hour of intratumoural H_2O_2 injection, thereby enabling radiosensitisation of hypoxic regions within the tumour. Therefore, this highlights that the timing and scheduling of H_2O_2 relative to IR is important, in order to maximise radiosensitisation of hypoxic regions. This is likely to be of greater benefit in the twice-weekly radiotherapy schedule currently being used in the Phase II clinical trial, where each fraction can be sensitised in this way from week 2 onwards. The other implication of reoxygenation by H_2O_2 is with regard to scheduling of intratumoural H_2O_2 within a course of radiotherapy, as H_2O_2 may be more effective towards the latter part of the RT schedule, when the relative proportion of hypoxic cells within the tumour is expected to be greater (Pajonk, Vlashi, & McBride, 2010).

A limitation of the *in vivo* experiments on reoxygenation was that the sample sizes were relatively small, but the findings were consistent between two tumour models. As expected, there was variability in the extent of hypoxia between xenograft tumours grown from the same cell line, but each tumour acted as its own control when measuring the change following IT injection. In non-injected control tumours, it was observed that the mean fluorescence intensity values were slightly lower with pimonidazole staining when compared to CCI-103F staining, although not statistically significant.

However, an unexpected finding from the in vivo experiments was that in xenografts injected with the control vehicle (sodium hyaluronate gel), there was a trend towards reduction in tumour hypoxia compared to that observed pre-injection. This was over and above the reduction seen in the non-injected control cohort. Although, this did not reach statistical significance, it is worthy of further investigation. On literature review, there is no definitive explanation for this observation, but a possible mechanism is via the agonist effect of sodium hyaluronate at the CD44 receptor. CD44 is a cell-surface adhesion glycoprotein which is upregulated in hypoxia and is also present on endothelial cells (Kotla et al., 2021). When sodium hyaluronate binds to

CD44, vascular permeability may be increased, thus increasing tumour oxygenation. It is important to further interrogate the possible mechanisms of the effect of sodium hyaluronate alone on tumour hypoxia. This may have relevance to clinical practice and may enable further quantification of the individual effect (on intratumoural hypoxia) of H_2O_2 within the combination. In the clinical trial, it was not possible to differentiate the separate effects of the two agents as it was not feasible to include intratumoural sodium hyaluronate (control vehicle alone) in combination with radiotherapy in the control arm. The reason for this is that it is not possible to safely inject H_2O_2 alone intratumourally, due to rapid breakdown of the compound and as it causes pain upon injection.

With regard to reoxygenation by H_2O_2, a recent study used topical H_2O_2 (33%) to treat non-melanoma skin cancers prior to surgical excision in a cohort of 11 patients. There was a significant reduction in the size of the lesions following application of H_2O_2 and in some cases, no surgical excision was required, as post-treatment biopsy demonstrated no evidence of malignancy. Patients experienced minimal discomfort during treatment and no long-term side toxicities were reported. Although the mechanisms of action have yet to be elucidated, it is most likely to be due to apoptotic/necrotic cell death (Mundi, Jordan, Doyle, & Moore, 2020). A further study using topical H_2O_2 in combination with photodynamic therapy in skin tumours, found that H_2O_2 was able to increase oxygenation at the treatment site (Manifold & Anderson, 2011).

6.1 Future directions

Intratumoural H_2O_2 represents a novel means of abrogating tumour hypoxia, which remains an important clinical problem. Despite identifying potential therapies to overcome hypoxia over many decades, none have been adopted into mainstream clinical practice. H_2O_2 is a relatively inexpensive and easily

available substance that is straightforward to use and store. The combination of H_2O_2 with RT represents a cost-effective treatment, which is relatively simple to deliver without additional infrastructure or advanced technology. Therefore, it is of particular relevance to low- and middle-income countries, where local disease control often represents an area of unmet need.

Having established reoxygenation as factor contributing to the mechanism of action of intratumoural H_2O_2, further staining will be performed on xenograft sections to investigate markers of oxidative stress and DNA damage (8-oxoguanine and phospho-ATM). A second method of hypoxia quantification using computer analysis of stained sections will provide a more objective means of quantifying hypoxia. A standard approach would be to set a threshold for a positive stain, to enable quantification of the fraction of positive pixels within a fluorescence image (Zaidi, Fu, Cojocari, McKee, & Wouters, 2019).

Within the Phase II KORTUC trial, markers of cell death and immune response in blood will be compared at baseline, 6- and 12-months post-RT. Circulating tumour DNA will be measured in blood at baseline, and at intervals up to 12 months. A novel imaging technique, super-resolution ultrasound (SRUS) is being utilised in a subset of patients to identify imaging derived biomarkers of tumour response. The Phase II trial will also test efficacy of H_2O_2 plus radiotherapy vs. radiotherapy alone, and it will be possible to monitor reoxygenation in this setting by employing opto-acoustic imaging to measure blood flow fluctuations, and track variation in oxygenated haemoglobin as a surrogate for tumour hypoxia.

With regard to other tumour types, intratumoural H_2O_2 injection (under CT/US guidance) has also been used in combination with external beam RT and interstitial brachytherapy in a patient with pelvic side wall recurrence from cervical cancer. This achieved a complete radiological response at 8 months

and maintained local control at 32 months post-treatment. There were no toxicities ≥ Grade 3, and gastrointestinal and genitourinary side effects were in keeping with that expected from RT alone (Nakata et al., 2020). Hu et al. reported on a cohort of 18 patients with cervical cancer who received external beam RT, with intravaginal gauze soaked with 3% H_2O_2 applied twice weekly. There were no acute toxicities ≥ Grade 3 and 10/18 patients achieved a complete response which was maintained at a median follow up of 28 months (Hu et al., 2021).

There are challenges with regard to safe application of H_2O_2 to deeper-seated tumours, especially where critical organs at risk are in close proximity. However, if efficacy is demonstrated in the Phase II KORTUC trial in breast cancer, there is potential for application of this treatment to other tumour sites, which are accessible for injection (or topical application), and in particular where hypoxia is recognised as a predominant feature.

References

Arriagada, R., Mouriesse, H., Sarrazin, D., Clark, R. M., & Deboer, G. (1985). Radiotherapy alone in breast cancer. I. Analysis of tumor parameters, tumor dose and local control: the experience of the Gustave-Roussy Institute and the Princess Margaret Hospital. *Int J Radiat Oncol Biol Phys, 11*(10), 1751-1757. doi:10.1016/0360-3016(85)90027-6

Baskar, R., Lee, K. A., Yeo, R., & Yeoh, K. W. (2012). Cancer and radiation therapy: current advances and future directions. *Int J Med Sci, 9*(3), 193-199. doi:10.7150/ijms.3635

Gorrini, C., Harris, I. S., & Mak, T. W. (2013). Modulation of oxidative stress as an anticancer strategy. *Nat Rev Drug Discov, 12*(12), 931-947. doi:10.1038/nrd4002

Hu, R., Saito, A. I., Mitsuhashi, T., Inoue, T., Ota, T., Ujihira, T., . . . Sasai, K. (2021). Radiosensitization using hydrogen peroxide in patients with cervical cancer. *Mol Clin Oncol, 15*(1), 142. doi:10.3892/mco.2021.2304

Kariya, S., Sawada, K., Kobayashi, T., Karashima, T., Shuin, T., Nishioka, A., & Ogawa, Y. (2009). Combination treatment of hydrogen peroxide and X-rays induces apoptosis in human prostate cancer PC-3 cells. *Int J Radiat Oncol Biol Phys, 75*(2), 449-454. doi:10.1016/j.ijrobp.2009.04.092

Katt, M. E., Placone, A. L., Wong, A. D., Xu, Z. S., & Searson, P. C. (2016). In Vitro Tumor Models: Advantages, Disadvantages, Variables, and Selecting the Right Platform. *Front Bioeng Biotechnol, 4*, 12. doi:10.3389/fbioe.2016.00012

Kotla, N. G., Bonam, S. R., Rasala, S., Wankar, J., Bohara, R. A., Bayry, J., . . . Pandit, A. (2021). Recent advances and prospects of hyaluronan as a multifunctional therapeutic system. *J Control Release, 336*, 598-620. doi:10.1016/j.jconrel.2021.07.002

Manifold, R. N., & Anderson, C. D. (2011). Increased cutaneous oxygen availability by topical application of hydrogen peroxide cream enhances the photodynamic reaction to topical 5-aminolevulinic acid-methyl ester. *Arch Dermatol Res, 303*(4), 285-292. doi:10.1007/s00403-011-1128-x

Mundi, N., Jordan, K., Doyle, P., & Moore, C. (2020). 33% hydrogen peroxide as a Neoadjuvant treatment in the surgical excision of non-melanoma skin

cancers: a case series. *J Otolaryngol Head Neck Surg, 49*(1), 33. doi:10.1186/s40463-020-00433-6

Nakata, M., Yoshida, K., Shimbo, T., Yoshikawa, N., Yoshioka, H., Hori, A., . . . Nihei, K. (2020). High-dose-rate interstitial brachytherapy with hypoxic radiosensitizer KORTUC II for unresectable pelvic sidewall recurrence of uterine cervical cancer: a case report. *J Contemp Brachytherapy, 12*(6), 606-611. doi:10.5114/jcb.2020.101695

Ogawa, Y., Takahashi, T., Kobayashi, T., Kariya, S., Nishioka, A., Mizobuchi, H., . . . Sonobe, H. (2003). Mechanism of hydrogen peroxide-induced apoptosis of the human osteosarcoma cell line HS-Os-1. *Int J Mol Med, 12*(4), 459-463. Retrieved from http://www.ncbi.nlm.nih.gov/pubmed/12964019

Ogawa, Y., Takahashi, T., Kobayashi, T., Kariya, S., Nishioka, A., Ohnishi, T., . . . Sonobe, H. (2003a). Apoptotic-resistance of the human osteosarcoma cell line HS-Os-1 to irradiation is converted to apoptotic-susceptibility by hydrogen peroxide: a potent role of hydrogen peroxide as a new radiosensitizer. *Int J Mol Med, 12*(6), 845-850. Retrieved from http://www.ncbi.nlm.nih.gov/pubmed/14612955

Ogawa, Y., Takahashi, T., Kobayashi, T., Toda, M., Nishioka, A., Kariya, S., . . . Yoshida, S. (2003). Comparison of radiation-induced reactive oxygen species formation in adult articular chondrocytes and that in human peripheral T cells: possible implication in radiosensitivity. *Int J Mol Med, 11*(4), 455-459. Retrieved from https://www.ncbi.nlm.nih.gov/pubmed/12632097

Ogawa, Y., Ue, H., Tsuzuki, K., Tadokoro, M., Miyatake, K., Sasaki, T., . . . Inomata, T. (2008). New radiosensitization treatment (KORTUC I) using hydrogen peroxide solution-soaked gauze bolus for unresectable and superficially exposed neoplasms. *Oncol Rep, 19*(6), 1389-1394. Retrieved from https://www.ncbi.nlm.nih.gov/pubmed/18497941

Pajonk, F., Vlashi, E., & McBride, W. H. (2010). Radiation resistance of cancer stem cells: the 4 R's of radiobiology revisited. *Stem Cells, 28*(4), 639-648. doi:10.1002/stem.318

Takahashi, T., Kitaoka, K., Ogawa, Y., Kobayashi, T., Seguchi, H., Tani, T., & Yoshida, S. (2004). Lysosomal dysfunction on hydrogen peroxide-induced apoptosis of osteoarthritic chondrocytes. *Int J Mol Med, 14*(2), 197-200. Retrieved from https://www.ncbi.nlm.nih.gov/pubmed/15254765

Tokuhiro, S., Ogawa, Y., Tsuzuki, K., Akima, R., Ue, H., Kariya, S., & Nishioka, A. (2010). Development of a novel enzyme-targeting radiosensitizer (KORTUC) containing hydrogen peroxide for intratumoral injection for patients with low linear energy transfer-radioresistant neoplasms. *Oncol Lett, 1*(6), 1025-1028. doi:10.3892/ol.2010.184

Zaidi, M., Fu, F., Cojocari, D., McKee, T. D., & Wouters, B. G. (2019). Quantitative Visualization of Hypoxia and Proliferation Gradients Within Histological Tissue Sections. *Front Bioeng Biotechnol,* *7*, 397. doi:10.3389/fbioe.2019.00397

Appendix

Appendix 1

a)

	26.4.18	IR alone								
Dose (Gy)	Plated cells	Well1	Well2	Well3	Mean	Std	PE	mean PE	mean SD	survival
0	62.5	26	34	25	28	4.9	45.3	48.27	4.47	100.00
	125	60	64	68	64	4.0	51.2			
2	125	33	41	43	39	5.3	31.2			
	250	40	64	71	68	4.9	27.0	29.10	5.12	60.29
4	250	27	40	45	43	3.5	17.0			
	500	43	60	70	65	7.1	13.0	15.00	5.30	31.08
6	625	36	45	53	45	8.5	7.1			
	1250	43	58	67	63	12.1	5.0	6.07	10.31	12.58
8	2500	47	42	47	45	2.9	1.8			
	5000	31	28	24	28	3.5	0.6	1.18	3.20	2.45
10	10000	35	43	38	39	4.0	0.4			
	20000	16	20	19	18	2.1	0.1	0.24	3.06	0.49

b)

	26.4.18	0.05mM H2O2 + IR								
Dose (Gy)	Plated cells	Well1	Well2	Well3	Mean	Std	PE	mean PE	mean SD	survival
0	62.5	36	35	26	32	5.5	51.7	47.47	4.08	100.00
	125	56	51	55	54	2.6	43.2			
2	125	32	30	34	32	2.0	25.6			
	250	58	72	55	62	9.1	24.7	25.13	5.54	52.95
4	250	46	55	50	50	4.5	20.1			
	500	61	59	52	57	4.7	11.5	15.80	4.62	33.29
6	625	45	56	47	49	5.9	7.9			
	1250	49	49	54	51	2.9	4.1	5.97	4.37	12.58
8	2500	59	56	63	59	3.5	2.4			
	5000	19	25	32	25	6.5	0.5	1.44	5.01	3.03
10	10000	23	32	34	30	5.9	0.3			
	20000	7	9	16	11	4.7	0.1	0.18	5.29	0.37

c)

	3.5.18	IR alone								
Dose (Gy	Plated cells	Well1	Well2	Well3	Mean	Std	PE	mean PE	mean SD	survival
0	62.5	30	35	35	33	2.9	53.3	48.53	5.06	100.00
	125	63	51	50	55	7.2	43.7			
2	125	44	51	34	43	8.5	34.4			
	250	70	66	61	66	4.5	26.3	30.33	6.53	62.50
4	250	45	31	44	40	7.8	16.0			
	500	52	44	49	48	4.0	9.7	12.83	5.93	26.44
6	625	39	29	22	30	8.5	4.8			
	1250	37	38	27	34	6.1	2.7	3.76	7.31	7.75
8	2500	53	44	39	45	7.1	1.8			
	5000	24	41	28	31	8.9	0.6	1.22	7.99	2.51
10	10000	47	49	32	43	9.3	0.4			
	20000	12	13	10	12	1.5	0.1	0.24	5.41	0.50

d)

	3.5.18	0.05mM H2O2 + IR								
Dose (Gy	Plated cells	Well1	Well2	Well3	Mean	Std	PE	mean PE	mean SD	survival
0	62.5	19	24	30	24	5.5	38.9	40.00	7.24	100.00
	125	41	56	57	51	9.0	41.1			
2	125	31	43	52	42	10.5	33.6			
	250	54	58	59	57	2.6	22.8	28.20	6.59	70.50
4	250	43	34	31	36	6.2	14.4			
	500	63	60	48	57	7.9	11.4	12.90	7.09	32.25
6	625	46	42	33	40	6.7	6.5			
	1250	45	29	34	36	8.2	2.9	4.67	7.42	11.67
8	2500	56	40	61	52	11.0	2.1			
	5000	19	34	25	26	7.5	0.5	1.31	9.26	3.27
10	10000	35	26	21	27	7.1	0.3			
	20000	12	19	12	14	4.0	0.1	0.17	5.57	0.43

e)

	14.5.18	IR alone								
Dose (Gy	Plated cells	Well1	Well2	Well3	Mean	Std	PE	mean PE	mean SD	survival
0	62.5	22	27	28	26	3.2	41.1	41.20	2.87	100.00
	125	52	49	54	52	2.5	41.3			
2	125	31	37	33	34	3.1	26.9			
	250	45	50	50	48	2.9	19.3	23.13	2.97	56.15
4	250	28	30	38	32	5.3	12.8			
	500	44	51	44	46	4.0	9.3	11.03	4.67	26.78
6	625	52	58	59	56	3.8	9.0			
	1250	42	42	61	48	11.0	3.9	6.44	7.38	15.63
8	2500	55	79	76	78	2.1	3.1			
	5000	31	50	64	57	9.9	1.1	2.12	6.01	5.15
10	10000	52	68	98	60	11.3	0.6			
	20000	24	35	62	30	7.8	0.1	0.37	9.55	0.91

f)

	14.5.18	0.05mM H2O2 + IR								
Dose (Gy	Plated ce	Well1	Well2	Well3	Mean	Std	PE	mean PE	mean SD	survival
0	62.5	21	31	17	23	7.2	36.8	38.67	9.47	100.00
	125	42	64	46	51	11.7	40.5			
2	125	31	38	29	33	4.7	26.1			
	250	42	63	50	52	10.6	20.7	23.40	7.66	60.52
4	250	50	58	49	52	4.9	20.9			
	500	56	47	50	51	4.6	10.2	15.57	4.76	40.26
6	625	35	43	57	45	11.1	7.2			
	1250	42	38	59	46	11.2	3.7	5.45	11.14	14.10
8	2500	53	61	98	57	5.7	2.3			
	5000	42	43	68	43	0.7	0.9	1.57	3.18	4.05
10	10000	59	61	73	64	7.6	0.6			
	20000	24	39	56	40	16.0	0.2	0.42	11.79	1.09

Tables a)-f)- Raw data from clonogenic survival curves comparing IR alone with H_2O_2 + IR in HN5 cell line (n=3). Data displays colony numbers in each well of a 6-well plate, according to cell seeding number, with calculated plating efficiency (PE). Percentage colony survival is normalised to untreated controls.

g)

	19.10.2018	IR alone								
Dose (Gy)	Plated cells	Well1	Well2	Well3	Mean	Std	PE	mean PE	mean SD	survival
0	100	52	41	33	42	9.5	42.0	42.00	6.95	100.00
	200	81	89	82	84	4.4	42.0			
2	500	65	66	76	69	6.1	13.8			
	1000	103	130	126	120	14.6	12.0	12.88	10.33	30.67
4	2000	66	85	65	72	11.3	3.6			
	5000	75	107	116	112	6.4	2.2	2.92	8.82	6.94
6	10000	80	71	81	77	5.5	0.8			
	20000	28	34	54	39	13.6	0.2	0.48	9.56	1.15
8	20000	11	21	34	16	7.1	0.1			
	50000	0	0	8	0	0.0	0.0	0.04	3.54	0.10
10	50000	2	2	14	2	0.0	0.0			
	100000	0	0	57	0	0.0	0.0	0.00	0.00	0.00

h)

	19.10.2018	0.05mM + IR								
Dose (Gy)	Plated cells	Well1	Well2	Well3	Mean	Std	PE	mean PE	mean SD	survival
0	100	46	42	31	40	7.8	39.7	39.33	6.67	100.00
	200	84	77	73	78	5.6	39.0			
2	500	56	70	66	64	7.2	12.8			
	1000	113	120	132	122	9.6	12.2	12.48	8.41	31.74
4	2000	53	62	90	68	19.3	3.4			
	5000	53	74	87	71	17.2	1.4	2.42	18.23	6.16
6	10000	44	47	54	48	5.1	0.5			
	20000	19	28	50	24	6.4	0.1	0.30	5.75	0.76
8	20000	8	24	28	26	2.8	0.1			
	50000	2	8	80	5	4.2	0.0	0.07	3.54	0.18
10	50000	5	10	9	8	2.6	0.0			
	100000	1	0	10	4	5.5	0.0	0.01	4.08	0.03

i)

	19.10.2018	IR alone								
Dose (Gy)	Plated cells	Well1	Well2	Well3	Mean	Std	PE	mean PE	mean SD	survival
0	100	57	53	47	52	5.0	52.3	49.08	8.63	100.00
	200	81	105	89	92	12.2	45.8			
2	500	71	96	91	86	13.2	17.2			
	1000	90	126	124	125	1.4	12.5	14.85	7.32	30.25
4	2000	64	70	74	69	5.0	3.5			
	5000	35	70	77	74	4.9	1.5	2.47	4.99	5.03
6	10000	22	39	58	40	18.0	0.4			
	20000	11	21	58	30	7.1	0.2	0.27	12.54	0.56
8	20000	9	18	30	14	6.4	0.1			
	50000	3	2	8	3	0.7	0.0	0.04	3.54	0.07
10	50000	1	1	9	4	4.6	0.0			
	100000	0	1	11	4	6.1	0.0	0.01	5.35	0.01

j)

	19.10.2018	0.1mM + IR								
Dose (Gy)	Plated cells	Well1	Well2	Well3	Mean	Std	PE	mean PE	mean SD	survival
0	100	49	38	43	43	5.5	43.3	41.92	6.66	100.00
	200	85	72	86	81	7.8	40.5			
2	500	76	67	77	73	5.5	14.7			
	1000	126	139	134	133	6.6	13.3	13.98	6.03	33.36
4	2000	60	69	79	69	9.5	3.5			
	5000	95	89	85	90	5.0	1.8	2.63	7.27	6.27
6	10000	61	63	79	68	9.9	0.7			
	20000	28	31	25	28	3.0	0.1	0.41	6.43	0.97
8	20000	5	17	25	21	5.7	0.1			
	50000	5	0	28	3	3.5	0.0	0.06	4.60	0.13
10	50000	1	0	4	2	2.1	0.0			
	100000	0	0	3	1	1.7	0.0	0.00	1.91	0.01

k)

	4.12.2018	IR alone								
Dose (Gy)	Plated cells	Well1	Well2	Well3	Mean	Std	PE	mean PE	mean SD	survival
0	100	49	41	53	48	6.1	47.7	40.33	4.86	100.00
	200	70	65	63	66	3.6	33.0			
2	500	57	66	68	64	5.9	12.7			
	1000	91	86	103	93	8.7	9.3	11.03	7.30	27.36
4	2000	49	34	41	41	7.5	2.1			
	5000	61	62	69	64	4.4	1.3	1.67	5.93	4.15
6	10000	30	16	43	30	13.5	0.3			
	20000	36	26	42	35	8.1	0.2	0.24	10.79	0.58
8	20000	9	5	9	7	2.8	0.0			
	50000	9	4	9	7	3.5	0.0	0.02	3.18	0.06

l)

	4.12.2018	0.05mM + IR								
Dose (Gy)	Plated cells	Well1	Well2	Well3	Mean	Std	PE	mean PE	mean SD	survival
0	100	42	41	39	41	1.5	40.7	37.83	4.26	100.00
	200	63	77	70	70	7.0	35.0			
2	500	47	66	57	57	9.5	11.3			
	1000	100	104	123	102	2.8	10.2	10.77	6.17	28.46
4	2000	45	40	47	44	3.6	2.2			
	5000	48	69	77	65	15.0	1.3	1.75	9.29	4.62
6	10000	25	23	26	25	1.5	0.2			
	20000	21	25	31	26	5.0	0.1	0.19	3.28	0.50
8	20000	5	0	5	3	3.5	0.0			
	50000	17	17	26	17	0.0	0.0	0.02	1.77	0.06

m)

	4.12.2018	0.1mM + IR								
Dose (Gy)	Plated cells	Well1	Well2	Well3	Mean	Std	PE	mean PE	mean SD	survival
0	100	49	36	50	45	7.8	45.0	39.92	7.42	100.00
	200	77	63	69	70	7.0	34.8			
2	500	42	45	40	42	2.5	8.5			
	1000	74	65	72	70	4.7	7.0	7.75	3.62	19.42
4	2000	31	22	39	31	8.5	1.5			
	5000	42	51	111	47	6.4	0.9	1.23	7.43	3.09
6	10000	23	18	26	22	4.0	0.2			
	20000	29	20	32	27	6.2	0.1	0.18	5.14	0.45
8	20000	4	2	5	4	2.1	0.0			
	50000	7	10	21	9	2.1	0.0	0.02	2.12	0.04

Tables g)-m)- Raw data from clonogenic survival curves comparing IR alone with H_2O_2 + IR in HCT116 cell line (n=2). Data displays colony numbers in each well of a 6-well plate, according to cell seeding number, with calculated plating efficiency (PE). Percentage colony survival is normalised to untreated controls.

Appendix 2

Nimalasena S, Gothard L, Anbalagan S, Allen S, Sinnett V, Mohammed K, Kothari G, Musallam A, Lucy C, Yu S, Nayamundanda G, Kirby A, Ross G, Sawyer E, Castell F, Cleator S, Locke I, Tait D, Westbury C, Wolstenholme V, Box C, Robinson SP, Yarnold J, Somaiah N. Intratumoral Hydrogen Peroxide With Radiation Therapy in Locally Advanced Breast Cancer: Results From a Phase 1 Clinical Trial. Int J Radiat Oncol Biol Phys. 2020 Nov 15;108(4):1019-1029. doi: 10.1016/j.ijrobp.2020.06.022. Epub 2020 Jun 22. PMID: 32585332.

International Journal of Radiation Oncology biology • physics

www.redjournal.org

Clinical Investigation

Intratumoral Hydrogen Peroxide With Radiation Therapy in Locally Advanced Breast Cancer: Results From a Phase 1 Clinical Trial

Samantha Nimalasena, FRCR,[*,†] Lone Gothard, HND,[*] Selvakumar Anbalagan, DPhil,[*] Steven Allen, FRCR,[†] Victoria Sinnett, MSc,[†] Kabir Mohammed, MSc,[†] Gargi Kothari, MBBS,[†] Annette Musallam, MPharm,[†] Claire Lucy,[†] Sheng Yu, PhD,[*] Gift Nayamundanda, MD,[*] Anna Kirby, MD,[*,†] Gill Ross, PhD,[†] Elinor Sawyer, PhD,[‡] Fiona Castell, FRCR,[§] Susan Cleator, PhD,[‖] Imogen Locke, MD,[†] Diana Tait, MD,[†] Charlotte Westbury, PhD,[¶] Virginia Wolstenholme, FRCR,[#] Carol Box, PhD,[*] Simon P. Robinson, PhD,[*] John Yarnold, FRCR,[*,†] and Navita Somaiah, DPhil[*,†]

Division of Radiotherapy and Imaging, the Institute of Cancer Research, London, UK; †The Royal Marsden NHS Foundation Trust, London, UK; ‡Guy's and St Thomas' NHS Foundation Trust, London, UK; §King's College Hospital NHS Foundation Trust, London, UK; ‖Imperial College Healthcare NHS Trust, London, UK; ¶Mount Vernon Cancer Centre, Northwood, UK; and #Barts Health NHS Trust, London, UK

Received Mar 24, 2020. Accepted for publication Jun 12, 2020.

Purpose: Hydrogen peroxide (H_2O_2) plays a vital role in normal cellular processes but at supraphysiological concentrations causes oxidative stress and cytotoxicity, a property that is potentially exploitable for the treatment of cancer in combination with radiation therapy (RT). We report the first phase 1 trial testing the safety and tolerability of intratumoral H_2O_2 + external beam RT as a novel combination in patients with breast cancer and exploratory plasma marker analyses investigating possible mechanisms of action.

Methods and Materials: Twelve patients with breast tumors ≥3 cm (surgically or medically inoperable) received intratumoral H_2O_2 with either 36 Gy in 6 twice-weekly fractions (n = 6) or 49.5 Gy in 18 daily fractions (n = 6) to the whole breast ±

Corresponding author: Navita Somaiah, PhD; E-mail: Navita.Somaiah@icr.ac.uk

The authors received funding from Kortuc Inc, Japan, and NHS funding to the NIHR Biomedical Research Centre at the Royal Marsden NHS Foundation Trust and the Institute of Cancer Research.

Disclosures: The authors declare no potential conflicts of interest.

All data generated and analyzed during this study are included in this article (and its supplementary files).

Supplementary material for this article can be found at https://doi.org/10.1016/j.ijrobp.2020.06.022.

Acknowledgments—We acknowledge the invaluable contribution of Professor Emeritus Yasuhiro Ogawa, University of Kochi, Japan, inventor of the KORTUC treatment, as scientific advisor to the UK Phase 1 trial. We are extremely grateful to him for training the UK team in the injection technique and for sharing his extensive clinical experience in treating Japanese cancer patients that has contributed immensely to the design of this trial.

Int J Radiation Oncol Biol Phys, Vol. 108, No. 4, pp. 1019–1029, 2020

https://doi.org/10.1016/j.ijrobp.2020.06.022

locoregional lymph nodes in a single-center, nonrandomized study. H_2O_2 was mixed in 1% sodium hyaluronate gel (final H_2O_2 concentration 0.5%) before administration to slow drug release and minimize local discomfort. The mixture was injected intratumorally under ultrasound guidance twice weekly 1 hour before RT. The primary endpoint was patient-reported maximum intratumoral pain intensity before and 24 hours postinjection. Secondary endpoints included grade ≥3 skin toxicity and tumor response by ultrasound. Blood samples were collected before, during, and at the end of treatment for cell-death and immune marker analysis.

Results: Compliance with H_2O_2 and RT was 100%. Five of 12 patients reported moderate pain after injection (grade 2 Common Terminology Criteria for Adverse Events v4.02) with median duration 60 minutes (interquartile range, 20-120 minutes). Skin toxicity was comparable to RT alone, with maintained partial/complete tumor response relative to baseline in 11 of 12 patients at last follow-up (median 12 months). Blood marker analysis highlighted significant associations of TRAIL, IL-1β, IL-4, and MIP-1α with tumor response.

Conclusions: Intratumoral H_2O_2 with RT is well tolerated with no additional toxicity compared with RT alone. If efficacy is confirmed in a randomized phase 2 trial, the approach has potential as a cost-effective radiation response enhancer in multiple cancer types in which locoregional control after RT alone remains poor.

Introduction

Breast cancer presents a global challenge, with an estimated incidence of 2 million patients worldwide, 80% of whom present with locally advanced disease.[1,2] In the United Kingdom, where women with locally advanced disease represent a minority (7%-13%) of the 55,000 new patient presentations, the lifetime morbidity of progressive local disease is significant.[3-5] Treatment is challenging in frail or elderly individuals who are unfit for or refuse surgery and for whom radiation therapy (RT) ± hormone therapy is often the most appropriate option for relief of breast ulceration, bleeding, and pain. Locally advanced inoperable primary or recurrent cancers infiltrating the breast/chest wall and/or axilla, with or without metastases, are typically associated with life expectancies measured in years rather than months and present significant challenges to patients and medical professionals. This represents an area of unmet clinical need, in which innovative approaches to enhance response to radiation would be highly beneficial.

An interaction at a cellular level between H_2O_2 and ionizing radiation (IR) was first reported in osteosarcoma (HS-Os-1) and prostate cancer (PC-3) cell lines, which demonstrated extreme resistance to either H_2O_2 or 30 Gy alone.[6,7] The addition of 0.1 mM H_2O_2 before IR resulted in enhanced cytotoxicity without causing DNA double strand breaks that classically mediate cell killing.[8,9] A novel mechanism was postulated to involve lysosomal membrane rupture with release of powerful oxidants, including heavy metal ions that permeabilize mitochondria and activate apoptosis.[10] In vivo use involved a mixture of 0.5% H_2O_2 in 0.83% sodium hyaluronate gel, the Kochi Oxydol-Radiation Therapy for Unresectable Carcinomas (KORTUC) strategy designed to minimize local pain at the injection site. Intratumoral injection of this H_2O_2 gel mixture into murine tumors before 30 Gy IR demonstrated clear evidence of growth delay greater than that achieved by either modality alone. No toxicity was noted.[11]

In this study we report the first systematically conducted phase 1 trial testing intratumoral H_2O_2 in combination with RT in locally advanced breast cancer (NCT02757651). The primary objective was assessment of safety and tolerability of H_2O_2 injections with moderately hypofractionated RT. Secondary endpoints included the proportion of patients requiring additional pain medication, incidence of grade ≥3 skin toxicity, and tumor response assessment. Exploratory analysis of plasma markers was also performed.

Methods and Materials

Study design

This nonrandomized study involved patients with locally advanced or locally recurrent breast cancer (with or without metastases) for whom RT was indicated for locoregional disease control. Patients were inoperable due to comorbidities or local disease extent, or surgery to the breast primary was not appropriate due to presence of metastatic disease.

The single-center study was conducted at The Royal Marsden NHS Foundation Trust (CCR4502). Approval by the Research Ethics Committee (REC) and the Medicines and Healthcare products Regulatory Agency (MHRA) was obtained before trial commencement (IRAS 203161, REC 16/LO/1566, EudraCT 2016-000833-40). Monitoring was undertaken by the Clinical Trials Unit at The Royal Marsden NHS Foundation Trust. The trial schema is shown in Figure 1.

Eligible patients were older than 18 years of age, had histologically confirmed breast cancer, and required breast RT for local control and/or palliation of locoregional symptoms. They had at least 1 breast tumor measuring ≥3 cm in diameter in a superficial location accessible for injection. Any combination of estrogen receptor (ER), progesterone receptor (PR), and HER2 expression was allowed. Exclusion criteria included prior RT to the breast and concomitant biological therapies other than trastuzumab, pertuzumab, and denosumab. Pregnancy was excluded in female patients of child-

bearing age. Patients were excluded if the anatomic location of the breast tumor, such as proximity to blood vessels or the brachial plexus, precluded safe access for intratumoral injection. This precaution minimized the risk of injection into a blood vessel causing embolism, an adverse effect that has not been described in the literature in relation to intratumoral H_2O_2.[12,13]

Drug formulation

A slow-release 0.5% H_2O_2 solution was created by mixing 0.4 mL of 3% H_2O_2 (2.0 mL sterile ampoules supplied by Stockport Pharmaceuticals, UK) with 2.0 mL OSTENIL (20 mg sodium hyaluronate in a 2.0-mL preloaded syringe provided by AAH Pharmaceuticals, UK), the latter licensed for intra-articular injection of arthritic joints.[14] The low molecular weight of H_2O_2 (34 g/mol) ensures rapid equilibration of drug within the gel. The mixture is a colorless, viscous solution (pH 6.8-7.8) stored at room temperature and stable for 2 hours after preparation, as determined by viscosity measurements (performed by Stockport Pharmaceuticals, UK). The gel allows slow release of H_2O_2 for at least 24 hours, as evidenced by generation of oxygen microbubbles during injection, a feature that provides a strong rationale for twice-weekly administration during RT.[15] In the trial, the drug and gel were mixed under aseptic conditions using 2 syringes connected via a 2-way tap. Once made, each syringe contained 2.4 mL of 0.5% H_2O_2, the contents of both syringes typically needed for tumors measuring 30 to 60 mm in diameter.

Radiation therapy

Six patients received 49.5 Gy in 18 daily fractions of 2.75 Gy, and 6 were treated with 36 Gy in 6 twice-weekly

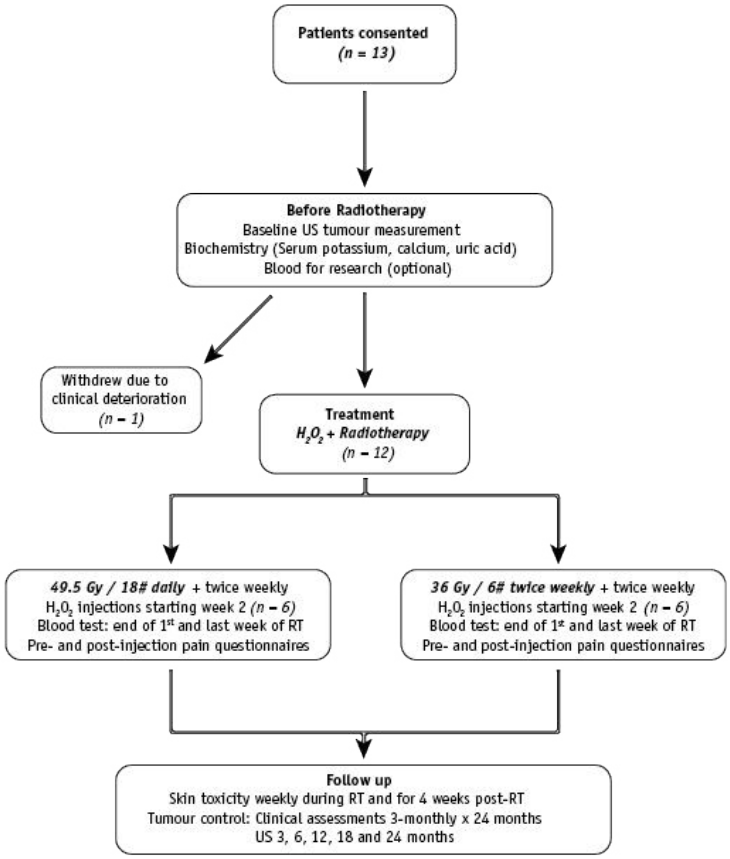

Fig. 1. Phase 1 trial schema. A nonrandomized study design testing intratumoral H_2O_2 in sodium hyaluronate gel in combination with 2 radiation therapy fractionation schedules in patients with locally advanced breast cancer and corresponding follow-up schedule. *Abbreviations:* RT = radiation therapy; # = radiation therapy fraction; US = ultrasound.

fractions of 6 Gy to the whole breast ± locoregional lymph nodes. The equivalent RT dose expressed in conventional 2-Gy fractions (EQD_2) was 57 Gy and 65 Gy for these 2 schedules, respectively (Fig. E1). Patients on the 6-Gy twice-weekly schedule, requiring lymph node irradiation in addition to the breast, were treated to a total dose of 30 Gy in 5 twice-weekly fractions of 6 Gy to the nodal regions, to not exceed brachial plexus tolerance dose (as per standard institutional guidelines).

The RT schedule was selected according to the patient's performance status and comorbidities, with fitter patients selected for the daily treatment schedule. RT was delivered using a linear accelerator with 6 to 10 MV photons, 3-dimensionally planned using data from a computed tomography planning scan and using standard tangentially opposed fields. Patients were simulated and treated in the supine position on a breast board with both arms abducted. The clinical target volume comprised the entire ipsilateral breast, including the deep fascia, but excluding underlying muscle or overlying skin (when not involved with disease). The RT dose was prescribed to the 100% isodose, ensuring the target volume was within the 95% to 107% isodose lines. Organs at risk including the heart, lung, and contralateral breast were outlined and standard guidelines for dose tolerances were followed. A standard treatment verification protocol was used, consisting of daily imaging for the first 3 days and subsequent weekly imaging. In cases in which there was skin involvement by tumor, treatment included 5 mm wax bolus throughout RT to maximize dose to skin, in keeping with standard practice. In patients treated with 49.5 Gy in 18 fractions, a sequential boost dose to the tumor bed (13.35 Gy in 5 daily fractions using minitangential opposed beams or a directly applied electron beam) was allowed, but this needed to be declared at time of trial entry. A tumor bed boost dose increased the EQD_2 to that comparable with 36 Gy in 6 fractions and with dose intensities previously reported in earlier patient cohorts treated with the same drug preparation.[16,17]

Intratumoral injections of H_2O_2 in sodium hyaluronate gel

Transdermal intratumoral KORTUC injections were administered twice weekly commencing in the second calendar week of RT. Each patient received 4 to 6 doses in total (median = 5 injections), the smaller number given to patients prescribed 6 fractions. The rationale for starting KORTUC in the second week was to allow for reduction in tumor interstitial pressure during the first week of RT, enabling technically easier and more tolerable injections for the patient. Injections were performed (23-gauge needle) under ultrasound (US) guidance by a trained radiologist or radiographer after 0.5% lignocaine injection to anesthetize the skin. For tumors measuring 30 to 60 mm in size, 2 syringes (4.8 mL) of 0.5% H_2O_2 in sodium hyaluronate gel were injected at each time point. Three syringes (7.2 mL) were required for tumors >60 mm in size.

Uniform and accurate delivery under US guidance via 2 to 3 differently angled needle tracks was aided by the immediate appearance of oxygen microbubbles as H_2O_2 degraded to oxygen and water within the tumor (Fig. 2A). The needle tip was positioned at the deepest aspect of the tumor and the gel released slowly while withdrawing the needle toward the surface. For smaller tumors, it was possible to achieve even distribution of the H_2O_2 gel mixture within the tumor via a single skin puncture site and by altering the angle of the needle (working from left to right or top to bottom within the tumor). For some larger tumors (eg, >60 mm) it was necessary to inject the tumor via more than 1 skin entry point from different directions to ensure even distribution of oxygen microbubbles throughout the tumor volume. The number of needle tracks within the tumor and skin entry points were decided by the radiologist during the US scan and guided by the extent and distribution of oxygen microbubbles during the injection procedure. If any gel tracked back to the skin surface during withdrawal of the needle, it was promptly wiped away with sterile gauze. If patients had >1 distinct tumor in the breast/axilla, the clinician/radiologist was required to clearly document the injected lesion (usually the largest) to aid response assessment. RT was delivered within 1 to 2 hours after H_2O_2 injection.

Treatment monitoring

Within each RT group (daily or twice-weekly fractions), a minimum gap of 1 week was stipulated between the first and second patient, during which acute toxicity data associated with intratumoral injections (pain, skin toxicity, and tumor lysis) were reviewed by an independent data monitoring committee. Based on predetermined criteria, the second and third patients in each group and subsequently the fourth, fifth, and sixth patients in each group were allowed to be treated concomitantly.

Primary endpoint

This related to the timing, severity, and duration of pain postinjection recorded via a self-reported questionnaire completed by patients at home. An 11-point numerical scale ranging from 0 ("no pain") to 10 ("worst possible pain") recorded severity and duration before and more than 24 hours after each H_2O_2 injection (Fig. E1). Patient-reported scores were used to calculate (1) the proportion of patients with pain scores ≥5 points greater than baseline after any of the intratumoral injections and (2) the requirement for additional pain medication.

Secondary endpoints

Secondary endpoints included acute RT-induced skin toxicity, serum biochemistry, and tumor response. Skin

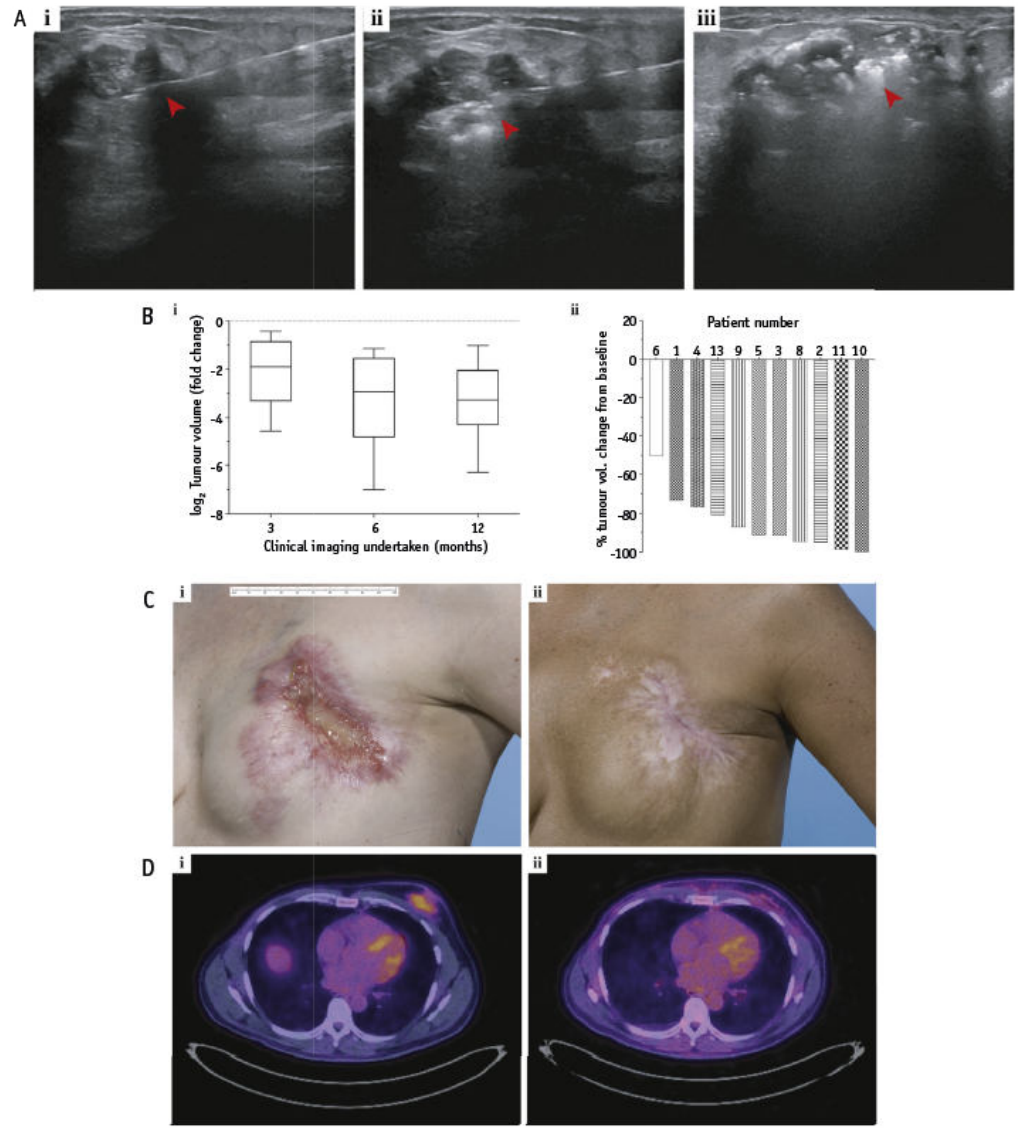

Fig. 2. Intratumoral H_2O_2 administration and tumor response. (A) Sequence of ultrasound images of a breast tumor showing H_2O_2 administration, red arrow indicating (i) needle entering under ultrasound guidance, (ii) H_2O_2 + sodium hyaluronate gel mixture being injected intratumorally, and (iii) breakdown of H_2O_2 with formation of echogenic oxygen microbubbles (white) within the tumor. (B) Tumor volume changes: (i) box plot showing the cumulative fold decrease (log2 transformed) for all 12 patients, at the indicated time points post-RT and (ii) waterfall plot showing % tumor volume change up to 12 months post-RT normalized to baseline tumor measurement (data represent tumor measurements at 9 and 12 months post-RT for 3 and 8 patients, respectively). (C) Clinical photographs of patient 10: (i) left breast with fungating tumor (baseline) and (ii) 12 months posttreatment with H_2O_2 + RT. (D) ^{18}F-FDG PET scans of patient 8: (i) high tracer uptake in left breast tumor at baseline and (ii) complete metabolic response at 12 months posttreatment. *Abbreviations:* FDG = fluorodeoxyglucose; PET = positron emission tomography; RT = radiation therapy.

toxicity was assessed weekly in all patients during and for 4 weeks after RT by a member of the clinical team. Standardized proformas recorded the degree of erythema and desquamation of the skin of the breast. In each of the RT groups, if no more than 1 of the first 3 patients had a persistent Common Terminology Criteria for Adverse Events (CTCAE) (v4.02) skin toxicity grade $\geq$3 at 6 weeks after RT, the independent data monitoring committee allowed recruitment to continue for a further 3 patients within that RT schedule. If moist desquamation was seen beyond skin folds, weekly assessments were continued until severity was reduced to grade $\leq$1. The proportion of patients with grade $\geq$3 skin toxicity at any time from the start of RT to 4 weeks post-RT and the worst grade of skin toxicity reported from the start of RT to 4 weeks post-RT were recorded in these cases. However, it was recognized that if cancer infiltrated skin, patients would typically experience grade $\geq$3 skin toxicity after RT alone.

In every patient, routine biochemistry including serum potassium, calcium, and uric acid were measured 2 days after the first H_2O_2 dose to rule out tumor lysis before proceeding with subsequent doses.[18]

Tumor response were assessed at 3, 6, and 12 months posttreatment. At each timepoint, 3-dimensional US measurements were obtained and the tumor volume was calculated on the assumption that breast tumors assume a hemiellipsoid shape, as previously demonstrated.[19] Maximum tumor dimension alone was not considered an accurate representation of tumor response, especially when tumors "flatten" after RT. Tumor volumes were compared against pretreatment measurements applying RECIST-like principles, with complete response (CR) defined as disappearance of the target lesion, partial response (PR) as at least a 30% reduction in tumor volume, and stable disease (SD) as less than a 30% reduction or 20% increase in tumor volume.

Statistical considerations

Based on the previously published data, 30% to 100% of patients experienced pain described as no worse than "mild" (or CTCAE grade 1) for several hours after injection.[16,20-22] A single case of tumor lysis syndrome (mild) was reported in a total of 139 breast cancer patients in the Japanese literature. Given this knowledge of the safety of H_2O_2 plus RT, the phase 1 trial required 12 patients to be recruited. Patients treated with once-daily and twice-weekly fractions of RT were analyzed as a single stratum, and the study population was defined as all patients who registered for the trial and received at least 1 dose of intratumoral H_2O_2. Tumor volumes were calculated using 3-dimensional measurements obtained from US scans.

Plasma markers

Blood samples were obtained pre-RT and at the end of the first and last weeks of RT. Blood (two 9-mL K3-EDTA tubes) was obtained by venipuncture and processed within 30 minutes. Plasma and buffy coat were isolated by centrifugation at 1600 $\times$ g for 10 minutes at room temperature and frozen in aliquots at -80°C. All the plasma samples subsequently underwent 1 freeze-thaw cycle before assay.

ELISA and Luminex assay

Frozen plasma samples were thawed on ice and brought to room temperature. They were spun at 10,000 $\times$ g for 10 minutes and the plasma supernatant assayed either by ELISA or Luminex assay as per the manufacturers' protocols. Results were measured against a normal plasma control obtained from a healthy donor (Cambridge BioScience Ltd). The absorbance for ELISA was obtained using a POLAR star Omega plate reader spectrophotometer (BMG Labtech). The Luminex Human XL Cytokine Discovery Panel (15-plex, #FCSTM18-15, R&D System) was carried out with a minimum of 100 events per bead using a Luminex 200 system with xPONENT v3.1 software (Millipore). The plasma samples were assayed in duplicate wells for individual targets at their corresponding time points (pre-RT, end of first week of RT, and post-H_2O_2 + RT), and the log2 fold change was calculated. Further information regarding the ELISA and Luminex analytes, their dilutions, and kit details used in this study are provided in Table E1.

Exploratory translational endpoints

Exploratory analyses of plasma biomarkers of cell death, inflammation, and immune response were conducted to test the feasibility of investigating novel mechanisms of action and biomarkers of response in trial patients. A linear mixed effect model was used to model the random effect of longitudinal data that the markers generated.[23] The model was built to study the effect of each marker and to quantify its significance in terms of association with tumor shrinkage over time. The difference between individual and temporal variability was treated as a random effect. The impact of each marker was regarded as a fixed effect. The model used was

Tumor_volume = marker + time + marker: time + random_effect (time)

The ":" sign denotes the variation of each plasma marker with time. Each marker was used to fit a mixed model individually with all patient samples, and 20 models were fitted in total. A P value for the coefficient of each marker was calculated to indicate whether the fixed effect had significance (at the 5% level). All graphs were generated using Graphpad Prism v8.1 (Mac OS), Graphpad Software (La Jolla, CA).

Results

Patient characteristics

Patient demographics, tumor characteristics, prior treatment, and RT target volumes are summarized in Table 1.

Thirteen patients (11 female, 2 male) were recruited to the study between February 2017 and August 2018. All patients had locally advanced or recurrent breast cancer and were inoperable due to comorbidities, local extent of disease, or metastatic disease. One patient withdrew due to clinical deterioration unrelated to the trial before starting RT and received no H_2O_2, so an additional (13th) patient was recruited. Median age was 77 years (range, 45-93). Three patients were wheelchair-bound due to comorbidities and frailty. Breast tumor stage was T2 in 5 of 12 patients and T4 in 7 of 12 patients. Six of 12 patients had N0 and 6 of 12 N1 disease (axillary node involvement). Eight of 12 patients had distant metastases. Breast tumor size varied from 30 mm to 164 mm (maximum dimension). Ten patients had ER+/HER2− disease, and 2 had triple negative disease. There were no patients with inflammatory breast cancer. All patients had received 1 to 4 previous lines of treatment for their breast cancer, and the majority had progressed on prior systemic treatment. Three patients had prior surgery for breast cancer but had locally recurrent disease. During RT, 7 of 12 patients continued taking concurrent hormone therapy, and 2 of 12 continued bisphosphonate therapy for metastatic bone disease.

Compliance with treatment protocol and follow-up

Compliance with H_2O_2 injections was 100% in all patients, including 1 with needle phobia. All patients received RT within the prescribed 1 to 2 hours of receiving the H_2O_2 injection, with a single exception of a patient given 1 RT fraction before H_2O_2 injection in error. Results are reported at a minimum follow-up of 12 months for all patients alive at the time of reporting (range, 2-24 months). Eleven patients completed 12 months of follow-up, and the 12th died of rapidly progressive metastatic disease slightly less than 2 months after RT.

Primary endpoint

The pain scores are summarized in Table 2, with respective grades detailed in Figure E1 (iii). Three of 12 patients experienced grade 1 (mild) tumor pain postinjection, and 5 of 12 experienced grade 2 pain (moderate severity, limiting activities of daily living) as per CTCAE v4.02.[24] The remainder did not report any additional pain after intratumoral injection. Median pain duration was 60 minutes with an interquartile range of 20 to 120 minutes.

Four of 12 patients reported pain $\geq$5 points above baseline during treatment. One patient was taking opiate analgesia (oral morphine) before starting RT to control pain resulting from a fungating breast tumor. Six of 12 patients required additional analgesia to manage their symptoms (paracetamol and codeine-based). In these cases, management included ensuring compliance with pre-existing painkillers and optimizing analgesia ± anxiolytics for the remainder of their treatment.

Table 1 Summary of patient demographics, tumor characteristics, previous lines of treatment, and RT treatment volumes

Patient	Age	Sex	PS* (ECOG)	Baseline TNM stage	Tumor phenotype	Prior treatment (no. of lines of therapy)	RT target volume
1	77	F	1	T2N1M1	$ER^+/HER2^-$	Endocrine (3)	Breast + axillary LN levels I-IV
2	69	F	0	T4N0M1	$ER^+/HER2^-$	Endocrine (2)	Breast
3	79	F	3	T4N0M0	$ER^+/HER2^-$	Endocrine (3)	Breast
4	80	M	2	T4N0M0	$ER^+/HER2^-$	Endocrine (2)	Breast
5	89	F	3	T2N0M0	$ER^+/HER2^-$	Endocrine (1)	Breast
6	78	F	2	T4N1M1	$ER^+/HER2^-$	Endocrine (2) Chemotherapy (1)	Breast + axillary LN levels I-IV
8	53	M	0	T2N0M1	$ER^-/HER2^-$	Surgery – Chemotherapy (4) RT (contralateral)	Breast
9	53	F	2	T2N1M1	$ER^+/HER2^-$	Surgery Endocrine (3) Chemotherapy (2) RT (contralateral)	Breast + axillary LN levels I-IV
10	45	F	0	T4N1M1	$ER^+/HER2^-$	Chemotherapy (1)	Breast + axillary LN levels I-IV
11	75	F	3	T4N1M1	$ER^+/HER2^-$	Surgery Endocrine (3)	Breast
12	45	F	1	T4N1M1	$ER^-/HER2^-$	Chemotherapy (2)	Breast + axillary LN levels I-IV
13	93	F	3	T2N0M0	$ER^+/HER2^-$	None	Breast

Abbreviations: ECOG = Eastern Cooperative Oncology Group; RT = radiation therapy; TNM = tumor, node, metastasis.
Patients 1, 3, 4, 5, 11, and 13 received 36 Gy/6 fractions, and 2, 6, 8, 9, 10, and 12 received 49.5 Gy/18 fractions.
* Performance status (Eastern Cooperative Oncology Group).

Table 2 Summary of pain scores and RT acute skin toxicity scores

Patient number	Maximum pain intensity		Extra analgesia required	Median difference in pain score (pre- and post-RT)	Effect of pain on ADLs	Maximum RT acute skin toxicity score	Bolus during RT
	Score	Period					
1	4	2 h	N	3	Y—housework, shopping	3	Y
2	0	0 min	N	0	N	3	Y
3	3	30 min	N	2.5	N	2	N
4	4	30 min	Y	0.5	N	2	N
5	0	0 min	N	0	N	0	N
6*	10	6 h	Y	5	N	1	N
8†	10	6 h	Y	6	Y—driving	2	N
9	6	5 h	N	4	N	2	N
10	8	2 h	Y	7	Y—housework	3	Y
11	0	0 min	N	0	N	3	Y
12‡	0	0 min	Y	0	N	3	Y
13	6	1 h	Y	5	N	0	N

Abbreviations: ADL = activities of daily living; CTCAE = Common Terminology Criteria for Adverse Events; RT = radiation therapy.

Pain intensity scored from 0 to 10 via patient self-assessment questionnaires (median calculated from difference in pain score pre- and post-H_2O_2 injection for each patient throughout treatment course (4-6 injections in total for each patient)); RT acute skin toxicity scored from 0 to 5 using CTCAE v4.02 by clinicians.

* Patient with needle phobia.

† Patient had significant breast pain before H_2O_2 injection and poor compliance with analgesia.

‡ Patient with significant breast pain and was taking opiate analgesia before RT, explaining the pain score of 0.

Secondary endpoints

Skin toxicity and tumor lysis

The highest grade of skin toxicity reported was grade 3 in 5 of 12 patients, grade 2 in 4 of 12 patients, grade 1 in 1 of 12 patients, and grade 0 in 2 of 12 patients (Table 2 and Fig. E1 [iv]). All 5 patients who experienced grade 3 skin toxicity had been treated with bolus during RT (due to skin involvement by tumor). There was no suggestion of enhancement of erythema due to local leakage of H_2O_2. The acute radiation skin toxicity observed in the trial was comparable to that expected with standard RT alone, including in patients with cancer infiltrating overlying skin.[25] There were no cases of tumor lysis syndrome.

Tumor response

Figure 2B (i) and Table E2 detail the tumor response based on US measurements at successive time points posttreatment. At the last imaging assessment percentage tumor volume reduction was between 50% and 100%, as shown in Figure 2B (ii). All evaluable patients in this study maintained locoregional control in the irradiated target lesion at last clinical follow-up (median, 12 months; range, 2-24 months). Patient 12 died of metastatic disease 6 weeks after RT and was not evaluable at the 3-month endpoint for tumor response.

As an illustrative example, Figure 2C shows tumor extent in patient 10 pre-RT and 12 months posttreatment (patient maintained CR at 18 months). Only 1 of 12 patients had >1 distinct tumor lesion within the RT treatment volume. In this patient only the tumor injected with H_2O_2 showed maintained PR at 12 months, whereas the 2 lesions receiving the same RT alone showed SD (the noninjected lesions acting as internal controls). With regard to tumor response assessment, there were discrepancies in 2 patients between US and clinical response assessments (Table E2). In patient 9, US measurements between 6 and 12 months suggested an increase in tumor size despite an excellent partial response on clinical examination. Radiology review of the US images at 12 months posttreatment indicated changes consistent with fibrosis rather than active tumor. Similarly, patient 8 demonstrated a CR on clinical assessment at 12 months, despite the presence of stable measurable disease on US. A staging positron emission tomography/computed tomography scan performed concurrently confirmed complete metabolic response in the H_2O_2 + RT-treated breast tumor, as shown in Figure 2D.

Exploratory secondary endpoint (post hoc analysis)

Ten of 12 patients consented to provide blood for research at the time points shown in Figure 3A. The exploratory target panel for ELISA and Luminex assays comprised 21 markers involved in cell death, the immune checkpoint, chemo-attraction, immune regulation, and angiogenesis (Table E3). Log2-transformed fold change of targets normalized to their baseline (pre-RT) expression was plotted for all patients, comparing levels after RT alone (at the end of the first week of treatment) and after H_2O_2 + RT (end of treatment) (Figs. 3B, E3). There was no consistent trend when comparing RT alone versus H_2O_2 + RT in this small exploratory cohort. However, upregulation of markers involved in inflammation, immune modulation,

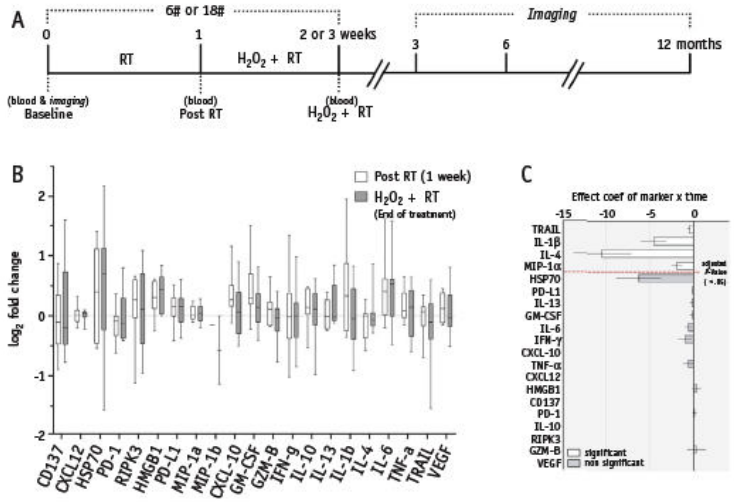

Fig. 3. Analysis of phase 1 trial plasma markers. (A) Scheme showing clinical imaging and blood sampling performed in this study. (B) Box and whisker plot depicting log2-transformed fold change of analyzed targets from individual patients. Values are normalized to their baseline expression for all 21 targets. (C) Plot shows the significant markers associated with tumor volume shrinkage, with multicomparison adjusted P value $< .05$. The bar shows the fixed effect of each marker with error bars, ranked by P values. A negative coefficient means that the marker is positively correlated with tumor shrinkage. *Abbreviation:* # = radiation therapy fraction.

and damage-associated molecular patterns (DAMPs) was noted.[26] Application of a linear mixed effect model identified 4 significant ($P < .05$) associations with tumor shrinkage, suggesting TRAIL mediated apoptosis with increased activated T cell signaling (IL-4, MIP-1α) and macrophage stimulation (IL-1β) (Fig. 3C and Table E4).

Discussion

This phase 1 study raised no concerns relating to local or systemic toxicity when intratumoral H_2O_2 is delivered with RT doses per fraction up to 6 Gy in patients with locally advanced primary or recurrent breast cancer unsuitable for primary surgery or palliative debulking. The intervention is well tolerated even by frail, older patients and those with needle phobia. In those patients with pre-existing pain symptoms, it was important and straightforward to optimize pain medication before starting treatment.

Commencing H_2O_2 injections in the second calendar week of RT ensured that there were no technical challenges (ie, resistance due to tissue turgor) to injecting the prescribed volume of drug in any of the patients. Given that H_2O_2 breaks down to O_2 within the tumor (2 molecules of H_2O_2 degrade to 1 molecule of O_2 and 2 molecules of water), it is hypothesized that this may contribute to reoxygenation of hypoxic areas, thereby alleviating radiation resistance. Therefore, aside from the classical DNA damage effects, another mechanism of synergy between H_2O_2 and RT may result from reoxygenation. This is currently being investigated in the laboratory setting. In tumors that do not reoxygenate spontaneously during fractionated RT, H_2O_2 is expected to be most effective after the second week of RT, when such tumors are likely to be enriched with hypoxic radioresistant subpopulations.[27-29]

Acute skin toxicity was no different to that expected after the same RT alone. As predicted, grade 3 radiation dermatitis occurred only in those patients with tumor involving skin, when a 5-mm layer of wax "blanket" ensured 100% prescribed RT dose to skin instead of approximately 70% of prescribed dose in patients without skin involvement.[30] Grade 3 skin desquamation managed with standard supportive measures including barrier creams and dressings ensured complete resolution of symptoms in every case. Overall, toxicity and tolerability were entirely consistent with extant literature, and these phase 1 data will contribute to an application for regulatory approval if the planned randomized phase 2 study confirms efficacy.

In view of the limitations of US in response assessment, magnetic resonance imaging has been selected as the imaging modality to monitor tumor response in the forthcoming phase 2 trial. In patients with locally advanced breast cancers treated with RT alone at equivalent doses to those used in this study, local control rates would be expected to be 45% to 57% at 3 years posttreatment, with lower rates associated with larger tumors.[31,32] Although it

is impossible to draw conclusions on efficacy in this phase 1 trial, anecdotal tumor responses are suggestive of enhanced antitumor effect. Because lifetime control of symptomatic locally advanced breast cancer is a major determinant of patient quality of life as well as survivorship, there is potential for an effective treatment to be globally beneficial, in which women with inoperable breast cancer often have limited access to effective treatment.[33,34] Intratumoral H_2O_2 injections are inexpensive and easy to administer, requiring minimal additional training and infrastructure.

Our study has also established that circulating plasma markers can be successfully quantified using the ELISA and Luminex platforms, providing insights into mechanisms of cell death after treatment. IR and H_2O_2 induce reactive oxygen species, inflammatory signaling, DNA damage, senescence, and cell death. In addition, IR can modulate the immunoinflammatory axis through the generation of ROS and DAMPs.[35] The wide range of potential mechanisms of interaction informed the choice of 21 markers in our exploratory panel.

The effect of H_2O_2 within the cell is concentration dependent, having a role in signaling and homeostasis at nanomolar concentrations (nM) and triggering cell death at supraphysiological (mM) concentrations.[36] The physiological outcome within the cell is modulated by antioxidant enzymes such as catalases, peroxidases, and thioredoxin-linked systems.[37] By affecting protein kinases and phosphatases, H_2O_2 influences a number of signaling cascades including ERK, JNK, MAPK, p38, TNFα, NFκB, IL-1β, IL-6, IL-8, MCP-1, and MIP.[36,38,39] Several publications have demonstrated apoptosis as the principal mode of cell death after H_2O_2 treatment.[10,40-42] The intrinsic mitochondrial pathway is thought to be the predominant mechanism of apoptosis.[43] One study reported apoptosis induction after exposure to H_2O_2 levels <0.4 mM and upregulation of RIP, a gene associated with necrosis, at higher concentrations.[44]

Exposure to H_2O_2 can result in increased expression of inflammatory cytokines.[45] IL-1 is a key mediator of T cell and dendritic cell function. Increased IL-1α levels occur in cells undergoing necrosis, whereas IL-1β signals toward apoptosis.[46,47] Another study reported that treating murine splenic T cells with H_2O_2 resulted in a significant increase in IL-4 production, a key regulator of humoral and adaptive immunity.[48] Both IL-1β and IL-4 were significantly associated with tumor shrinkage in our study.

In our plasma analysis, a significant association between TRAIL and tumor shrinkage was also found. Intracellular ROS such as H_2O_2 is thought to mediate apoptosis via death receptor ligands such as TRAIL.[43] A study in an astroglial cell line demonstrated an increase in TRAIL gene expression in cells treated with H_2O_2 in a dose-dependent manner up to a concentration of 0.8 mM.[49] TRAIL-dependent apoptosis regulates the priming of $CD8^+$ memory T cells by $CD4^+$ T_H1 cells.[50] In a study using a murine macrophage cell line (B10R), exposure to H_2O_2 increased the transcription of the chemokines MIP-1α, MIP-1β, MIP-2, and MCP-1.[51] MIP-1β was undetectable in 7 of 10 patients, but MIP-1α expression was detected to a varying degree in all cases, suggesting activation of $CD8^+$ T lymphocytes.

In summary, the analysis of blood biomarkers showed correlations with clinical tumor response and suggest an inflammatory/immune response associated with apoptotic cell death. These mechanisms of action are potentially relevant to an interaction between IR and drug. However, in this cohort, all of whom received H_2O_2 + RT, it is difficult to distinguish the contribution of H_2O_2 over and above that of RT alone. The plasma analyses have been valuable in informing the selection of markers to investigate in a subsequent trial.

Conclusions

The results from this phase 1 trial confirm intratumoral H_2O_2 in combination with RT is a safe and simple intervention with the potential for high global impact if efficacy is confirmed in the forthcoming randomized phase 2 trial. Proof of concept in breast cancer could lead to rapid evaluation in other challenging and accessible primary sites, including cancers of the head and neck, cervix uteri, and soft tissue sarcomas, where locoregional control with RT alone is poor.

References

1. Ginsburg O, Bray F, Coleman MP, et al. The global burden of women's cancers: A grand challenge in global health. *Lancet* 2017; 389:847-860.
2. American Cancer Society. Global Cancer Facts & Figures 4th Edition. Available at: https://www.cancer.org/content/dam/cancer-org/research/cancer-facts-and-statistics/global-cancer-facts-and-figures/global-cancer-facts-and-figures-4th-edition.pdf. Accessed August 4, 2020.
3. Cancer Research UK. Available at: https://www.Cancerresearchuk.Org/health-professional/cancer-statistics/statistics-by-cancer-type/breast-cancer/incidence-invasive#heading-three. Accessed August 4, 2020.
4. National Cancer Registration and Analysis Service. Available at: http://www.Ncin.Org.Uk/publications/survival_by_stage. Accessed August 4, 2020.
5. Public Health Scotland. Available at: http://www.Isdscotland.Org/health-topics/cancer/detect-cancer-early/. Accessed August 4, 2020.
6. Ogawa Y, Takahashi T, Kobayashi T, et al. Mechanism of hydrogen peroxide-induced apoptosis of the human osteosarcoma cell line HS-Os-1. *Int J Mol Med* 2003;12:459-463.
7. Kariya S, Sawada K, Kobayashi T, et al. Combination treatment of hydrogen peroxide and x-rays induces apoptosis in human prostate cancer PC-3 cells. *Int J Radiat Oncol Biol Phys* 2009;75:449-454.
8. Eriksson D, Stigbrand T. Radiation-induced cell death mechanisms. *Tumour Biol* 2010;31:363-372.
9. Katsube T, Mori M, Tsuji H, et al. Most hydrogen peroxide-induced histone H2AX phosphorylation is mediated by ATR and is not dependent on DNA double-strand breaks. *J Biochem* 2014;156:85-95.
10. Ogawa Y, Takahashi T, Kobayashi T, et al. Apoptotic-resistance of the human osteosarcoma cell line HS-Os-1 to irradiation is converted to apoptotic-susceptibility by hydrogen peroxide: A potent role of hydrogen peroxide as a new radiosensitizer. *Int J Mol Med* 2003;12: 845-850.

11. Akima R, Ogawa Y, Morita-Tokuhiro S, et al. New enzyme-targeting radiosensitizer (KORTUC) containing hydrogen peroxide & sodium hyaluronate for intra-tumoral injection using mice transplanted with SCC VII tumor. *Int J Cancer Clin Res* 2016;3:1-6.
12. Ogawa Y. Paradigm shift in radiation biology/radiation oncology-exploitation of the "H_2O_2 effect" for radiotherapy using low-LET (linear energy transfer) radiation such as x-rays and high-energy electrons. *Cancers (Basel)* 2016;8:28.
13. Sleigh JW, Linter SP. Hazards of hydrogen peroxide. *Br Med J (Clin Res Ed)* 1985;291:1706.
14. Puhl W, Bernau A, Greiling H, et al. Intra-articular sodium hyaluronate in osteoarthritis of the knee: A multicenter, double-blind study. *Osteoarthritis Cartilage* 1993;1:233-241.
15. Morita-Tokuhiro S, Ogawa Y, Yokota N, et al. Development of a novel enzyme-targeting radiosensitizer (new KORTUC) using a gelatin-based hydrogel instead of a sodium hyaluronate. *Cancers (Basel)* 2016;8:10.
16. Aoyama N, Ogawa Y, Yasuoka M, et al. Therapeutic response to a novel enzyme-targeting radiosensitization treatment (Kochi oxydol-radiation therapy for unresectable carcinomas) in patients with recurrent breast cancer. *Oncol Lett* 2016;12:29-34.
17. Aoyama N, Ogawa Y, Yasuoka M, et al. Therapeutic response to a novel enzyme-targeting radiosensitization treatment (KORTUC II) for residual lesions in patients with stage IV primary breast cancer, following induction chemotherapy with epirubicin and cyclophosphamide or taxane. *Oncol Lett* 2017;13:69-76.
18. Rampello E, Fricia T, Malaguarnera M. The management of tumor lysis syndrome. *Nat Clin Pract Oncol* 2006;3:438-447.
19. Wapnir IL, Wartenberg DE, Greco RS. Three dimensional staging of breast cancer. *Breast Cancer Res Treat* 1996;41:15-19.
20. Miyatake K, Kubota K, Ogawa Y, et al. Non-surgical care for locally advanced breast cancer: Radiologically assessed therapeutic outcome of a new enzyme-targeting radiosensitization treatment, Kochi oxydol-radiation therapy for unresectable carcinomas, type II (KORTUC II) with systemic chemotherapy. *Oncol Rep* 2010;24:1161-1168.
21. Ogawa Y, Kubota K, Ue H, et al. Phase I study of a new radiosensitizer containing hydrogen peroxide and sodium hyaluronate for topical tumor injection: A new enzyme-targeting radiosensitization treatment, Kochi oxydol-radiation therapy for unresectable carcinomas, type II (KORTUC II). *Int J Oncol* 2009;34:609-618.
22. Ogawa Y, Kubota K, Ue H, et al. Safety and effectiveness of a new enzyme-targeting radiosensitization treatment (KORTUC II) for intratumoral injection for low-LET radioresistant tumors. *Int J Oncol* 2011;39:553-560.
23. Lindstrom MJ, Bates DM. Newton-Raphson and EM algorithms for linear mixed-effects models for repeated-measures data. *J Am Stat Assoc* 1988;83:1014-1022.
24. U.S. Department of Health and Human Services. National Institutes of Health. National Cancer Institute. Available at: https://ctep.Cancer.Gov/protocoldevelopment/electronic_applications/docs/ctcae_v5_quick_reference_8.5x11.Pdf. Accessed August 4, 2020.
25. Yee C, Wang K, Asthana R, et al. Radiation-induced skin toxicity in breast cancer patients: A systematic review of randomized trials. *Clin Breast Cancer* 2018;18:e825-e840.
26. Garg AD, Galluzzi L, Apetoh L, et al. Molecular and translational classifications of damps in immunogenic cell death. *Front Immunol* 2015;6:588.
27. Pajonk F, Vlashi E, McBride WH. Radiation resistance of cancer stem cells: The 4 r's of radiobiology revisited. *Stem Cells* 2010;28:639-648.
28. Zips D, Zophel K, Abolmaali N, et al. Exploratory prospective trial of hypoxia-specific PET imaging during radiochemotherapy in patients with locally advanced head-and-neck cancer. *Radiother Oncol* 2012;105:21-28.
29. Lock S, Perrin R, Seidlitz A, et al. Residual tumour hypoxia in head-and-neck cancer patients undergoing primary radiochemotherapy, final results of a prospective trial on repeat FMISO-PET imaging. *Radiother Oncol* 2017;124:533-540.
30. Bray FN, Simmons BJ, Wolfson AH, et al. Acute and chronic cutaneous reactions to ionizing radiation therapy. *Dermatol Ther (Heidelb)* 2016;6:185-206.
31. Arriagada R, Mouriesse H, Sarrazin D, et al. Radiotherapy alone in breast cancer. I. Analysis of tumor parameters, tumor dose and local control: The experience of the Gustave-Roussy Institute and the Princess Margaret Hospital. *Int J Radiat Oncol Biol Phys* 1985;11:1751-1757.
32. Bedwinek J, Rao DV, Perez C, et al. Stage III and localized stage IV breast cancer: Irradiation alone vs irradiation plus surgery. *Int J Radiat Oncol Biol Phys* 1982;8:31-36.
33. Lievens Y, Gospodarowicz M, Grover S, et al. Global impact of radiotherapy in oncology: Saving one million lives by 2035. *Radiother Oncol* 2017;125:175-177.
34. Abdel-Wahab M, Fidarova E, Polo A. Global access to radiotherapy in low- and middle-income countries. *Clin Oncol (R Coll Radiol)* 2017;29:99-104.
35. Galluzzi L, Buque A, Kepp O, et al. Immunogenic cell death in cancer and infectious disease. *Nat Rev Immunol* 2017;17:97-111.
36. Gough DR, Cotter TG. Hydrogen peroxide: A Jekyll and Hyde signalling molecule. *Cell Death Dis* 2011;2:e213.
37. Sena LA, Chandel NS. Physiological roles of mitochondrial reactive oxygen species. *Mol Cell* 2012;48:158-167.
38. Veal EA, Day AM, Morgan BA. Hydrogen peroxide sensing and signaling. *Mol Cell* 2007;26:1-14.
39. Sies H. Hydrogen peroxide as a central redox signaling molecule in physiological oxidative stress: Oxidative eustress. *Redox Biol* 2017;11:613-619.
40. Takahashi A, Hanson MG, Norell HR, et al. Preferential cell death of CD8+ effector memory (CCR7-CD45RA-) T cells by hydrogen peroxide-induced oxidative stress. *J Immunol* 2005;174:6080-6087.
41. Whittemore ER, Loo DT, Watt JA, et al. A detailed analysis of hydrogen peroxide-induced cell death in primary neuronal culture. *Neuroscience* 1995;67:921-932.
42. Clement MV, Ponton A, Pervaiz S. Apoptosis induced by hydrogen peroxide is mediated by decreased superoxide anion concentration and reduction of intracellular milieu. *FEBS Lett* 1998;440:13-18.
43. Tochigi M, Inoue T, Suzuki-Karasaki M, et al. Hydrogen peroxide induces cell death in human trail-resistant melanoma through intracellular superoxide generation. *Int J Oncol* 2013;42:863-872.
44. Xiang JM, Wan CY, Guo R, et al. Is hydrogen peroxide a suitable apoptosis inducer for all cell types? *BioMed Res Int* 2016;2016:7343965.
45. Di Marzo N, Chisci E, Giovannoni R. The role of hydrogen peroxide in redox-dependent signaling: Homeostatic and pathological responses in mammalian cells. *Cells* 2018;7:156.
46. Hogquist KA, Nett MA, Unanue ER, et al. Interleukin 1 is processed and released during apoptosis. *Proc Natl Acad Sci U S A* 1991;88:8485-8489.
47. England H, Summersgill HR, Edye ME, et al. Release of interleukin-1α or interleukin-1β depends on mechanism of cell death. *J Biol Chem* 2014;289:15942-15950.
48. Obata F, Hoshino A, Toyama A. Hydrogen peroxide increases interleukin-12 p40/p70 molecular ratio and induces Th2-predominant responses in mice. *Scand J Immunol* 2006;63:125-130.
49. Kwon D, Choi IH. Hydrogen peroxide upregulates TNF-related apoptosis-inducing ligand (TRAIL) expression in human astroglial cells, and augments apoptosis of T cells. *Yonsei Med J* 2006;47:551-557.
50. Janssen EM, Droin NM, Lemmens EE, et al. CD4+ T-cell help controls CD8+ T-cell memory via TRAIL-mediated activation-induced cell death. *Nature* 2005;434:88-93.
51. Jaramillo M, Olivier M. Hydrogen peroxide induces murine macrophage chemokine gene transcription via extracellular signal-regulated kinase- and cyclic adenosine 5'-monophosphate (cAMP)-dependent pathways: Involvement of NF-kappa B, activator protein 1, and cAMP response element binding protein. *J Immunol* 2002;169:7026-7038.